

**ENZYMATIC REACTION BASED BIOSENSOR FOR
SPECIFIC DETECTION OF ORGANOPHOSPHATE
PESTICIDES**



Miss Chonticha Sahub

จุฬาลงกรณ์มหาวิทยาลัย
CHULALONGKORN UNIVERSITY

**A Dissertation Submitted in Partial Fulfillment of the
Requirements
for the Degree of Doctor of Philosophy in Chemistry
Department of Chemistry
FACULTY OF SCIENCE
Chulalongkorn University
Academic Year 2018
Copyright of Chulalongkorn University**

ตัวรับรู้ชีวภาพบนพื้นฐานปฏิกิริยาของเอนไซม์สำหรับการตรวจวัดอย่างจำเพาะของสารมาส์ทรูพีซ
และสัตว์กลุ่มออร์แกโนฟอสเฟต



วิทยานิพนธ์นี้เป็นส่วนหนึ่งของการศึกษาตามหลักสูตรปริญญาวิทยาศาสตรดุษฎีบัณฑิต
สาขาวิชาเคมี ภาควิชาเคมี
คณะวิทยาศาสตร์ จุฬาลงกรณ์มหาวิทยาลัย
ปีการศึกษา 2561
ลิขสิทธิ์ของจุฬาลงกรณ์มหาวิทยาลัย

Dissertation Title ENZYMATIC REACTION BASED BIOSENSOR FOR
 SPECIFIC DETECTION OF ORGANOPHOSPHATE
 PESTICIDES
By Miss Chonticha Sahub
Field of Study Chemistry
Thesis Advisor Assistant Professor Boosayarat Tomapatanaget, Ph.D.

Accepted by the FACULTY OF SCIENCE, Chulalongkorn University in
Partial Fulfillment of the Requirement for the Doctor of Philosophy

..... Dean of the FACULTY OF
 SCIENCE
(Professor Polkit Sangvanich, Ph.D.)

DISSERTATION COMMITTEE

..... Chairman
(Associate Professor Vudhichai Parasuk, Ph.D.)

..... Advisor
(Assistant Professor Boosayarat Tomapatanaget, Ph.D.)

..... Examiner
(Professor Thawatchai Tuntulani, Ph.D.)

..... Examiner
(Associate Professor FUANGFA UNOB, Ph.D.)

..... Examiner
(Numpon Insin, Ph.D.)

..... External Examiner
(Gamolwan Tumcharern, Ph.D.)

ชลธิชา สาหับ : ตัวรับรู้ชีวภาพบนพื้นฐานปฏิกิริยาของเอนไซม์สำหรับการตรวจวัดอย่างจำเพาะของสารฆ่าศัตรูพืชและสัตว์ในกลุ่มออร์แกโนฟอสเฟต. (ENZYMATIC REACTION BASED BIOSENSOR FOR SPECIFIC DETECTION OF ORGANOPHOSPHATE PESTICIDES) อ.ที่ปรึกษาวิทยานิพนธ์หลัก : ผศ. ดร.บุญรัตน์ ธรรมพัฒน์กิจ

ในงานวิจัยนี้มีวัตถุประสงค์เพื่อออกแบบและพัฒนาตัวรับรู้ชีวภาพในสองแพลตฟอร์ม โดยอาศัย กราฟีนควอนตัมดอท (GQDs) และปฏิกิริยาของเอนไซม์ สำหรับตรวจวัดยาฆ่าศัตรูพืชและสัตว์ในกลุ่มออร์แกโนฟอสเฟต (OPs) ตัวรับรู้ชีวภาพในแพลตฟอร์มแรกสามารถเตรียมได้อย่างง่ายในรูปของสารละลายกราฟีนควอนตัมดอทและเอนไซม์ (GQDs/Enz) จากนั้นได้พัฒนาเซนเซอร์ GQDs/Enz แพลตฟอร์มในรูปของไฮบริดไฮโดรเจล (GQDs/Enz/Gels) ที่สามารถฟอร์มตัวได้ดีในน้ำ เพื่อการตรวจวัดออร์แกโนฟอสเฟตที่มีประสิทธิภาพมากยิ่งขึ้น โดยเพิ่มความเสถียรให้กับเอนไซม์ และความว่องไวในการตรวจวัด ทำให้ได้การตรวจวัดที่ง่าย และสะดวก

ตัวรับรู้ชีวภาพ GQDs/Enz และ GQDs/Enz/Gels ถูกเตรียมขึ้นและพิสูจน์เอกลักษณ์ด้วยเทคนิคอินฟราเรดสเปกโทรสโกปี กล้องจุลทรรศน์อิเล็กตรอนแบบส่องกราด และกล้องจุลทรรศน์อิเล็กตรอนแบบส่องผ่าน ในงานวิจัยนี้ได้อาศัยกลไกการทำงานของเอนไซม์ 2 ชนิด คือ อะซิติลโคลีนเอสเตอเรสและโคลีนเอสเตอเรส ซึ่งในสภาวะปกติจะผลิตไฮโดรเจนเปอร์ออกไซด์ ที่ส่งผลกระทบต่อลดลงของความเข้มสัญญาณแสงโฟโตลูมิเนสเซนซ์ของกราฟีนควอนตัมดอท ที่ความยาวคลื่น 467 นาโนเมตร เมื่อมีออร์แกโนฟอสเฟตในระบบ ออร์แกโนฟอสเฟตจะยับยั้งการทำงานของเอนไซม์ ทำให้ปริมาณไฮโดรเจนเปอร์ออกไซด์ลดลง และส่งผลกระทบต่อการคืนกลับมาของสัญญาณแสงโฟโตลูมิเนสเซนซ์ของกราฟีนควอนตัมดอท จากผลการทดลองพบว่า ตัวรับรู้ชีวภาพ GQDs/Enz สามารถใช้ในการตรวจวัดออร์แกโนฟอสเฟตได้อย่างจำเพาะกับไดโครออส และเมทิลพาราออกซอน โดยมีขีดจำกัดของการตรวจวัดเท่ากับ 0.78 และ 0.34 ไมโครโมลาร์ ในช่วงความเป็นเส้นตรงเท่ากับ 0.45-45 และ 0.40-4 ไมโครโมลาร์ ตามลำดับ นอกจากนี้ตัวรับรู้ชีวภาพในรูปแบบเจล GQDs/Enz/Gels ที่เตรียมได้จากโมเลกุล 4b จะช่วยเพิ่มสัญญาณโฟโตลูมิเนสเซนซ์ของกราฟีนควอนตัมดอท และเพิ่มขีดความสามารถในการตรวจวัด ได้ประมาณ 10-100 เท่า โดยขีดจำกัดของการตรวจวัดที่มีประสิทธิภาพขึ้นของไดโครออส และเมทิลพาราออกซอน เท่ากับ 26.10×10^{-3} และ 6.79×10^{-3} ไมโครโมลาร์ ในช่วงความเป็นเส้นตรง 12.5×10^{-3} -125 และ 1.25×10^{-3} - 62.5 ไมโครโมลาร์ ตามลำดับ ซึ่งตัวรับรู้ชีวภาพทั้งสองแพลตฟอร์มนี้ให้ความจำเพาะเจาะจง และความว่องไวในการตรวจวัดสูง จึงสามารถพัฒนาไปสู่การวิเคราะห์ปริมาณยาฆ่าแมลงในอาหาร แหล่งน้ำ และสิ่งแวดล้อมอื่น ๆ ได้ต่อไปในอนาคต

CHULALONGKORN UNIVERSITY

ภาควิชา	ภาควิชาเคมี	ลายมือชื่อนิสิต
สาขาวิชา	เคมี
ปีการศึกษา	2561	ลายมือชื่อ อ.ที่ปรึกษาวิทยานิพนธ์หลัก

5672887123 : DOCTOR OF PHILOSOPHY

Graphene quantum dots / Organophosphates / Photoluminescence/
Acetylcholinesterase/ Choline Oxidase

Chonticha Sahub : ENZYMATIC REACTION BASED BIOSENSOR FOR
SPECIFIC DETECTION OF ORGANOPHOSPHATE PESTICIDES.
ADVISOR: Asst. Prof. Boosayarat Tomapatanaet, Ph.D.

This research aims to design and develop two-biosensor platforms based on graphene quantum dots (GQDs) *via* enzymatic reaction for determining organophosphate pesticides (OPs). A first platform consisting of GQDs and active enzyme, GQDs/Enz platform, is simply fabricated in aqueous solution. Ongoing development of GQDs/Enz platform for effective OPs sensing by hybrid hydrogel (GQDs/Enz/Gels) was of great interest to improve the sensitivity and enzyme stability under the benefit of easy to be used for sensing approach.

The GQDs/Enz and GQDs/Enz/Gels were constructed and characterized by general methods such as FT-IR, SEM and TEM. Based on the concept, H₂O₂ generated *in situ* by the active enzymatic reaction of acetylcholinesterase and choline oxidase enables to react with GQDs resulting in photoluminescence (PL) quenching of GQDs at 467 nm. The PL recovery of GQDs was observed in the system with OPs due to enzymatic inhibition process by OPs. With a selectivity study of sensing platform toward OPs, GQDs/Enz platform exhibited a significant fluorescent change in case of dichlorvos and methyl-paraoxon. In quantitative analysis, the limits of detection (LOD) of GQDs/Enz platform for dichlorvos and methyl paraoxon are 0.78 μM and 0.34 μM in linear range of 0.45-45 and 0.40-4 μM , respectively. Furthermore, novel incorporation of GQDs and enzyme in hydrogels (GQDs/Enz/Gels) based gelator 4b enables to significantly enhance the PL intensity of GQDs and effectively improve 10-100 folds in the limit of detection and in linearity range towards dichlorvos and methyl-paraoxon (26.10 $\times 10^{-3}$ and 6.79 $\times 10^{-3}$ μM in linear range of 12.5 $\times 10^{-3}$ -125 μM and 1.25 $\times 10^{-3}$ -62.5 μM , respectively). In this approach, the biosensors are expected to offer the promising selective and sensitive determination of the OPs and a benefit for easy checking of OPs in food, water and environment in future.

Department:	Department of Chemistry	Student's Signature
	
Field of Study:	Chemistry	Advisor's Signature
	
Academic Year:	2018	

ACKNOWLEDGEMENTS

I would like to express my deepest appreciation to my thesis supervisor Asst. Prof. Dr. Boosayarat Tomapatanaget, Prof. Dr. Jonathan W. Steed and Prof. Dr. Thawatchai Tuntulani for their kindness, opportunity, suggestion, assistance, encouragement, inspiration in this research and introducing the new knowledges about nanomaterial and supramolecular chemistry especially supramolecular hydrogels. In addition, I would like to thank Assoc. Prof. Dr. Vudhichai Parasuk, Asst. Prof. Dr. Fuangfa Unob, Dr. Numpon Insin and Dr. Gamolwan Tumcharern for their valuable suggestions and comments as thesis committee and thesis examiner.

I would like thank Associate Professor Dr. Thumnoon Nhujak and his student for their advice and assistance in UHPLC-MS technique, Miss Manunya Tepakidareekul for synthesis of graphene quantum dots, Miss Piyanan Pranee for assistance in morphology studies by using the scanning electron microscopy, Jessica L. Andrews, James P. Smith and Maya A. Mohamad Arif for their support, suggestion and assistance in Durham University, UK. I wish like to express my sincere thanks to Miss Siriboon Mukdasai for her useful recommendation and encouragement. I would like to thank all members in the Supramolecular Chemistry Research Unit (SCRU) and JWS group for their friendship, support, suggestion and assistance.

Additionally, I would like to acknowledge department of Chemistry of both Chulalongkorn University, Thailand and Durham University, United Kingdom, the Ratchadapisek Sompoch Endowment Fund (2016), Chulalongkorn University (CU-59-020-FW), the Thailand Research Fund (RSA6080012) and the 90th Anniversary of Chulalongkorn Fund (Ratchadapisek Sompoch Endowment Fund), Development and Promotion of Science and Technology Talents Project (DPST) for research grant. And financial supports.

Finally, I would like to express my deepest gratitude to my parents, my sisters, and all of my friends for their love, care, kindness, encouragement and other supports throughout my life.

Chonticha Sahub

TABLE OF CONTENTS

	Page
ABSTRACT (THAI)	iii
ABSTRACT (ENGLISH).....	iv
ACKNOWLEDGEMENTS.....	v
TABLE OF CONTENTS.....	vi
LIST OF FIGURES	ix
LIST OF TABLES.....	xvi
CHAPTER I.....	1
1.1 Introduction.....	1
1.2 Research objective	1
1.3 Literature reviews	2
1.4 Scope of this research	12
1.5 Benefits of this research.....	12
CHAPTER II Graphene quantum dots for organophosphate sensing.....	13
2.1 Introduction.....	13
2.2 Analytical measurement	14
2.3 Experimental.....	15
2.3.1 Materials.....	15
2.3.2 Preparation of the graphene quantum dots (GQDs).....	15
2.3.3 Preparation of GQDs/AChE/ChOx (GQDs/Enz) biosensors	15
2.3.4 UV-visible and photoluminescence (PL) studies of GQDs.....	16
2.3.5 Impact of H ₂ O ₂ toward the GQDs	17
2.3.6 Responsibility of H ₂ O ₂ -generated <i>in situ</i> by GQDs/Enz.....	18
2.3.7 The detection of organophosphate by GQDs/Enz.....	18
2.3.8 Effect of interfering ions	21
2.3.9 Organophosphate detection in real samples	21

2.4 Results and discussions.....	23
2.4.1 Structural morphology characterizations of GQDs and GQDs/Enz.....	24
2.4.2 Infrared spectroscopy studies	25
2.4.3 UV-visible and photoluminescence (PL) studies of GQDs.....	28
2.4.4 Role of GQDs toward peroxidase-catalytic reaction of H ₂ O ₂	29
2.4.5 Responsibility of H ₂ O ₂ -generated <i>in situ</i> by GQDs/Enz.....	32
2.4.6 Signal amplification for increasing responsive sensing of GQDs/Enz	34
2.4.7 OPs detection by using the GQDs/Enz nanomaterial.....	37
2.4.8 Effect of interfering ions	41
2.4.9 Determination of organophosphate in real samples	43
CHAPTER III Hybrid hydrogels for organophosphate detection.....	45
3.1 Introduction.....	45
3.2 Experimental.....	46
3.2.1 Materials	46
3.2.2 Synthesis of compound 1 to 6b	46
3.2.2.1 4,4'-methylenebis(2,6-diethylphenyl isocyanate)	47
3.2.2.2 Compound 1	48
3.2.2.3 Compound 2c	49
3.2.2.4 Compound 3	50
3.2.2.5 Compound 4b	51
3.2.2.6 Compound 4a	52
3.2.2.7 Compound 4c	53
3.2.2.8 Compound 5	54
3.2.2.9 Compound 6b	55
3.2.2.10 Compound 6a	56
3.2.3 Gel screening test	57
3.2.4 Preparation of hybrid GQDs/Gels	57
3.2.5 Impact of H ₂ O ₂ toward the GQDs/Gels	58
3.2.6 Preparation of hybrid GQDs/Enz/Gels.....	58

3.2.7 The determination of organophosphate pesticides	59
3.2.8 Rheology	61
3.2.9 Scanning electron microscopy.....	61
3.3 Result and discussions	62
3.3.1 Characterization of compound 1-6b	63
3.3.2 Gel screening.....	65
3.3.3 Preparation of hybrid GQDs/Gels	69
3.3.3.1 The effect of GQDs toward GQDs/Gels formation.....	71
3.3.3.2 The effect of pH toward GQDs/Gels formation.....	73
3.3.3.3 The rheological properties.....	76
3.3.4 Preparation of hybrid GQDs/Enz/Gels materials	77
3.3.5 Impact of H ₂ O ₂ toward GQDs/Gels	82
3.3.6 Responsibility of H ₂ O ₂ -generated <i>in situ</i> by the hybrid GQDs/Enz/Gels	84
3.3.7 Signal amplification for increasing responsive sensing of GQDs/Enz/Gels	89
.....	89
3.3.8 Study on the detection of GQDs/Enz/Gel toward organophosphate	91
3.3.9 Comparison of the GQDs/Enz in aqueous and in hydrogel state	94
3.3.10 Lab on chips	96
CHAPTER IV	98
4.1 Conclusion	98
4.2 Suggestions for future works	99
REFERENCES	100
APPENDIX.....	108
VITA.....	120

LIST OF FIGURES

Chapter I

- Figure 1.1** Irreversible inhibitor of acetylcholinesterase (AChE) by organophosphate pesticides (OPs) [6]. 2
- Figure 1.2** Sensing assembly of the nanostructured films of AChE and CdTe quantum dots (QDs) [10]. 4
- Figure 1.3** (A) Proposed mechanism and (B) dose–response curve for methyl-paraoxon detection [2]. 4
- Figure 1.4** Schematic illustration of highly-efficient peroxidase-like activity of graphene dots (GDs) for the detection of H₂O₂ and glucose [21]. 5
- Figure 1.5** Quantum confinement effect of conjugated π -domains in GQDs (a) The suggested energy levels of C₄₂H₁₈, C₉₆H₃₀, C₁₃₂, C₁₃₂H₃₄, and C₂₂₂H₄₂. The size-dependent energy levels in these H-passivated small GQDs are in agreement with the molecule orbital calculation. The intrinsic state depends on size. The energy-level offset between the intrinsic state and the edge state determines its optical properties. (b) The structure of all materials [25]. 6
- Figure 1.6** (A) Diagram for the synthesis of GQDs and GO, the black dots in the GO represent oxygen atoms and (B) UV–vis absorption of CA and the GQDs, and PL spectra of the GQDs and GO with different excitation wavelength [24]. 7
- Figure 1.7** Schematic representation of the proposed mechanism of stabilization of GDH by using PEI [32]. 8
- Figure 1.8** (A) BAmoc–peptides. (B) Schematic representation showing the self-assembly of BPmoc–peptides to form a nanofiber network (gel) and H₂O₂-triggered gel degradation. (C) Schematic representation of O_x–BPmoc–F₃ hybrid gels before and after the response to analytes [49]. 10
- Figure 1.9** Schematic representation of triethylammonium salt gelators (1a-2b), carbon-dot gel and their photoluminescence properties [56]. 11

Chapter II

- Figure 2.1** Proposed GQDs/Enz system to determine the organophosphate pesticide. 13
- Figure 2.2** Synthetic pathway of graphene quantum dots (GQDs) [24]. 15
- Figure 2.3** The magnification TEM image of GQDs (A), TEM images of GQDs (B) GQDs/Enz biosensor (C) Inset of (B) and (C) are the frequency (%) of size of GQDs and GQDs/Enz biosensor by TEM image, respectively. 24

Figure 2.4 ATR-FTIR spectra of citric acid and GQDs.....	25
Figure 2.5 ATR-FTIR spectra of citric acid, GQDs, GQDs (in Tris), bi-enzyme, BSA and GQDs/Enz (in Tris and Tris-BSA).....	26
Figure 2.6 The proposed formation of GQDs/Enz with BSA platform.	27
Figure 2.7 (A) UV-Vis absorption spectra of the GQDs, inset (A) is the GQDs solution observed under visible light. (B) Photoluminescent spectra of the GQDs with different excitation wavelength (λ_{ex} 300 to 440 nm), inset (B) is the photoluminescence brightness of GQDs under UV light.	28
Figure 2.8 (A) Time-dependent photoluminescent changes of 5×10^{-4} g/ml of the GQDs after interacted with 0.1 M H_2O_2 and (B) Concentration-dependent fluorescence changes at 30 min after interacted with different concentration of H_2O_2	29
Figure 2.9 Linear relationship between $(I-I_0)/I_0$ of GQDs and concentration of H_2O_2	30
Figure 2.10 Stern-Volmer plots for photoluminescence of GQDs with H_2O_2 concentration ranging from 0 to 0.05 M.	30
Figure 2.11 The normalized I/I_0 photoluminescent response at λ_{em} 467 nm of GQDs, GQD/Enz (GQDsAChE/ChOx) and GQDs/ChOx after the addition of ACh. Concentration of AChE and ChOx were 1 and 0.125 U/ml, respectively, where 1U is equivalent to amount of enzyme that hydrolyses acetylcholine or substrate to produce 1 mmol of choline or product per minute.	32
Figure 2.12 Time-dependent photoluminescence changes of GQDs/Enz after interacted with 1 mg/ml of acetylcholine (ACh) in Tris buffer pH 8, the concentration of GQDs, AChE and ChOx are 5×10^{-4} g/mL, 1 U/mL and 0.125 U/mL, respectively.	33
Figure 2.13 Normalized I/I_0 photoluminescence responses at λ_{em} 467 nm of GQDs upon the interaction of various concentrations of AChE and ChOx and incubation time.	34
Figure 2.14 The PL intensity of GQDs/Enz at pH 3 to 12.	36
Figure 2.15 The PL intensity of GQDs/Enz before (black bar) and after incubation with ACh for 30 min (red bar) at various pH from 5 to 9.	36
Figure 2.16 (A) Photoluminescence responses of GQDs/Enz biosensor after incubation with various concentration of dichlorvos 0-100 ppm. (B) % Inhibition efficiency (I%) of 1 and 10 ppm of different OPs toward GQDs/Enz biosensor.	37
Figure 2.17 % Inhibition efficiency (I%) of GQDs/Enz biosensor after incubation with various concentration of dichlorvos from 0.025 to 100 ppm (A) and methyl-paraoxon	

from 1×10^{-5} to 20 ppm (B). The insets of (A) and (B) showed the linear rang of dichlorvos detection from 0.1 to 10 ppm and methyl-paraoxon from 0.1 to 1 ppm, respectively.39

Figure 2.18 Colorimetric of **GQDs/Enz** biosensor in visible (A) and UV light (B) at various concentration of dichlorvos organophosphate (OP) at 0, 1, 10, 100 ppm and blank (no dichlorvos and ACh).40

Figure 2.19 Effect of interference (1×10^{-5} M) to the inhibition efficiency (%) of AChE of **GQDs/Enz** biosensor in the presence of dichlorvos (1×10^{-5} M or 2 ppm) after incubation for 30 min.41

Figure 2.20 The PL intensity of GQDs in the presence of various ions (1×10^{-5} M). I_0 and I were the intensity of GQDs before and after incubation with various ions for 30 min.42

Chapter III

Figure 3.1 Hybrid hydrogels of **GQDs/Enz/Gels** and proposed mechanism of organophosphate pesticide detection.45

Figure 3.2 The molecular structures of compound **1-6b**.46

Figure 3.3 Synthetic pathway of 4,4'-methylenebis(2,6-diethylphenyl isocyanate). .47

Figure 3.4 Synthetic pathway of compound **1**.48

Figure 3.5 Synthetic pathway of compound **2c**.49

Figure 3.6 Synthetic pathway of compound **3**.50

Figure 3.7 Synthetic pathway of compound **4b**.51

Figure 3.8 Synthetic pathway of compound **4a**.52

Figure 3.9 Synthetic pathway of compound **4c**.53

Figure 3.10 Synthetic pathway of compound **5**.54

Figure 3.11 Synthetic pathway of compound **6b**.55

Figure 3.12 Synthetic pathway of compound **6a**.56

Figure 3.13 Preparation of **GQDs/Enz/Gels** for organophosphate pesticides (OPs) detection.60

Figure 3.14 The molecular structures of compound **1-6b**.63

Figure 3.15 NMR spectra of compounds **4a-4c** and D_2O experiment of compound **4b**.64

- Figure 3.16** The assigned behavior of solution (S), insoluble (I), rapid precipitate formed from solution (P), partial gel (PG), gel (G) and collapsed gel (CG).65
- Figure 3.17** Gel formations of 1wt% of compounds **4b** in various solvents.68
- Figure 3.18** Proposed primary, secondary and tertiary structures of hybrid GQDs hydrogel materials (**GQDs/Gels**).....69
- Figure 3.19** Comparison between hybrid **GQDs/Gels** from **4a** and **4b** that formed by method 1 (M1) and method 2 (M2).69
- Figure 3.20** The gelation behavior by 0.3%wt of **4b** (A) and 0.5%wt of **4b** (B) at various amount of GQDs at 0 (b, h), 0.5 (c, i), 1 (d, j), 2 (e, k) and 3 mg/mL (f, l). For GQDs solution at 2 mg/mL (a, g) in 10 mM phosphate buffer pH 8 for 24 h. The left picture was taken in normal light and right picture was taken under 365 nm UV light.72
- Figure 3.21** Photographs of gel behavior at 30 min (A) gel formation studies of gelators **4a**, **4b** and **4c** without GQDs in various concentration of phosphate buffer pH 8; the **GQDs/Gels** from 1wt% gelators **4a**, **4b** and **4c** in water (B); and 0.5% wt gelator under different concentration of phosphate buffer (C) and different wt% of gelator **4b**, in 10 mM phosphate buffer pH 8 (D) respectively.73
- Figure 3.22** (A) Stress sweep and (B) frequency-sweep rheology of gelator **4b** and **GQDs/Gels** from **4b** in different conditions.....76
- Figure 3.23** The fluorescent images of **GQDs**, **GQDs/Enz**, **GQDs/Gels** and **GQDs/Enz/Gels** before (A) and after incubation in acetylcholine for 30 (B), 60 (C) and 120 min (D). The **GQDs/Enz/Gels** were prepared by cooling down of **GQDs/Gels** from 1 to 5 min, and then, enzymes were added and kept at 5 °C for 24 h prior activity tests. (E) The temperature of **GQDs/Gel** after cooling at room temperature from 0-15 min.77
- Figure 3.24** SEM image of gelator **4b** in 10 mM phosphate buffer.....78
- Figure 3.25** (A) Preparation of partial **GQDs/Gels** (stage 1) and **GQDs/Enz/Gels** hybrid hydrogels (stage 2). (B) SEM images of the partial gels in stage 1 that was prepared for 1 min and the hybrid hydrogels in stage 2 that was prepared for 30 min before dropping on stuff and dried for 2 days.....79
- Figure 3.26** FT-IR spectra of starting materials and xerogel of the hybrid hydrogels.81
- Figure 3.27** (A) Illustration of peroxidase-catalytic reaction of **GQDs/Gels**. (B) Comparison between concentration of **4b** (0.5 and 1 wt%) toward naked-eyed brightness quenching by slow passing of H₂O₂ from top to bottom of vials at room temperature. (C) Concentration-dependent PL changes of **GQDs/Gels** after interaction

with H₂O₂ between 0 and 1250 mM at 37 °C for 20 min. Inset of C is Stern-Volmer plots from PL of **GQDs/Gels** after interaction with H₂O₂ at concentration ranging from 0 to 125 mM.....82

Figure 3.28 Stress sweep and (A) frequency-sweep(B) rheology of **GQDs/Gels** before (S1) and after (S2) adding enzyme, and **GQDs/Enz/Gels** after reacting with acetylcholine (S3).84

Figure 3.29 Fluorescent intensity of **GQDs/Gels** from gelator **4b** showed stable intensity after re-heating and forming gel again in a cuvette for 15 minutes. The **GQDs/Gels** was prepared under condition of 1.25 mg/ml of GQDs with 0.3125 wt% of **4b** in 12.5 mM phosphate buffer pH 8.....85

Figure 3.30 Fluorescent intensity of **GQDs/Gels** after addition of ACh and dichlorvos (DV) in a range of 1.25×10^{-8} to 1.25×10^{-4} M.....85

Figure 3.31 (A) Scheme of H₂O₂-responsive in situ of **GQDs/Enz/Gels** biosensor (stage 3; S3). (B) The PL quenching of biosensor after adding acetylcholine. (C) In comparison of relative enzyme activity between in aqueous solution and gel phase after incubated in 5, 25 and 37 °C for 4 h.86

Figure 3.32 (A) Relative F/F₀ of **GQDs/Gels**. (B) Relative enzyme activity (%) of **GQDs/Enz/Gels** that were kept in 5 °C and room temperature from 4h to 15 days. ...88

Figure 3.33 Optimized condition such as temperature (A), pH (B), concentration of two enzymes (C) and acetylcholine (D) for sensing application.89

Figure 3.34 (A) Proposed mechanism of hybrid **GQDs/Enz/Gels** for organophosphate pesticide detection. (B) PL intensity of **GQDs/Enz/Gels** upon increment of dichlorvos concentration between 1.25×10^{-9} to 1.25×10^{-4} M (λ_{ex} 360 nm). (C) Comparison of inhibition efficiency (%) of AChE in hybrid hydrogels after incubated in 1.25×10^{-6} and 12.5×10^{-6} M of four OPs. (D) and (E) Inhibition efficiency (%) of AChE in this material after incubation in various concentration of dichlorvos and methyl-paraoxon. Insets of D and E showed linear range of dichlorvos and methyl-paraoxon detections in log concentration of 1.25×10^{-8} to 1.25×10^{-4} M and 1.25×10^{-9} to 0.625×10^{-4} M, respectively.92

Figure 3.35 PL emission spectra of **GQDs/Enz** (A) and **GQDs/Enz/Gels** (B) upon the increasing of methyl-paraoxon (MP) at concentration between 1.25×10^{-9} to 1.25×10^{-5} M (λ_{ex} 360 nm).....94

Figure 3.36 Photographs of hybrid **GQDs/Enz/Gels** sensory chips in the presence of various concentration of dichlorvos (DV) and time of measurement.....96

Figure 3.37 RGB of green value of 50 μ L **GQDs/Enz/Gels** on glass slide 2h after addition of 10 μ L of dichlorvos (DV) in a range of 1×10^{-6} to 1×10^{-3} M and followed by

10 μL of 80 mM ACh. The final concentration of these hydrogels is 1.25 mg/mL of GQDs, 0.3125% wt of **4b**, 20 U/mL of AChE and 2 U/mL of ChOx.97

Chapter IV

Figure 4.1 Proposed **GQDs/Enz** and **GQDs/Enz/Gels** biosensor systems for detection of organophosphate pesticide.....98

Appendix

Figure A1. The $^1\text{H-NMR}$ of 4,4'-methylenebis(2,6-diethylphenyl isocyanate) in DMSO- d_6 109

Figure A2. The $^1\text{H-NMR}$ of compound **1** 109

Figure A3. The $^1\text{H-NMR}$ of compound **2c** 110

Figure A4. The $^1\text{H-NMR}$ of compound **3** 110

Figure A5. The $^1\text{H-NMR}$ of compound **5** 111

Figure A6. The $^1\text{H-NMR}$ of compound **6a** 111

Figure A7. The $^1\text{H-NMR}$ of compound **6b** 112

Figure A8. ESI mass spectrum of compound **1**. 113

Figure A9. ESI mass spectrum of compound **2c**..... 113

Figure A10. ESI mass spectrum of compound **3**. 113

Figure A11. Accurate mass spectrum of compound **4a** 114

Figure A12. Accurate mass spectrum of compound **4b**..... 114

Figure A13. ESI mass spectrum of compound **4c**..... 114

Figure A14. ESI mass spectrum of compound **5**. 115

Figure A15. ESI mass spectrum of compound **6a**. 115

Figure A16. ESI mass spectrum of compound **6b**. 115

Figure A17. Linear range of dichlorvos detections in tap water by using **GQDs/Enz** platform with spiked dichlorvos in log concentration of 0.2 ppm to 4 ppm..... 116

Figure A18. Linear range of dichlorvos detections in field water 1 by using **GQDs/Enz** platform with spiked dichlorvos in log concentration of 0.2 ppm to 4 ppm..... 116

Figure A19. Linear range of dichlorvos detections in field water 2 by using **GQDs/Enz** platform with spiked dichlorvos in log concentration of 0.2 ppm to 4 ppm..... 117

Figure A20. Linear range of dichlorvos detections in Milli-Q water by using LC/MS method with spiked dichlorvos in concentration of 1 ppm to 5 ppm..... 117

Figure A21. Linear range of dichlorvos detections in tap water by using LC/MS method with spiked dichlorvos in concentration of 1 ppm to 5 ppm..... 118

Figure A22. Linear range of dichlorvos detections in field water 1 by using LC/MS method with spiked dichlorvos in concentration of 1 ppm to 5 ppm..... 118

Figure A23. Linear range of dichlorvos detections in field water 2 by using LC/MS method with spiked dichlorvos in concentration of 1 ppm to 5 ppm..... 119



LIST OF TABLES

Chapter II

Table 2.1 Various conditions in H ₂ O ₂ -responsive study of GQDs.	17
Table 2.2 Parameters used in signal amplification of GQDs/Enz	18
Table 2.3 Amount of components used in dichlorvos detection studies.	20
Table 2.4 Amount of components used in various type of OPs detection.	20
Table 2.5 The analytical comparison between this work and other works.	40
Table 2.6 The determination of dichlorvos in real samples by using this biosensor and LC/MS.....	43

Chapter III

Table 3.1 Various conditions used in gels screening test.....	57
Table 3.2 Various conditions used in GQDs/Gels preparation.	58
Table 3.3 Parameters used in signal amplification of GQDs/Enz/Gels	59
Table 3.4 Final concentration of component in GQDs/Enz/Gels for organophosphate detection.....	60
Table 3.5 Gel formation studies of compounds 1-6b	65
Table 3.6 GQDs/Gels formation studies of compounds 1-6b	70
Table 3.7 GQDs/Gels formation studies in various concentration of gelator 4b and GQDs.	72
Table 3.8 Gel formation studies of gelators 4a-4c in a range of pH between 6-9.	75
Table 3.9 Gel formation studies of gelators 4a-4c in different concentration of phosphate buffer pH 8.....	75
Table 3.10 Summarized values of storage modulus and loss modulus of GQDs/Gels in various condition.....	76
Table 3.11 The comparison of linear range and LOD between GQDs/Enz and GQDs/Enz/Gels	93

CHAPTER I

1.1 Introduction

Currently, pesticides are widely used in agricultural products. Most of them are found to contaminate fresh fruits and vegetables, which are seriously toxic to human. Therefore, the sensitive and reliable determination of organophosphate pesticide residues is of great importance. Nowadays, graphene quantum dots (GQDs) are currently attractive materials because of their low toxicity and small particle size. Apart from the interesting properties of GQDs, their performances show a benefit of photoluminescence property for using in various applications such as photoluminescence indicator for phenolic compound [1]. According to peroxidase-mimicking catalytic and photoluminescence properties, GQDs are attractive candidates for sensing purpose. This work aims to develop the pesticide sensor by GQDs and active enzyme, **GQDs/Enz** platform, for monitoring the organophosphate pesticides. In this concept, H_2O_2 generated from the active enzymatic reaction of acetylcholinesterase and choline oxidase [2] can react with GQDs, resulting in turn-off fluorescence of GQDs. Turn-on fluorescence of GQDs is observed in the presence of organophosphate. Definitely, the fluorescence changes of **GQDs/Enz** reasonably correspond to the amount of pesticide. Furthermore, we also aim to construct a highly sensitive and convenient organophosphate sensing system based on a hybrid hydrogel system integrating GQDs, enzymes and small-molecule hydrogels called **GQDs/Enz/Gels** to selectively detect organophosphate with extremely high sensitivity. In this approach, **GQDs/Enz** platform and hybrid **GQDs/Enz/Gels** material are expected to offer the promising determination of the organophosphate pesticides in real samples and offer scope for development of rapid and environmentally friendly detection without involving any sophisticated instruments or skilled personnel.

1.2 Research objective

- 1) To synthesize the graphene quantum dots/enzyme platform (**GQDs/Enz**)
- 2) To synthesize the hybrid graphene quantum dots/enzyme/hydrogels (**GQDs/Enz/Gels**) based on a new low molecular weight gelator
- 3) To develop the graphene quantum dots/enzyme platform and hybrid graphene quantum dots/enzyme/hydrogels for organophosphate pesticide determination

1.3 Literature reviews

Generally, pesticides are widely used in agricultural products to control or kill unwanted insects, weeds, rodents, fungi, bacteria, or other organisms [3]. The Pesticide Data Program (PDP) reported that pesticide residues were found in 73% of all fresh fruits and vegetables in 2005 [4]. Organophosphate pesticides (OPs) are one type of insecticide frequently used in agricultural industry, for example, dichlorvos, paraoxon and parathion, etc. The Official of Agricultural Economics of Thailand (OAE) has reported the importation of insecticide more than 21,000 tons in 2017 with a tendency of an increase every year [5]. Several organophosphate pesticides (OPs) can directly disturb the active site of acetylcholinesterase (AChE).

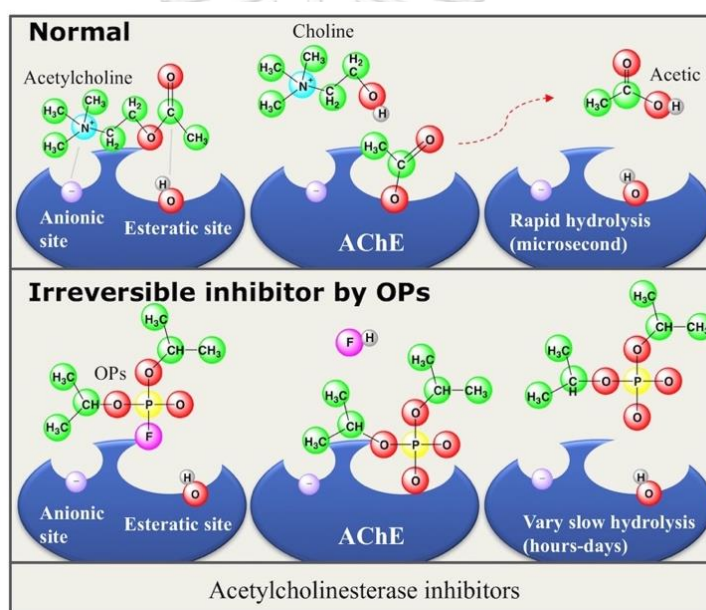
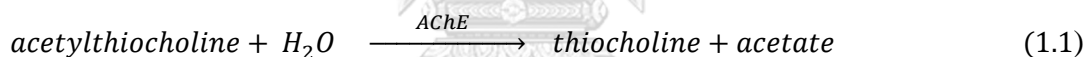


Figure 1.1 Irreversible inhibitor of acetylcholinesterase (AChE) by organophosphate pesticides (OPs) [6].

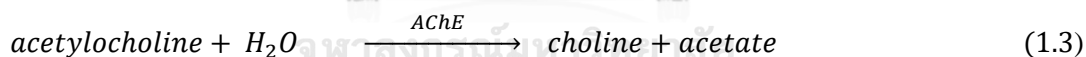
Normally, acetylcholinesterase (AChE) can hydrolyze neurotransmitter acetylcholine to choline and acetate. In the presence of organophosphate compounds, they will covalently bond with an active site of acetylcholinesterase (AChE) enzyme in nervous system by impacting on the insect's nerve impulses and subsequently to kill the insect [6, 7] as shown in Figure 1.1. This process is called irreversible inhibitor of AChE, leading to increase of the extremely high level of acetylcholine that causes organ

failure and eventual death [6]. Furthermore, OPs can contaminate in food, soil, water and environment which seriously impact to a merit of the human life and health. Hence, the UK Health and Safety Executive (HSE) has set a maximum residue limit for organophosphate pesticide such as dichlorvos at 0.01 ppm in fruits and vegetables [8], and the United States Environmental Agency (EPA) has set a maximum residue limit for dichlorvos at 10 ppm in natural water [3]. Because of high toxicity of pesticides, the sensitive and reliable determination of the organophosphate pesticide residues is of the great importance. Analytical techniques such as GC/MS and LC/MS are usually used to determine the amount of pesticide but these techniques are expensive, time consuming, and require an expertise [9].

Photoluminescence and UV-visible spectroscopies are widely used for monitoring amount of organophosphates due to the simple detection and low detection limit. Furthermore, acetylcholinesterase has been usually used for determination of organophosphate in pesticide. The determination of organophosphate pesticides can be carried out by monitoring the thiocholine, electron or H_2O_2 generated from the inhibition of AChE enzymatic mechanism as shown in equations 1.1-1.2 or 1.3-1.4.



or



In the previous reports, nanostructured films of AChE and CdTe quantum dots (QDs) was prepared to detect the pesticide, by monitoring the electron transfer of product corresponding to the amount of pesticide [10]. It can be explained that AChE can catalyze mimic acetylthiocholine neurotransmitter to generate the dithio-bis-choline, proton and electron. The electron transfer of product effected on the CdTe QDs to give the highly sensitive quenching of photoluminescent (PL) intensity of QDs as shown in Figure 1.2.

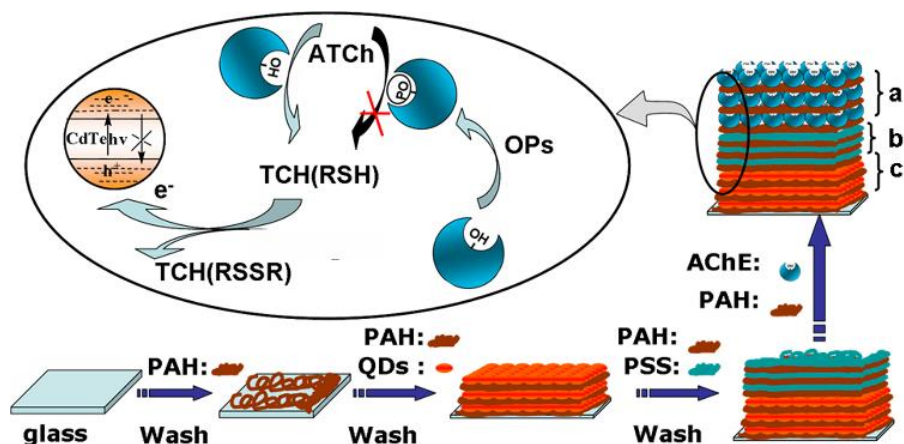


Figure 1.2 Sensing assembly of the nanostructured films of AChE and CdTe quantum dots (QDs) [10].

Liang and co-workers have employed the Fe_3O_4 magnetic nanoparticle peroxidase mimetic-based colorimetric method for the determination of organophosphates [2]. They found that Fe_3O_4 could catalyze the oxidation of 3,3',5,5'-tetramethylbenzidine (TMB) in the presence of H_2O_2 to allow a color reaction as shown in Figure 1.3A. In contrast, no color reaction occurred in the presence of organophosphate. Figure 1.3B, the decrease in absorbance intensity as the increase of methyl-paraoxon is indicative of increasing inhibition of enzyme activity. Moreover, the similar response in case of acetate and sarin pesticides was observed.

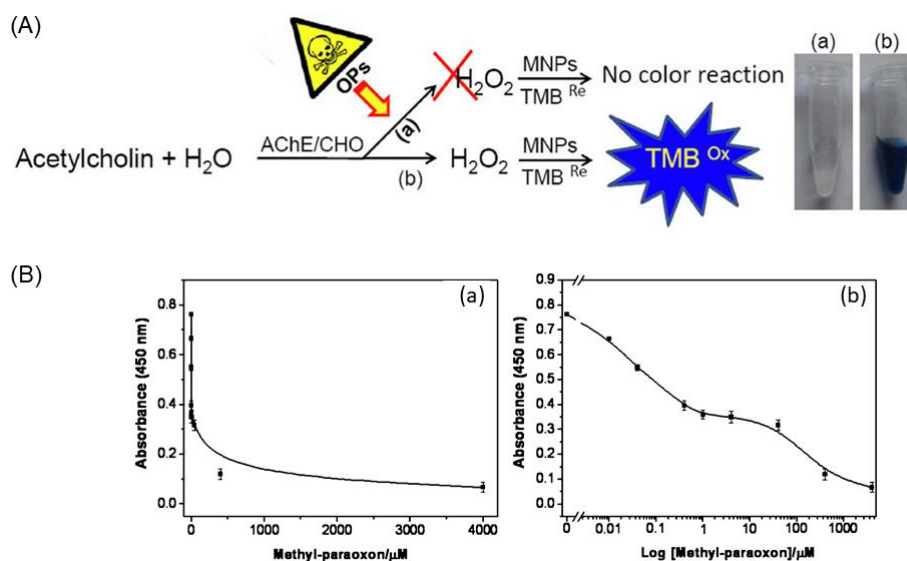


Figure 1.3 (A) Proposed mechanism and (B) dose–response curve for methyl-paraoxon detection [2].

As such previous reports, the determination of organophosphate pesticides by taking an advantage of inhibition of acetylcholinesterase enzyme were reported with its particular challenges of chemistry for examples of electrochemical method [11-14], fluorescence probe [10, 15, 16] and colorimetric detection [2, 17-19]. All of methods are sensitive to detect organophosphate pesticides, but most of the biosensor probes were prepared by a complicated method, highly toxic materials and the use of a large amount of enzymes, leading to high cost. In this work, we attempt to employ an easy and low cost method and a touch on green chemistry in synthesizing the effective photoluminescence GQDs/enzyme biosensor for organophosphate detection.

H_2O_2 is a well-known oxidizing agent that is widely used for determination not only in organophosphates but also in the important compounds in clinical diagnostics such as glucose. Recently, Song [20] revealed that the graphene oxide (GO) exhibited the peroxidase-like catalytic activity for the oxidation of TMB in the presence of H_2O_2 for determination of glucose as shown in Figure 1.4. In addition, Zheng and co-workers [21] reported better catalytic oxidation of TMB activity from the smaller sized graphene dots (GDs or GQDs). The catalytic activity was suggested via the electron transfer process. TMB fabricated on graphene can donate lone-pair electrons from amino groups to graphene and most of electron on graphene also transfers from the top of valence band to the lowest unoccupied molecular orbital (LUMO) of H_2O_2 [22].

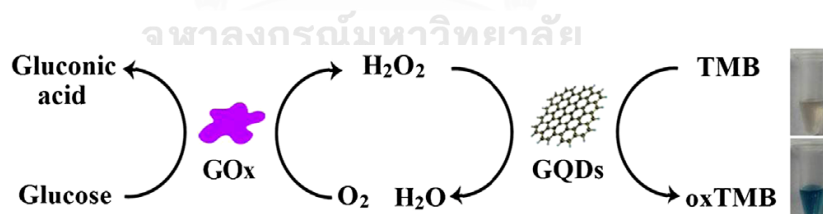


Figure 1.4 Schematic illustration of highly-efficient peroxidase-like activity of graphene dots (GDs) for the detection of H_2O_2 and glucose [21].

Graphene quantum dots (GQDs), the small size materials less than 100 nm (typical size in range of 2-20 nm) are currently outstanding [23]. They are composed of the surface state of sp^2 hybridization and the diverse functionalities at their edge such -OH and -COOH groups [24]. They are attractive materials because of their unique optical and electronic properties including the quantum confinement, tunable band gap, stable fluorescence, high surface area and edge effect. As previous report [25], they found that the green fluorescence of these GQDs not only depends on the size, but also stem from bright edge state. For large GQDs, the energy level of intrinsic state is lower than the edge state, which leads to the weak PL as shown in Figure 1.5.

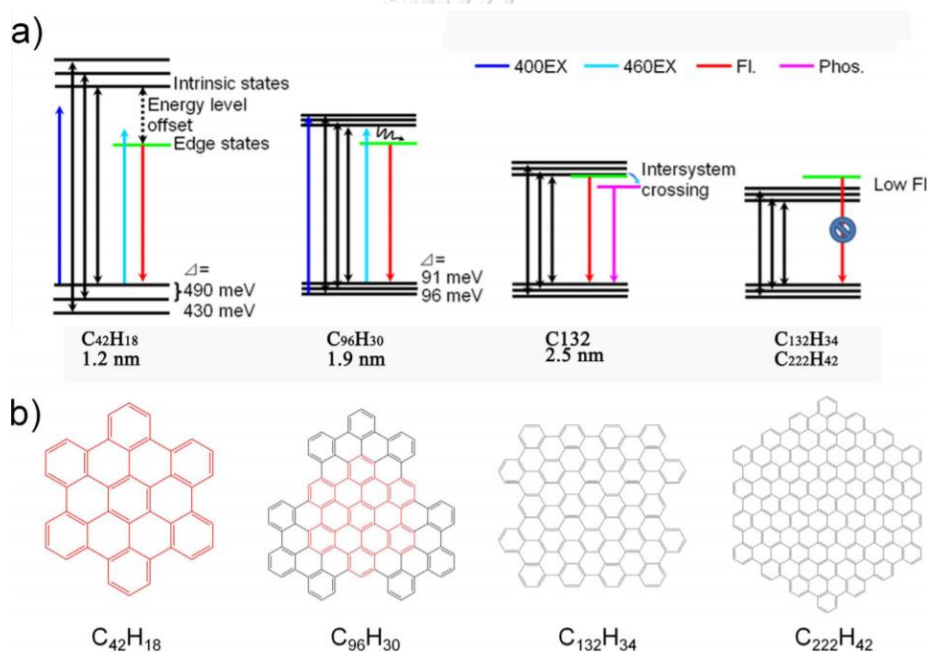


Figure 1.5 Quantum confinement effect of conjugated π -domains in GQDs (a) The suggested energy levels of C₄₂H₁₈, C₉₆H₃₀, C₁₃₂, C₁₃₂H₃₄, and C₂₂₂H₄₂. The size-dependent energy levels in these H-passivated small GQDs are in agreement with the molecule orbital calculation. The intrinsic state depends on size. The energy-level offset between the intrinsic state and the edge state determines its optical properties. (b) The structure of all materials [25].

The modified size, surfaces and edges of GQDs lead to the change of band gap and photoluminescence that adapt to a specific target [26]. The tunable size, surface and edge of GQDs can attribute to their excellent properties, including high photoluminescence (PL), high water solubility, low toxicity and biocompatibility [24, 27-29]. The GQDs in aqueous solution have been broadly used in various applications, for example, sensing of hydroquinone, glucose, biothiols, heavy metal ions [1, 21, 26,

30]. Taking on a board the ideas of using peroxidase-mimicking catalyst of graphene materials, the GQDs are attractive candidates for this sensing purpose.

GQDs were synthesized by bottom-up and top-down methods. Lately, Dong [24] reported a low cost bottom-up method by using pyrolysis of citric acid as shown in Figure 1.6. This GQDs exhibited sp^2 clusters with $-COOH$ and $-OH$ groups at the edge of graphene and also exposed a strong fluorescence emission at 460 nm. The GQDs exposed a narrow absorbance spectrum implying that they were composed of uniform sp^2 clusters in size. In addition, GQDs showed the same emission spectrum even using different wavelength excitation. The GQDs perform the excitation independence of fluorescence response. In contrast, GO showed the different emission spectrum with a broad UV-vis spectrum, implying that GO was the non-uniform sp^2 clusters.

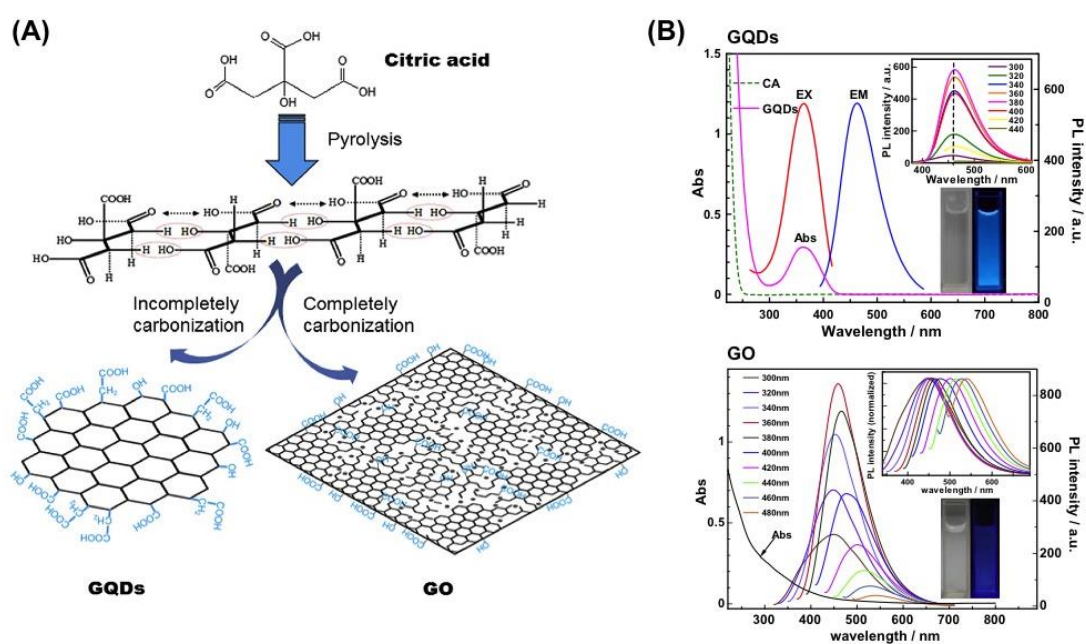


Figure 1.6 (A) Diagram for the synthesis of GQDs and GO, the black dots in the GO represent oxygen atoms and (B) UV-vis absorption of CA and the GQDs, and PL spectra of the GQDs and GO with different excitation wavelength [24].

According to the previous researches, most of researchers reported the biosensors prepared by a complicated method, highly toxic materials and the use of a large amount of enzymes to prepare biosensors, leading to high cost. In this work, we attempt to use the easy and low cost method to synthesize the effective

photoluminescence GQDs/enzyme platform by using GQDs containing $-\text{COOH}$ and $-\text{OH}$ edge for easily enzymatic interaction [31]. As anticipated, the photoluminescence quenching mechanism of GQDs should possibly be caused by the electron transfer from valence band of higher electron density of GQDs to the LUMO of H_2O_2 [20-22].

Additionally, the immobilized enzyme on the materials is very important to enhance the sensitivity and stability of the enzyme [31-33]. In 2013, Galan[32] reported the successful procedure by using polyethyleneimine (PEI) for stabilizing an enzyme glutamate dehydrogenase (GDH) in solution. They found that the cationic polymer PEI could prevent the dissociation of the enzyme, causing the better stability of GDH enzyme as shown in Figure 1.7. Moreover, Nery and co-workers [33] studied the immobilized methods such as physical adsorption, entrapment in gel, layer-by-layer, covalent linkage and encapsulation of glucose oxidase paper-based devices. They found that the layer-by-layer of alginate-PEI (storage at 4 °C) could stabilize enzymatic activity up to 60% after 20 weeks.

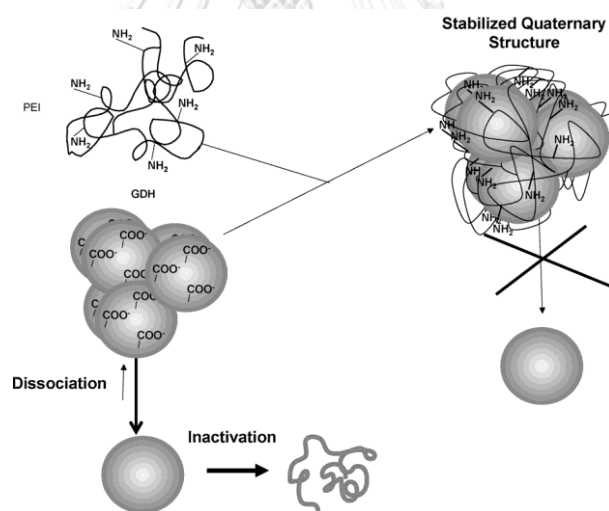


Figure 1.7 Schematic representation of the proposed mechanism of stabilization of GDH by using PEI [32].

However, the experiment in aqueous phase still exposed some typical drawback, for instance, not easy to be used for OPs sensing in field work. Moreover, a lot of π -system in GQDs might lead to the aggregation under increasing temperature and long-term storage. To overcome this weak point, the immobilization of GQDs and enzyme in soft materials is of a great interest.

Soft materials such as supramolecular hydrogels were attractive and recently achieved in numerous utilization, including controlled drug release [34, 35], stabilized and immobilized enzyme [36-40], pharmaceutical polymorph control [41-43], anion-cation or metal ions sensing [44-48], and biosensor [49-51]. The supramolecular hydrogels are flexible materials that compose of the self-assembly of small molecules (low molecular weight gelators, LMWG) and large amount of water (typically higher than 99%) using non-covalent interaction, resulting in the formation of hydrophobic fibrillar network and large hydrophilic cavities of water [38, 52-54]. It means that they address the solid phase on analytical time scale and also display the fluid behavior [54, 55]. Additionally, hydrogels have been extensively studied in the context of simply encapsulated and stabilized enzymes into hydrogels without a chemical crosslinking (chemical modification technique) [37, 38].

Peptide-based hydrogelators have been developed by Hamachi group. The BYmoc-peptides were synthesized to obtain the water gelation by varying Y including of BAmoc boronoarylmethoxycarbonyl, BPmoc: boronophenylmethoxycarbonyl, BNmoc: borononaphthylmethoxycarbonyl and FFX: F, phenylalanine; X: OH, isoleucine (I), leucine (L) or phenylalanine (F) as illustrated in Figure 1.8A. The results showed that the BPmoc-F₃ based on phenylalanine demonstrated a good gel formation in 100 mM MES buffer solution (pH 7.0). Interestingly, this hydrogel can exhibit a H₂O₂-responsive nanofiber by the degradation of a matrix that consists H₂O₂ as shown in Figure 1.8B. Moreover, the peptide-based hydrogelators have been applied to Logic-gate response by encapsulation of multiple enzymes (see Figure 1.8C). Then information in the form of molecular input is achieved by the enzyme and converted into H₂O₂, which eventually gives rise to a gel-sol change as output, that can be further applied in medical diagnosis and treatment such as cancer and diabetes. However, the sol-gel change output is difficult to identify.

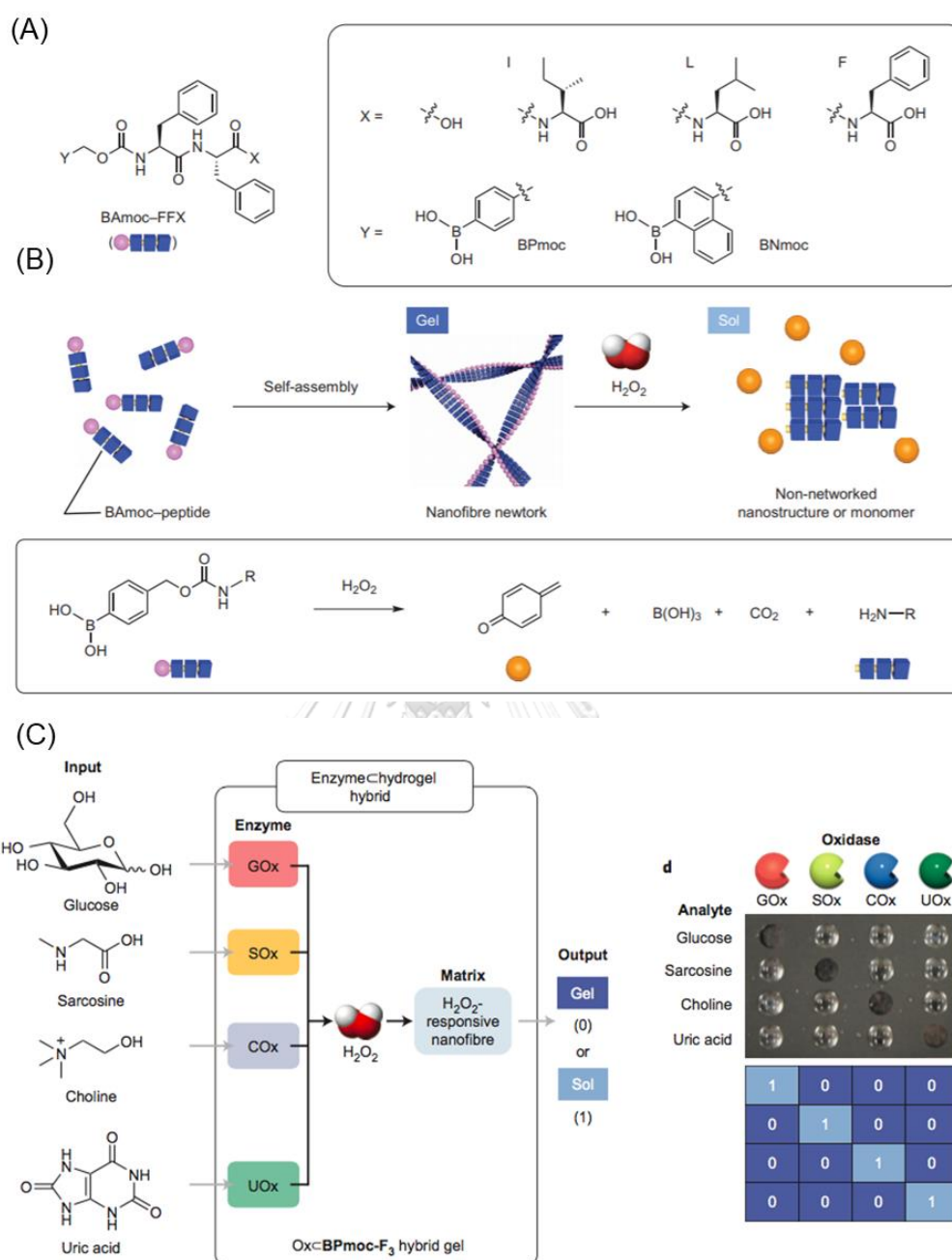


Figure 1.8 (A) BAmoc-peptides. (B) Schematic representation showing the self-assembly of BPmoc-peptides to form a nanofiber network (gel) and H_2O_2 -triggered gel degradation. (C) Schematic representation of Ox-BPmoc-F₃ hybrid gels before and after the response to analytes [49].

In 2015, Cayuela and Steed group [56] have reported the sensitive and switchable supramolecular gels for heavy metal sensing. They found that gelator **1a** (see Figure 1.9) based urea and ionisable salicylic acid system have established the key of gel formation in water depending on the carboxyl-terminal group of salicylic acids and the non-steric hindrance around the urea carbonyl group of gelator. Interestingly, this gelator containing 2wt% (about 10 mM) of ionic liquid (BMIMBF₄) can rather improve the fluorescence properties of carbon dot *via* an aggregated prevention in aqueous solution. Additionally, the carbon dot nanogel materials effectively exhibited the selectivity for heavy metal detection especially Ag⁺ ion. However, the ionic liquid BMIMBF₄ can induce a significant cytotoxic effect to CCO cell line (from the ovaries of Channel catfish) and HeLa cells (from the human cervical carcinoma) with EC₅₀ at 5.01±0.32 and 4.42±0.18 mM, respectively [57], (EC₅₀ is The half maximal effective concentration, defined as the concentration of ionic liquid that resulted in 50 % growth inhibition). Hence, the BMIMBF₄ might not be suitable for preparation of biosensor regarding to the enzymatic reaction.

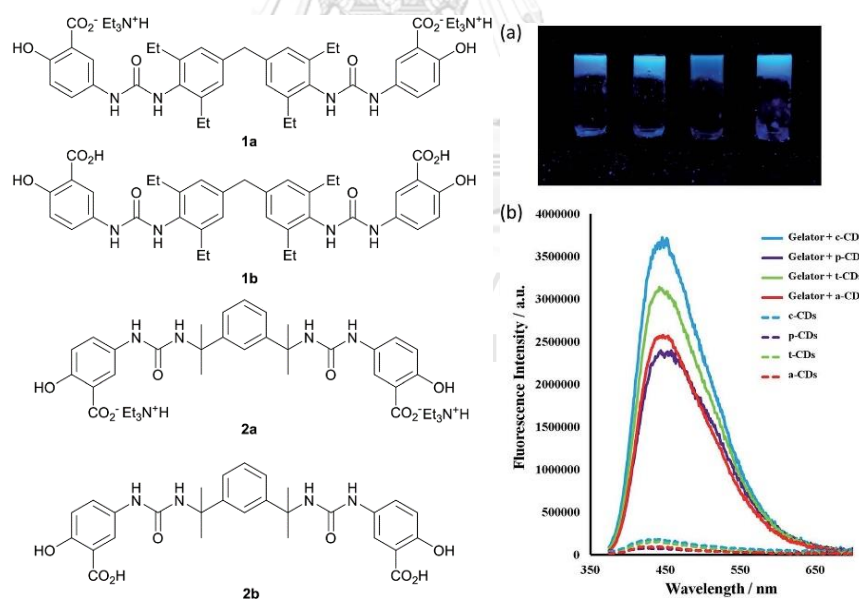


Figure 1.9 Schematic representation of triethylammonium salt gelators (1a-2b), carbon-dot gel and their photoluminescence properties [56].

Hence, the immobilization of the amphiphilic GQDs and enzyme molecules into the biocompatible hydrogels is apprehensively challenged for amplifying a signal and maintaining the enzyme activity in biological applications such as, clinical diagnoses and organophosphate pesticides sensing.

1.4 Scope of this research

In this work, we attempt to design the easy-to-use and low cost sensors by using graphene quantum dots (GQDs) and enzymatic reactions for determination of the organophosphate pesticides (OPs). A first platform consisting of GQDs and active enzyme, **GQDs/Enz** platform is simply fabricated in aqueous solution [58], while on going platform by **GQDs/Enz/Gels** based on bis-(urea)-amino-gelator, is continuously developed in well-defined model of hydrogels for improving the enzyme stability, sensitivity and especially easy-to-use for detection of organophosphate pesticides.

We expect that these GQDs enable indirectly detection the organophosphates by monitoring the fluorescent response of reaction between GQDs and H_2O_2 generated from AChE and ChOx enzyme reaction. These approaches would give high impact for its application as fluorescence sensor for food and environment.

1.5 Benefits of this research

Obtain an inexpensive and simple biosensor for specific detection of organophosphate pesticides in food, water and environment.

CHAPTER II

Graphene quantum dots for organophosphate sensing

2.1 Introduction

This work explored the detection of organophosphate pesticide by using GQDs as a direct photoluminescence probe via enzymatic reaction. We aim to develop the pesticide sensor by GQDs and active enzyme (acetylcholinesterase; AChE and choline oxidase; ChOx) with bovine serum albumin (BSA), GQDs/Enz platform, for monitoring the organophosphate pesticides. In this concept as shown in Figure 2.1, H_2O_2 , generated from the active enzymatic reaction of acetylcholinesterase and choline oxidase, [2] can react with GQDs, resulting in a “turn-off” fluorescence of GQDs. A “turn-on” fluorescence of GQDs has been recovered in the presence of organophosphate in the system. Definitely, fluorescence changes of GQDs/Enz biosensor reasonably correspond to the amount of pesticide. In this approach, GQDs/Enz biosensor is expected to highlight the promising selective determination of the organophosphate pesticides and an attractive material for easy checking of organophosphate pesticides in water with easy-to-prepare and low toxic to environment.

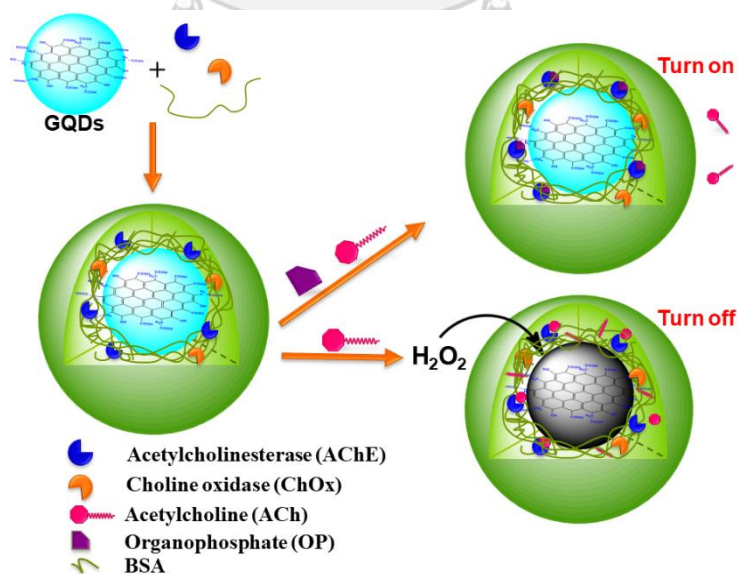


Figure 2.1 Proposed GQDs/Enz system to determine the organophosphate pesticide.

2.2 Analytical measurement

Transmission electron microscopy (TEM) was performed on a JEOL JEM 2010 with a field emission gun operated at 200 kV. The TEM micrographs were used to determine size of the deposited particles by counting approximately 200 particles (ImageJ software, Scion Corporation). IR spectrophotometric measurement of dried particle samples was performed on Thermo, Nicolet 6700 FT-IR. Absorption spectra were measured by a Varian Cary 50 UV-Vis spectrophotometer. Fluorescence spectra were performed on a Varian spectrofluorometer equipped and PTI QuantaMasterTM spectrofluorometer with a personal computer data processing unit. The light source is Cary Eclipse a pulsed xenon lamp and a detector is a photomultiplier tube. Ultra high performance liquid chromatography coupled with mass spectrometry (UHPLC-MS) used in this experiment was performed on Agilent Technologies Model 1290 (CA, USA) including vacuum degasses, binary pump, agilent jet weaver, autosampler and vacuum oven and Agilent Technologies Model 6490 MS (CA, USA) including a triple quadrupole mass analyzer, electrospray ionization (ESI) interface and MassHunter software processing. A UHPCL separation was performed on an Eclipse XDB-C18 with 4.6 mm × 50 mm, 1.8 μm from Agilent (USA).



2.3 Experimental

2.3.1 Materials

Citric acid monohydrate ($C_6H_8O_7 \cdot H_2O$) was provided from Merck. Acetylcholinesterase (AChE, 217 units/mg) from *Electrophorus electricus* (electric eel), choline oxidase (ChOx, 14 units/mg) from *Alcaligenes* sp. and bovine serum albumin (BSA) were obtained from Sigma-aldrich. Organophosphate pesticides including dichlorvos, methyl-paraoxon, malathion and parathion were purchased from Sigma-aldrich. Tris-HCl was obtained from Carlo Erba. Milli-Q (MQ) was performed by ultra pure water system, Merck and used throughout the experiment.

2.3.2 Preparation of the graphene quantum dots (GQDs)

Graphene quantum dots were prepared following Dong's method[24] as illustrated in Figure 2.2. The starting citric acid (2 g, 0.01 mol) in 5 mL beaker was heated to 200 °C for 30 min and obtained orange solution. Then the prepared GQDs liquid was added dropwise to 100 mL of 10 mg/mL NaOH solution under vigorous stirring. After that, the solution was adjusted to pH 8.0 by 1 M HCl solution, then purified by dialysis 2,000 Da 15 h in 5 mM of Tris buffer pH 8.0 and stored at 5 °C for using in sensor application within 2 months. The GQDs were solidified by freeze-drying, and then they were weighed and characterized by UV-visible, fluorescent spectrofluorometer, ATR-FTIR spectroscopy and TEM techniques.

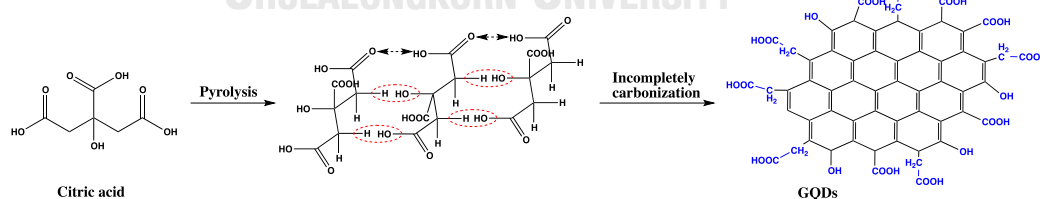


Figure 2.2 Synthetic pathway of graphene quantum dots (GQDs) [24].

2.3.3 Preparation of GQDs/AChE/ChOx (GQDs/Enz) biosensors

The stock solutions of acetylcholinesterase (AChE) and choline oxidase (ChOx) at concentration of 100 and 12.5 U/mL, respectively, were prepared in Tris-BSA (1% of BSA in 50 mM pH 8 of Tris buffer). The 3.6 mg or 493.2 unit (U) of AChE was

dissolved in 4.93 mL of Milli-Q water. The 3.6 mg or 50.4 unit (U) of ChOx was dissolved in 4.03 L of Milli-Q water. Then both enzymes were divided to portion of 1 mL tube separately with 0.1 mL per tube and stored at -20 °C for using within a year. The stock solution of both enzymes was diluted 10 times by 0.9 mL of Tris-BSA and kept in 5 °C for using in sensor experiment (the diluted enzymes need to use within a day).

In 5 mL vial, 0.1 mL of GQDs solution (1×10^{-2} g/mL) was added to 0.4 mL of 50 mM of Tris buffer solution pH 8. After that, 0.2 mL of AChE (10 U/mL) and 0.2 mL of ChOx (1.25 U/mL) were added to the solution mixture and stirred for 5 min prior to incubation at 5 °C for 24 h to obtain **GQDs/Enz** biosensor.

2.3.4 UV-visible and photoluminescence (PL) studies of GQDs

Typically, a stock solution of GQDs (1×10^{-2} mg/mL) was collected from refrigerator and left to room temperature before using. Stock solution of Tris buffer solution at concentration of 0.05 M was prepared by dissolving 3.03 g of Tris in Milli-Q water in 500 mL beaker. Then the pH was adjusted to 8 by 1M of HCl. The mixture was transferred to a volumetric flask and adjusted to 500 mL by Milli-Q water and stored in 5 °C for using within 6 months.

The 0.1 mL of stock solution of GQDs was pipetted into 5 mL vial. Then 0.8 mL of 0.05 M of Tris buffer solution pH 8 and 1.1 mL of Milli-Q water were added to GQDs solution. The sample was stirred for 2 min and measured by UV-visible and fluorescence spectrometry upon parameter as following condition.

<i>Parameter in fluorescent spectroscopy</i>	
<i>Excitation (nm)</i>	<i>300-440 (362 was selected)</i>
<i>Excitation Slit</i>	<i>5</i>
<i>Emission Slit</i>	<i>5</i>
<i>PMT</i>	<i>700</i>
<i>Scan rate (nm/min)</i>	<i>600</i>
<i>Start (nm)</i>	<i>310-450 (372 was selected)</i>
<i>End (nm)</i>	<i>700</i>
<i>Emission (nm)</i>	<i>467</i>

2.3.5 Impact of H₂O₂ toward the GQDs

The GQDs was reasonably utilized for H₂O₂-responsive study by following the photoluminescence intensity after adding H₂O₂. Initially, stock solution of 2 M of H₂O₂ was prepared in a 5 mL volumetric flask and then adjusted to 5 mL by Milli-Q water. The 0.10 mL of 1x10⁻² mg/mL of GQDs was pipetted into 5 mL vial followed by 0.8 mL of 0.05 M of Tris buffer solution pH 8 and 1 mL of Milli-Q water.

To study of time independent fluorescent change, the 0.1 mL of stock solution of H₂O₂ was added to the prepared GQDs and stirred for 1.5 min under ambient condition. The sample was transferred to a cuvette. At 2 min, the photoluminescence (PL) intensity was measured (λ_{ex} 362 nm) assigned to “0” min, and then PL was recorded every 5 min to 60 min.

To study the concentration of H₂O₂, the various volumes of stock solution of H₂O₂ were added to the prepared GQDs. Then, the samples were adjusted to 2 mL by Milli-Q water to obtain various concentration of H₂O₂ from 0 to 0.2 M (see Table 2.1). The samples were stirred under ambient condition and measured the PL intensity at 30 min ($\lambda_{\text{ex/em}}$ 362/467 nm). The experiment was repeated 3 times.

Table 2.1 Various conditions in H₂O₂-responsive study of GQDs.

Final [H ₂ O ₂] (M)	Volume of stock solution (mL)				Time (min)
	GQDs	Tris buffer	Milli-Q	H ₂ O ₂	
0.100	0.100	0.800	1.000	0.100 (2 M)	0, 5, 10, 15, ... 60
0.000	0.100	0.800	1.100	0.000	30
0.001	0.100	0.800	1.096	0.004 (0.5 M)	30
0.005	0.100	0.800	1.080	0.020 (0.5 M)	30
0.010	0.100	0.800	1.090	0.010 (2 M)	30
0.025	0.100	0.800	1.075	0.025 (2 M)	30
0.050	0.100	0.800	1.050	0.050 (2 M)	30
0.075	0.100	0.800	1.025	0.075 (2 M)	30
0.100	0.100	0.800	1.000	0.100 (2 M)	30
0.015	0.100	0.800	0.950	0.150 (2 M)	30
0.200	0.100	0.800	0.900	0.200 (2 M)	30

2.3.6 Responsibility of H₂O₂-generated *in situ* by GQDs/Enz

The enzyme activity of GQDs/Enz were carried out by addition of acetylcholine (ACh). A stock solution of acetylcholine of 10 mg/mL was prepared in volumetric flask 100 mL and stored at 5 °C for using all experiment.

The 0.9 mL of Milli-Q water were added to the solution of 0.9 mL of GQDs/Enz biosensor, and followed by 0.2 mL of acetylcholine stock solution. The sample was stirred for 1.5 min under ambient condition and transferred to a cuvette. At 2 min, the photoluminescence (PL) intensity was measured (λ_{ex} 362 nm) assigned to “0” min. Then, PL was recorded every 5 min to 60 min.

Parameters such as pH and concentration of enzyme were carried out to improve the signal of sensor or signal amplification. In pH studies, the GQDs/Enz samples were performed in various pH from 5 to 9 by using acetate (pH 5), phosphate (pH 6-7) and Tris (pH 8-9) buffer solution. In concentration studies, the GQDs/Enz was prepared under various concentration of enzymes in Tris buffer pH 8 as shown in Table 2.2. Then, their enzymatic activity was studied and repeated 3 times.

Table 2.2 Parameters used in signal amplification of GQDs/Enz.

Exp.	Parameter	Studied range	unit
1.	Incubation-time	0-60	min
2.	Concentration of AChE	0.005-1	U/mL
3.	Concentration of ChOx	0.125-0.25	U/mL
4.	pH	5-9	-

2.3.7 The detection of organophosphate by GQDs/Enz

The stock solutions of organophosphate pesticides including, dichlorvos (mol. wt. = 220.98 gmol⁻¹), malathion (mol. wt. = 330.36 gmol⁻¹), methyl-paraoxon (mol. wt. = 247.14 gmol⁻¹) and parathion (mol. wt. = 291.26 gmol⁻¹) were prepared at concentrations of 1000 ppm (they can be converted to molar by using mol. wt.). In 10 mL volumetric flask, the 10 mg of each organophosphate pesticide was carefully dissolved by 10 mL of 50 % EtOH in water under fume hood and well protecting prior to kept at -20 °C for using within 6 months. At the experiment time, the

organophosphate pesticides were diluted by water to obtain various concentration of stock organophosphate in 5% EtOH in water for experiment in each time.

Each portion of the **GQDs/Enz** biosensors was achieved in the same stock solution for using in one experiment as followed condition. Under 20 condition (60 samples), 12 mL of AChE (10 U/mL) and 12 mL of ChOx (1.25 U/mL) in Tris-BSA were firstly added to 6 mL of GQDs stock solution (1×10^{-2} M) and then the solution was added by 24 mL of Tris buffer solution (50 mM pH 8). The solution was stirred for 5 min prior to incubation at 5 °C for 24 h. Stocks of graphene quantum dots immobilized enzymes (**GQDs/Enz**) were divided into 60 vials with 0.9 mL per vial and kept at 5 °C prior to use. All sample components were shown in Table 2.3. Then the solution of 0.7 mL of MQ-water and 0.2 mL of different concentration of dichlorvos pesticide was added to the biosensor solution and incubated in a water bath at 25 °C for 15 min. The mixture solution was added by 0.2 mL acetylcholine (10 mg/mL) and incubated by stirring for 30 min.

The PL signals were monitored by fluorescence spectroscopy and the measurements were repeated 3 times. The percentage of enzyme inhibition (I%) was plotted against the concentration of organophosphate pesticide to construct the calibration curve and subsequently afford the limit of detection for sensing application.

Other organophosphate pesticides including, parathion, malathion, and methyl-paraoxon at the concentration of 1 and 10 ppm were further examined for the inhibition efficiency (I%) towards AChE. Amounts of all components were used in fluorescent spectrophotometry studies as shown in Table 2.4. In addition, the percentage of enzyme inhibition (I%) by dichlorvos (as mentioned above) and methyl-paraoxon (1×10^{-5} to 20 ppm) reliably provide the limit of detection (LOD).

Table 2.3 Amount of components used in dichlorvos detection studies.

Final [OPs] (ppm)	Stock sol ⁿ of OPs (ppm)	Volume of stock solution (mL)						V _{total} (mL)
		GQDs	Tris	Enz	Milli-Q	OPs	ACh	
0 (control)	0	0.1	0.4	0.4	1.1	-	-	2
0 (control)	0	0.1	0.4	0.4	0.9	-	0.2	2
0	0	0.1	0.4	0.4	0.7	0.2	0.2	2
0.025	0.25	0.1	0.4	0.4	0.7	0.2	0.2	2
0.05	0.5	0.1	0.4	0.4	0.7	0.2	0.2	2
0.1	1	0.1	0.4	0.4	0.7	0.2	0.2	2
0.15	1.5	0.1	0.4	0.4	0.7	0.2	0.2	2
0.2	2	0.1	0.4	0.4	0.7	0.2	0.2	2
0.4	4	0.1	0.4	0.4	0.7	0.2	0.2	2
0.6	6	0.1	0.4	0.4	0.7	0.2	0.2	2
0.8	8	0.1	0.4	0.4	0.7	0.2	0.2	2
1	10	0.1	0.4	0.4	0.7	0.2	0.2	2
2	20	0.1	0.4	0.4	0.7	0.2	0.2	2
4	40	0.1	0.4	0.4	0.7	0.2	0.2	2
6	60	0.1	0.4	0.4	0.7	0.2	0.2	2
8	80	0.1	0.4	0.4	0.7	0.2	0.2	2
10	100	0.1	0.4	0.4	0.7	0.2	0.2	2
20	200	0.1	0.4	0.4	0.7	0.2	0.2	2
50	500	0.1	0.4	0.4	0.7	0.2	0.2	2
100	1000	0.1	0.4	0.4	0.7	0.2	0.2	2
V _{total} (mL)		2	8	8	14.6	3.6	3.8	40
V _{total} (mL) for 3 times		6	24	24	43.8	10.8	11.4	120

Table 2.4 Amount of components used in various type of OPs detection.

Final [OPs] (ppm)	Stock sol ⁿ (ppm)	Volume of stock solution (mL)					
		GQDs	Tris	Enz	Milli-Q	OPs	ACh
0 (control)	0	0.1	0.4	0.4	1.1	-	-
0 (control)	0	0.1	0.4	0.4	0.9	-	0.2
1 of dichlorvos	10	0.1	0.4	0.4	0.7	0.2	0.2
1 of malathion	10	0.1	0.4	0.4	0.7	0.2	0.2
1 of methyl-paraoxon	10	0.1	0.4	0.4	0.7	0.2	0.2
1 of parathion	10	0.1	0.4	0.4	0.7	0.2	0.2
10 of dichlorvos	100	0.1	0.4	0.4	0.7	0.2	0.2
10 of malathion	100	0.1	0.4	0.4	0.7	0.2	0.2
10 of methyl-paraoxon	100	0.1	0.4	0.4	0.7	0.2	0.2
10 of parathion	100	0.1	0.4	0.4	0.7	0.2	0.2

2.3.8 Effect of interfering ions

The stock solutions of metal ions including Cd^{2+} ($\text{Cd}(\text{NO}_3)_2 \cdot 4\text{H}_2\text{O}$), Co^{2+} ($\text{Co}(\text{NO}_3)_2 \cdot 6\text{H}_2\text{O}$), Cu^{2+} ($\text{CuSO}_4 \cdot 5\text{H}_2\text{O}$), Ni^{2+} ($\text{Ni}(\text{NO}_3)_2 \cdot 6\text{H}_2\text{O}$), Hg^{2+} (HgCl_2), Pb^{2+} ($\text{Pb}(\text{NO}_3)_2$), Na^+ (NaCl), NH_4^+ (NH_4Cl), Na^+ (NaNO_3), NH_4^+ ($(\text{NH}_4)_3\text{PO}_4$) and Mg^{2+} ($\text{Mg}(\text{NO}_3)_2$) were prepared in Milli-Q water at the concentration of 1×10^{-3} M.

The directly interfering ions toward GQDs were studied as follows. Each metal solution (0.02 mL) was added to 1.98 mL of 5×10^{-4} mg/mL of GQDs in Tris buffer solution pH 8. The mixture was stirred for 30 min under ambient condition. The PL intensity was studied via fluorescent spectroscopy (λ_{ex} at 362 nm and λ_{em} at 467 nm).

The interfering ions toward OPs detection was studied as follows. The portion of **GQDs/Enz** biosensor was prepared as the same method as OP detection part. In each 5 mL vial, the 0.02 mL of stock solution of each metal ions was added to 0.9 mL of **GQDs/Enz** followed by 0.68 mL of MQ-water. Then 0.2 mL of dichlorvos pesticide (1×10^{-5} M) was added to the mixture solution and incubated for 15 min, after that the mixture was added by 0.2 mL acetylcholine (10 mg/mL) and incubated at 25 °C with stirring for 30 min. The PL intensity was studied using fluorescent spectroscopy (λ_{ex} at 362 nm and λ_{em} at 467 nm).

2.3.9 Organophosphate detection in real samples

The organophosphate detection in real samples was carried out as following: (1) tap water sample, field water samples from Roi Et province and Chulalongkorn University which were collected and kept at room temperature for a day. Then, the top layer of water samples was filtrated through a 0.2 μm Millipore filter; (2) the water samples (instead of MQ-water) and the spiked organophosphate pesticide with difference concentration were injected in the **GQD/Enz** biosensor and then the mixture was incubated at 25 °C for 15 min; (3) the **GQDs/Enz** biosensor was added by acetylcholine and then incubated at 25 °C for 30 min; (4) the PL spectrum was recorded and the calibration curve of PL intensity against concentration of organophosphate pesticide was constructed. The amount organophosphate pesticide in the real sample water was determined from this calibration curve.

A UHPLC-MS method was used to compare the detection affinity of our biosensor. Real samples were prepared according to the procedures from literature [59, 60]. The calibration curve was constructed by standard addition of dichlorvos. The UHPLC-MS was completely run within 6 min under the flow rate of 0.4 mL/min, and injection volume of 2 μ L. The mobile phases A and B were 0.1% formic acid and acetonitrile, respectively. As the first 0.2 min, 75% mobile phase A was set with an isocratic run until 3.8 min. The electrospray MRM scan mode with positive ion was used to determine the dichlorvos with the transition of the precursor ion of 220.95 to the product ion of 108.9.



2.4 Results and discussions

As well-known, H_2O_2 is widely utilized for many clinical diagnostics because it is an important by-product in many bio-reactions for example the catalytic reaction of glucose and choline by glucose oxidase and choline oxidase, respectively[49].

In previous research, carbon material species such as graphene oxide (GO) and graphene dots (GDs) were explored as the peroxide-responsive materials, which exhibited the catalytic properties toward the oxidation of 3,3,5,5,-tetramethylbenzidine (TMB) by reacting with H_2O_2 for glucose detection [20, 21].

The graphene quantum dots with small size (typically in size 2-10 nm) are of great interest in materials because they illustrated a high photoluminescent (PL) intensity, low toxicity, easy and cheap preparation. In this work, the GQDs were synthesized followed by Dong's method. We expected that the GQDs could demonstrate a good capability to catalyze H_2O_2 and show a different PL property. In addition, the responsive- H_2O_2 of GQDs with enzyme platform (**GQDs/Enz**) were performed in Tris-BSA buffer solution pH 8. With an advantage of enzyme inhibition, the **GQDs/Enz** might be realized for further organophosphate pesticide sensors.

2.4.1 Structural morphology characterizations of GQDs and GQDs/Enz

The TEM images were used to study the structural morphologies of graphene quantum dots (GQDs) as shown in Figure 2.3A and B, respectively. The images of GQDs showed their spherical shape with average particle size of about 5 nm, which were calculated from 200 particles in TEM images by the ImageJ software.

After incubation of GQDs with bi-enzyme, acetylcholine (AChE) and choline oxidase (ChOx) in Tris-BSA pH 8.0. The BSA is protein that used to stabilize some restriction enzymes and to prevent adhesion of the enzyme to reaction tubes, pipet tips, and other vessels. The TEM image of **GQDs/Enz** biosensor showed core and light shell as illustrated in Figure 2.3C. Noticeably that, image showed an insignificant increment of average particle size of core shell to 6 nm, which is similar size to the normal GQDs. Approximately particle size of one **GQDs/Enz** particle with the entrapment layer was about 20-30 nm (yellow arrow). Regarding to the remark increase of particle size of this platform, it is possibly due to a large globular protein of BSA and enzyme coated on GQDs.

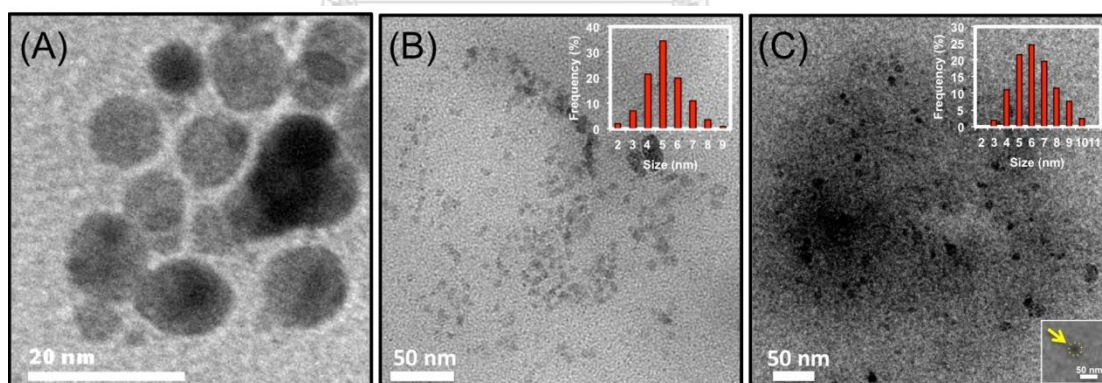


Figure 2.3 The magnification TEM image of GQDs (A), TEM images of GQDs (B) **GQDs/Enz** biosensor (C) Inset of (B) and (C) are the frequency (%) of size of GQDs and **GQDs/Enz** biosensor by TEM image, respectively.

2.4.2 Infrared spectroscopy studies

Attenuated total reflectance Fourier transform infrared spectroscopy (ATR-FTIR) was employed to characterize the functional groups and formation of biosensor platform. Firstly, IR spectra of citric acid anhydrous (starting material) and prepared GQDs were compared in Figure 2.4. The comparison of spectra presented significant changes in the position and the peak shape. The broad transmission bands of GQDs were observed at 3000-3500 cm^{-1} ($\nu_{\text{O-H}}$) and sharp transmission bands at 1561 cm^{-1} (ν_{asCOO^-}), 1379 cm^{-1} (ν_{sCOO^-}) and 1057 cm^{-1} ($\nu_{\text{C-OH}}$) belonging to the characteristic peak of -COOH and -OH group. It was implied that the GQDs are surrounded by -COOH and -OH group.

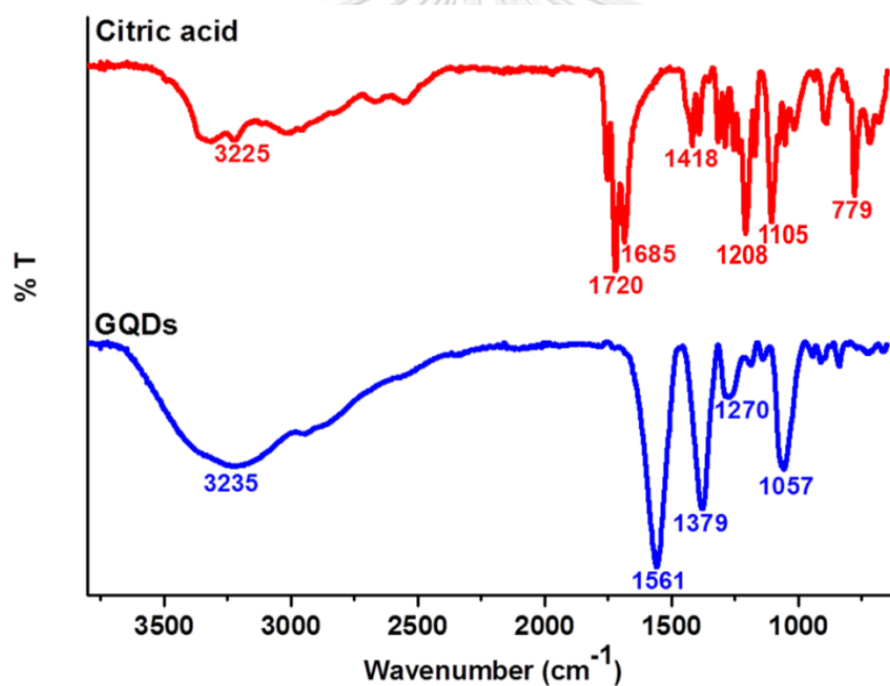


Figure 2.4 ATR-FTIR spectra of citric acid and GQDs.

The ATR-FTIR spectra of GQDs, bi-enzyme (AChE/ChOx), bovine serum albumin (BSA) and **GQDs/Enz** (GQDs/AChE/ChOx) were showed in Figure 2.5. The transmission peaks of **GQDs/Enz** biosensor (in Tris-BSA) were slightly shifted from the starting materials. However, the appearance of the additional peak at 1627 cm^{-1} belonging to the characteristic amide peak [61] of bi-enzyme is indicative of the incorporated **GQDs/Enz** biosensor. Furthermore, the correlated FT-IR spectrum of **GQDs/Enz** biosensor in Tris-BSA showed a characteristic amide peak of enzyme and BSA at 1643 cm^{-1} [61, 62].

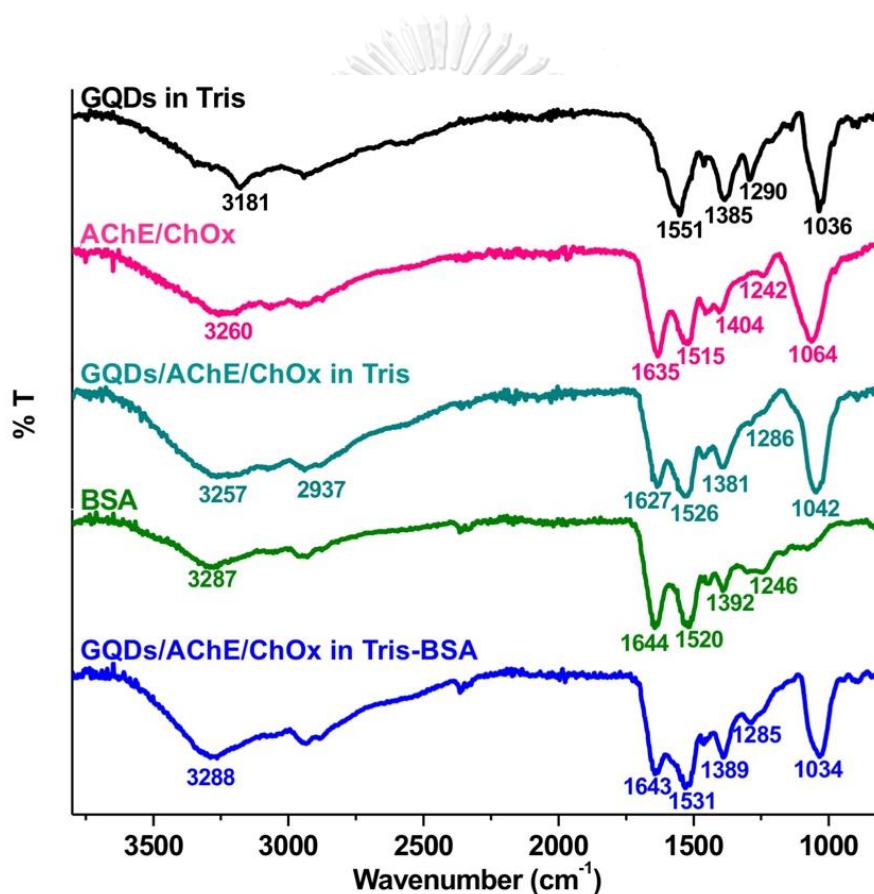


Figure 2.5 ATR-FTIR spectra of citric acid, GQDs, GQDs (in Tris), bi-enzyme, BSA and **GQDs/Enz** (in Tris and Tris-BSA).

Generally, the enzyme and BSA are proteins which contain the rich amino and carboxyl groups. Possibly, these results have been well explained that the GQDs were entrapped with the enzyme and BSA by the hydrogen bonding and electrostatic interactions of carboxylic groups at the edge of GQDs with amino and carboxyl groups of AChE, ChOx and BSA [14, 61-63]. As anticipated, we proposed an incorporation of GQDs and enzyme in the BSA layer as shown in Figure 2.6.

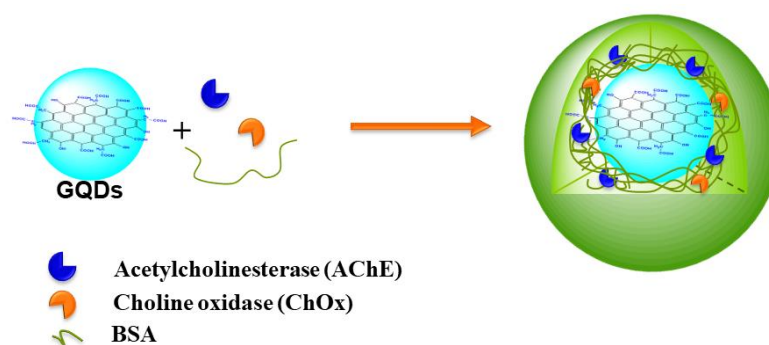


Figure 2.6 The proposed formation of GQDs/Enz with BSA platform.



2.4.3 UV-visible and photoluminescence (PL) studies of GQDs

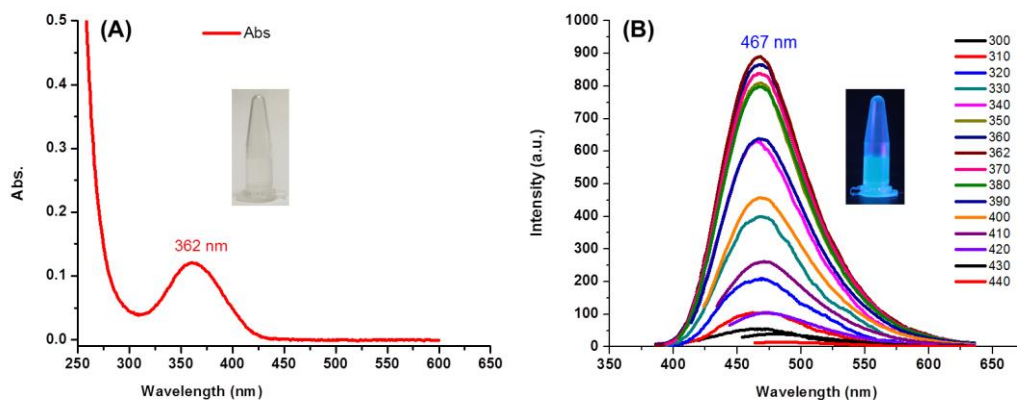


Figure 2.7 (A) UV-Vis absorption spectra of the GQDs, inset (A) is the GQDs solution observed under visible light. (B) Photoluminescent spectra of the GQDs with different excitation wavelength (λ_{ex} 300 to 440 nm), inset (B) is the photoluminescence brightness of GQDs under UV light.

UV-Vis spectrum of GQDs was illustrated in Figure 2.7A demonstrating an absorption band at 362 nm. Additionally, the GQDs showed one strong emission band at 467 nm under various excitation wavelength (λ_{ex}) from 300 to 440 nm (Figure 2.7B) and showed blue luminescence under UV light with λ_{ex} 365 nm (Figure 2.7A inset). The excitation-independent photoluminescence of GQDs may attribute to the uniform size and the surface state of sp^2 hybridization for GQDs[24]. Apart from a well-defined properties, the excitation-dependent carbon dot based luminescent nanomaterials performed a particular properties of the different size and emission band of each sp^2 cluster [64, 65].

From the TEM, ATR-FTIR, UV-Vis and fluorescent results, the results clearly indicated that the GQDs showed the uniform size with abundant sp^2 structure, which was surrounded by hydroxyl and carboxyl groups.

2.4.4 Role of GQDs toward peroxidase-catalytic reaction of H₂O₂

As a well-known aspect, the carbon material species such as graphene oxide (GO) and graphene dots (GDs) showed the tremendous properties as the peroxidase-like catalytic materials[20, 21]. To verify the peroxide-responsive GQDs in this work, the photoluminescent property of GQDs was investigated upon an increment of reaction-time and concentration of H₂O₂.

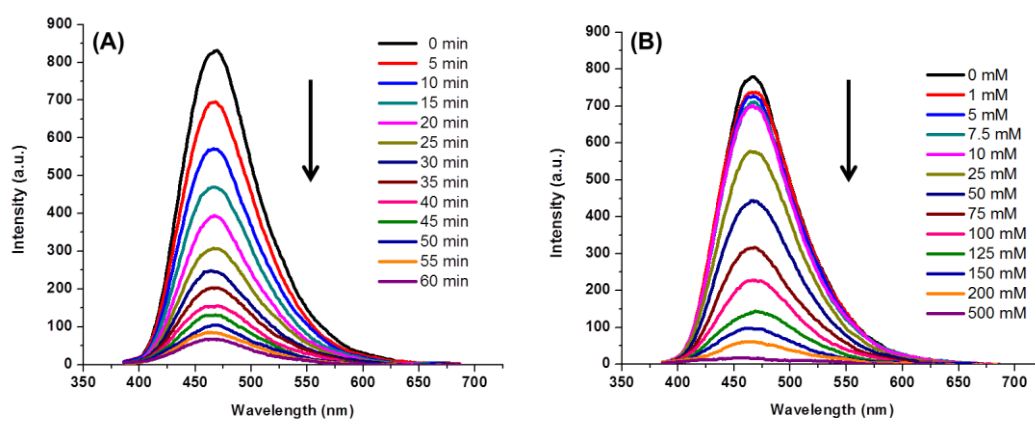


Figure 2.8 (A) Time-dependent photoluminescent changes of 5×10^{-4} g/ml of the GQDs after interacted with 0.1 M H₂O₂ and (B) Concentration-dependent fluorescence changes at 30 min after interacted with different concentration of H₂O₂.

From Figure 2.8A, the PL intensity of GQDs solution in the presence of 0.1 M of H₂O₂ as a function of time was investigated. The emission bands of GQDs at 467 nm presented a rapidly decrease in the range of 0-30 min. At time over 30 to 60 min, the bands demonstrated a very small decrease. By considering the time efficiency for sensing ability, the optimum catalytic time of GQDs was preferred at 30 min.

Next, the peroxidase-like catalytic activity of GQDs was first investigated by varying the concentration of H₂O₂. From the PL spectra in Figure 2.8B, the PL intensity of GQDs was significantly decreased as a function of concentration of H₂O₂ from 0 to 500 mM. The good linearity in the H₂O₂ concentration range of 1-125 mM with a $R^2 = 0.9849$ was shown in Figure 2.9.

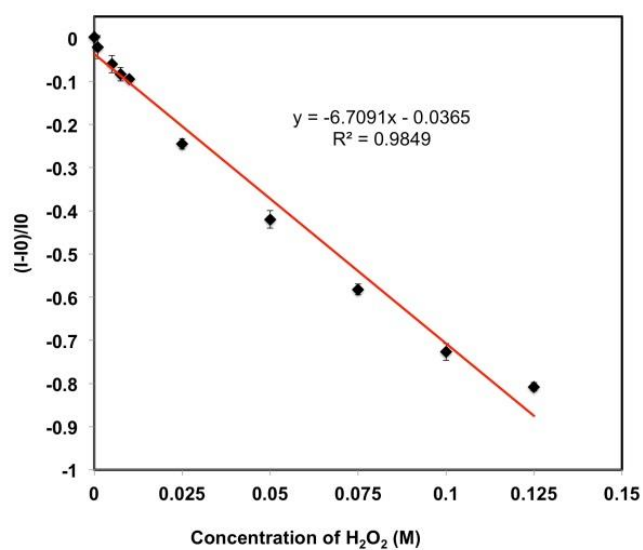


Figure 2.9 Linear relationship between $(I-I_0)/I_0$ of GQDs and concentration of H_2O_2 .

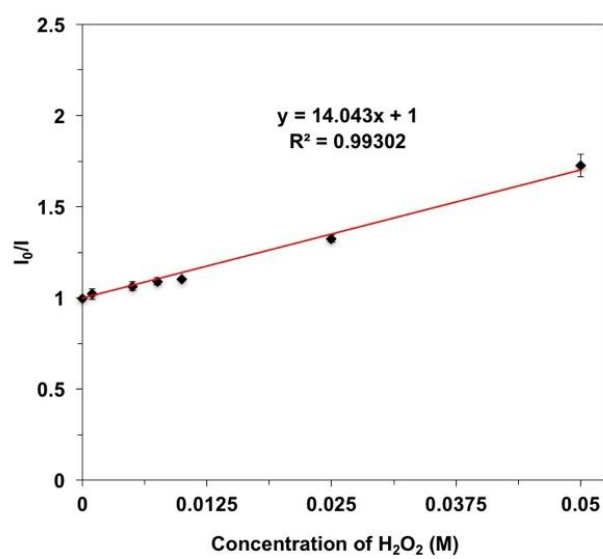


Figure 2.10 Stern-Volmer plots for photoluminescence of GQDs with H_2O_2 concentration ranging from 0 to 0.05 M.

Additionally, the affinity between GQDs and H₂O₂ quencher was evaluated *via* the Stern-Volmer equation as represented in equation 2.1, where the I₀ and I are the PL of GQDs in absence and presence of H₂O₂ (concentration range of 0-50 mM) and K_{sv} is the Stern Volmer constant [66, 67]. From the Stern-Volmer plots as in Figure 2.10, the relative photoluminescence intensity of GQDs correspond to the concentration of H₂O₂ and the Stern-Volmer constant, K_{sv}, is 14.04 L/mol.

$$\frac{I_0}{I} = 1.0 + K_{SV}[Analytes] \quad (2.1)$$

Taking on a board of the peroxidase-like catalytic activity of carbon materials such as graphene oxide and graphene dots, it was stemmed from the electron transfer process[20, 26] from abundant electrons on the surface of small particles GQDs to the LUMO of H₂O₂ resulting in the PL quenching of the GQDs. The mechanism of this process was illustrated in equation 2.2-2.3 [20, 21, 26].



2.4.5 Responsibility of H₂O₂-generated *in situ* by GQDs/Enz

The enzyme immobilization on the materials has been considerably realized since they take a benefit to encourage stability and sensitivity of enzyme[14]. As anticipated, the GQDs with the edge of carboxyl and hydroxyl group might easily interact to acetylcholinesterase (AChE) and choline oxidase (ChOx) through hydrogen bonding interaction. If the immobilization of enzymes in this platform was successfully performed, H₂O₂ generated *in situ* by active AChE and ChOx upon the addition of acetylcholine could encourage the PL quenching of this material.

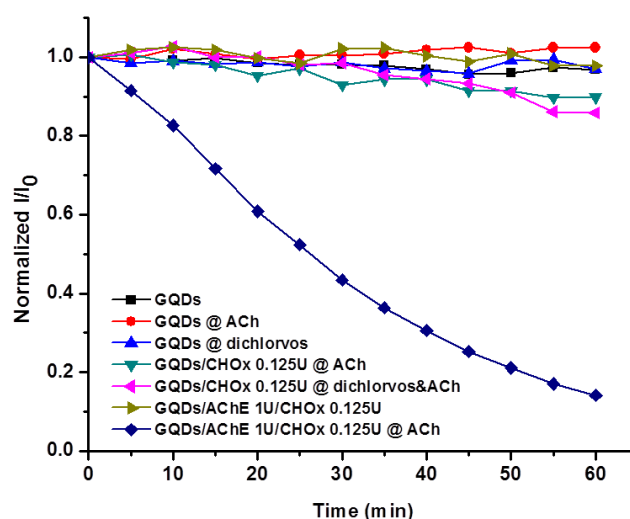


Figure 2.11 The normalized I/I_0 photoluminescent response at λ_{em} 467 nm of GQDs, GQD/Enz (GQDsAChE/ChOx) and GQDs/ChOx after the addition of ACh. Concentration of AChE and ChOx were 1 and 0.125 U/ml, respectively, where 1U is equivalent to amount of enzyme that hydrolyses acetylcholine or substrate to produce 1 mmol of choline or product per minute.

To verify the factor that affect to photoluminescent quenching of GQDs, the variety of system including acetylcholine (ACh), dichlorvos (organophosphate), one enzyme and bi-enzyme (AChE and ChOx) were investigated in Figure 2.11. From the normalized I/I_0 photoluminescent responses at 467 nm of all samples in each system, the blue line assigned to the factors of bi-enzyme in the presence of ACh in the system demonstrated the significant decrease of the normalize PL (from 1 to 0.14) of GQDs/Enz platform upon increment of time (from 0 to 60 min). This phenomenon is analogue to the photoluminescent quenching of direct H₂O₂ added. In the case of other

system without both enzymes of AChE and ChOx incorporated on GQDs, no significantly photoluminescent quenching have been observed. It implied that the photoluminescent quenching of GQDs in the biosensor platform was occurred by H_2O_2 generated *in situ* by enzymatic reaction of active AChE and ChOx as following in equations 2.4 and 2.5. Additionally, the GQDs would reduce H_2O_2 to water and a consequent $GQDs^+$ species induce the PL quenching (as in equation 2.2-2.3).

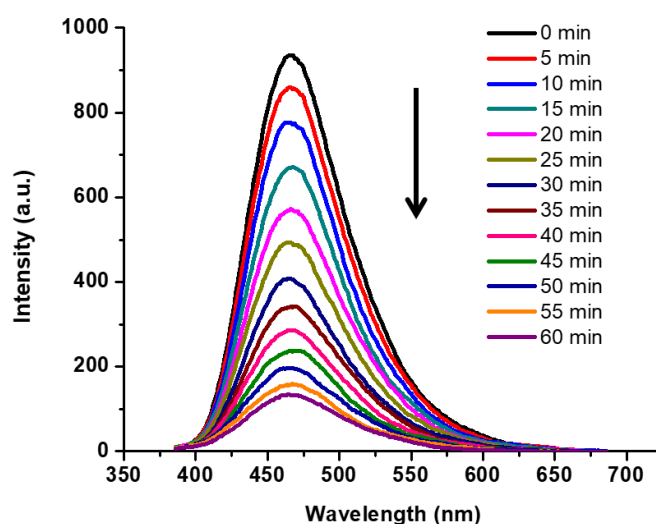
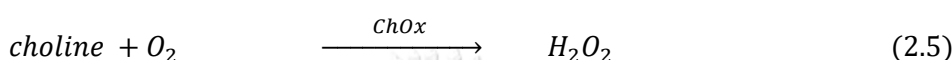
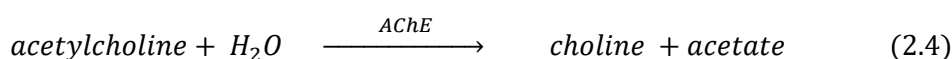


Figure 2.12 Time-dependent photoluminescence changes of **GQDs/Enz** after interacted with 1 mg/ml of acetylcholine (ACh) in Tris buffer pH 8, the concentration of GQDs, AChE and ChOx are 5×10^{-4} g/mL, 1 U/mL and 0.125 U/mL, respectively.

The time-dependent enzymatic reaction relied on **GQDs/Enz** biosensor in the presence of acetylcholine was investigated in Tris buffer pH 8 as shown in Figure 2.12. The spectra showed the decrement of emission band at 467 nm upon an increment of time to 60 min, which is the point with a respect to a large amount of H_2O_2 generated by enzymatic reaction.

2.4.6 Signal amplification for increasing responsive sensing of GQDs/Enz

To improve the sensitivity by signal amplification, the proper amount of enzyme, incubation time and pH need to be properly considered in this research.

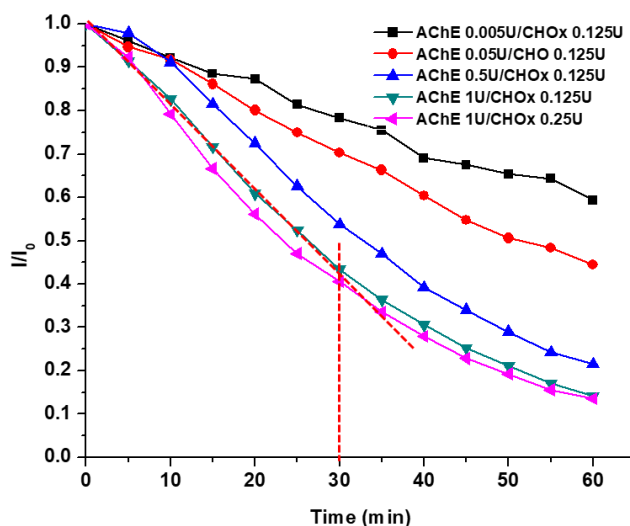


Figure 2.13 Normalized I/I_0 photoluminescence responses at λ_{em} 467 nm of GQDs upon the interaction of various concentrations of AChE and ChOx and incubation time.

Firstly, the different amount of bi-enzyme in GQDs/Enz biosensor under varying the ACh incubation time was investigated by monitoring the PL intensity in Tris buffer solution pH 8.0. The Figure 2.13 showed the decrement of PL intensity at 467 nm upon the increment of incubation time from 0 to 60 min and concentration of AChE/ChOx from 0.005/0.0125 to 1/0.25 U/mL. It means that the reaction rate of turning acetylcholine to H_2O_2 is increased upon the increment of incubation time and amount of enzyme catalysis.

In comparison of the concentration of AChE/ChOx at 1/0.125 and 1/0.25 U/mL in green and purple line, respectively, the PL showed high significantly decrease as in Figure 2.13. To improve the sensitivity by the highest change of PL, the use of highest amount of enzyme was appropriately selected. However, the cost-effective use should be considerably realized. The concentration of enzyme in this research was chosen as 1 U/ml AChE and 0.125 U/mL ChOx, which were lower than the employing amount of enzyme in previous researches [2, 10, 18].

Next, the incubation time was examined upon the addition of acetylcholine from 0 to 60 min. The normalized PL intensity of the GQDs in the presence of 1 U/ml AChE and 0.125 U/mL ChOx revealed completely quenching as a function of reaction time of 60 min (green line of Figure 2.13). Interestingly, a dramatical decrease of PL at over 50 % quenching was observed at 30 min (red dotted line of Figure 2.13). Hence the incubation time of 30 min for the reaction of **GQDs/Enz** biosensor with acetylcholine under the concentration of GQDs, AChE and ChOx at 5×10^{-4} g/mL, 1 U/mL and 0.125 U/mL, respectively, was selected for all further manipulation.

Another key factor of this study is the pH effect. The maximum PL intensity at 467 nm of the **GQDs/Enz** biosensor in varying pH from 3 to 12 showed the increasing tendency ranged pH 8-9 (Figure 2.14). At the point higher than 9, the maximum PL intensities were slightly decreased and remained unchanged. Hence, the pH range between 5 to 9 was chosen to study the PL quenching by H_2O_2 -generated *in-situ* of this biosensor after adding acetylcholine. As the results, a large quenching of the maximum PL intensity was observed especially pH 7-9 as shown in Figure 2.15.

As widely known, the organophosphates were gradually unstable at high temperature and high pH for example, hydrolysis half-life of dichlorvos at 25°C at pH 6.0, pH 7.0 and pH 8.0 was 46, 2.8 days and 0.91 days, respectively [68, 69]. In comparative work, many researchers reported the suitable pH at 8 to obtain the highest activity of free AChE and ChOx enzymes[70-72]. As reasonable consistency with above, a similar fluorescent quenching of **GQDs/Enz** biosensor at pH 7-9 pursued us to study the organophosphate detection at pH 8 for all manipulation.

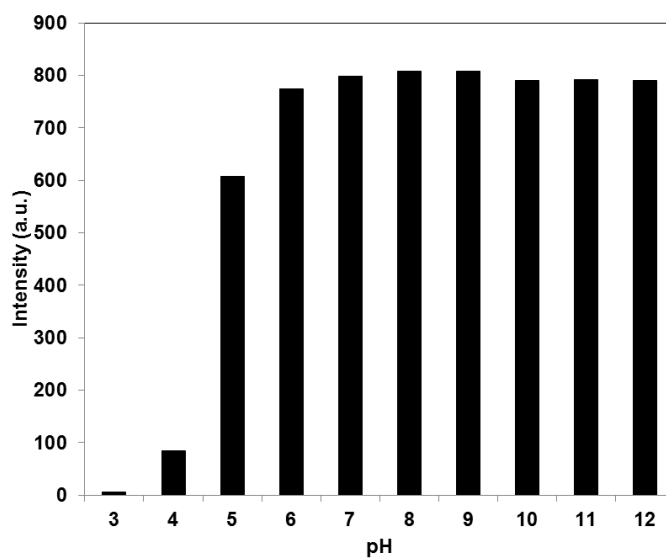


Figure 2.14 The PL intensity of GQDs/Enz at pH 3 to 12.

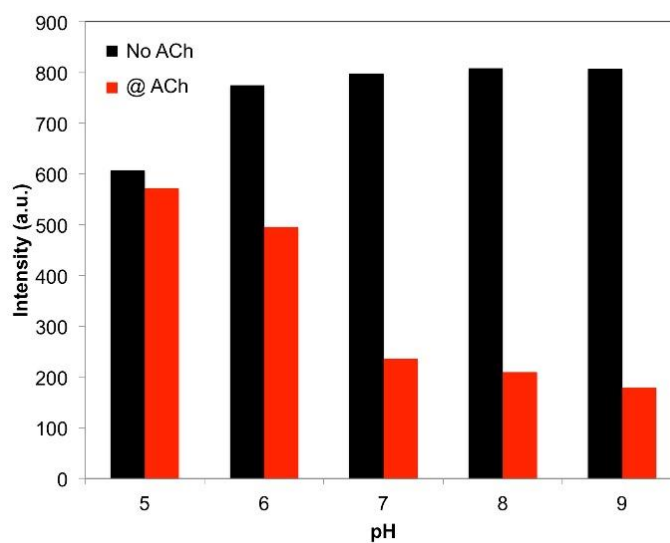


Figure 2.15 The PL intensity of GQDs/Enz before (black bar) and after incubation with ACh for 30 min (red bar) at various pH from 5 to 9.

2.4.7 OPs detection by using the GQDs/Enz nanomaterial

To investigate the organophosphate pesticide sensing properties, the PL spectra of this biosensor toward dichlorvos were shown in Figure 2.16. The PL intensity of **GQDs/Enz** was significantly increased upon the increment of dichlorvos. This indicated that organophosphate pesticides (OPs) actually inhibited the activity of enzyme acetylcholinesterase (AChE) and led to the decrease of H_2O_2 resulting in turn-on PL intensity of GQDs in the presence of OPs as demonstrated in Figure 2.1 (see introduction part of this chapter). Collectively, these results demonstrated that **GQDs/Enz** biosensor can assemble onto indirect detection of the amount of OPs through the inhibition of AChE enzymatic reaction, thereby inducing a fluorescence recovery.

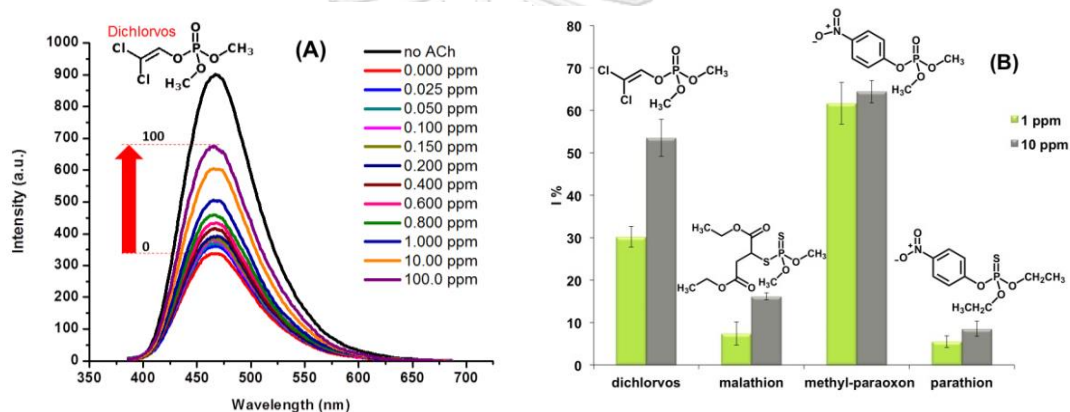


Figure 2.16 (A) Photoluminescence responses of **GQDs/Enz** biosensor after incubation with various concentration of dichlorvos 0-100 ppm. (B) % Inhibition efficiency (I%) of 1 and 10 ppm of different OPs toward **GQDs/Enz** biosensor.

Four selected organophosphates (OPs) including methy-paraoxon, dichlorvos, malathion and parathion at concentration of 1 ppm and 10 ppm were further examined in a regard to an inhibition efficiency (I%) of AChE enzymatic reaction as shown Figure 2.16B. The I% was calculated via equation 2.6, where $K_{30\text{without}}$ and $K_{30\text{withOP}}$ are the photoluminescent quenching with and without OP after incubation in ACh for 30 min ($K_{30} = F_0 - F_{30}/30$, where F_0 and F_{30} are PL intensity of **GQDs/Enz** in the absence and presence of ACh followed by incubation for 30 min)[10].

$$I(\%) = \left(\frac{K_{30without} - K_{30withOP}}{K_{30without}} \right) \times 100 \quad (2.6)$$

Of particular concentration of OPs at 1 ppm addressed the % inhibition of methy-paraoxon, dichlorvos, malathion and parathion at $62 \pm 5\%$, $30 \pm 2\%$, $7 \pm 3\%$ and $6 \pm 1\%$, respectively. However, the % inhibition efficiency in both concentrations of OPs showed the similar tendency change for all OPs. Taking such a previous work in the inhibition capacity of OPs toward AChE, a possible effect of the electrophilicity at a phosphorus atom has been reliably considered since the inhibition capacity of the oxo-forms is more efficient than the thio-form [13, 16, 19]. Another factor is steric effect of OPs to the active center of AChE containing a deep and narrow gorge [10, 73]. In these regards, the inhibition capacity of dichlorvos and methyl-paraoxon is more efficient than that of malathion and-parathion. Concerning on the different inhibition capacity of OPs, it was a possible attribution of the reciprocal absorption capacity of OPs on the nanomaterial surface. According to the chemical structure of OPs, dichlorvos pesticide has more hydrophobic structure than methyl-paraoxon. This was possibly rationalized that the hydrophobic dichlorvos did not prefer passing through hydrophilic phase of **GQDs/Enz** biosensor resulting in a lower inhibition capacity [10]. Such the inhibition of dichlorvos and methyl-paraoxon has been extensively studied in sensing applications.

The % inhibition efficiency (I%) of enzyme was plotted toward the concentration of dichlorvos and methyl-paraoxon as shown in Figure 2.17A and B. The suitably linear range of 0.1 to 10 ppm for dichlorvos (inset Figure 2.17A) showed the % inhibition efficiency (I%) of $27.173 + 22.488\log[\text{dichlorvos}]$, $R^2 = 0.99$ and $n = 3$. Normally, the detection limit of pesticide by sensory system is acceptable at 10% inhibition based on AChE activity [73]. Consequently, detection limit of dichlorvos by **GQDs/Enz** biosensor was 0.172 ppm (0.778 μM). In comparison, this value is lower than a potentiometric detection [11], the enzymatic immobilization on working electrode for an amperometric detection [12], the luminescence quenching probe of Tb^{3+} complex [74] and an optical mode [75] as shown in Table 2.5. Interestingly, the PL changes of **GQDs/Enz** biosensor are covered in the range of a maximum residue limit of dichlorvos at 10 ppm in natural water authorized by the United States

Environmental Agency (EPA) [3]. In the case of methyl-paraoxon, the linear range of 0.1-1 ppm (Figure 2.17B) with the equation of $I\% = 55.253 + 42.158\log[\text{methyl-paraoxon}]$, $R^2 = 0.99$ and $n = 3$ demonstrated the detection limit of 0.084 ppm (0.342 μM). This value is lower than the spectrophotometric cutinase assay [76] and conductometric detection [77] as shown in Table 2.5. Although this sensing platform provided an excellent analytical LOD for methyl-paraoxon over dichlorvos, a dramatic increase of dichlorvos usage in agriculture in Thailand [78] urged us to focus on studying dichlorvos sensing purpose by this sensing platform.

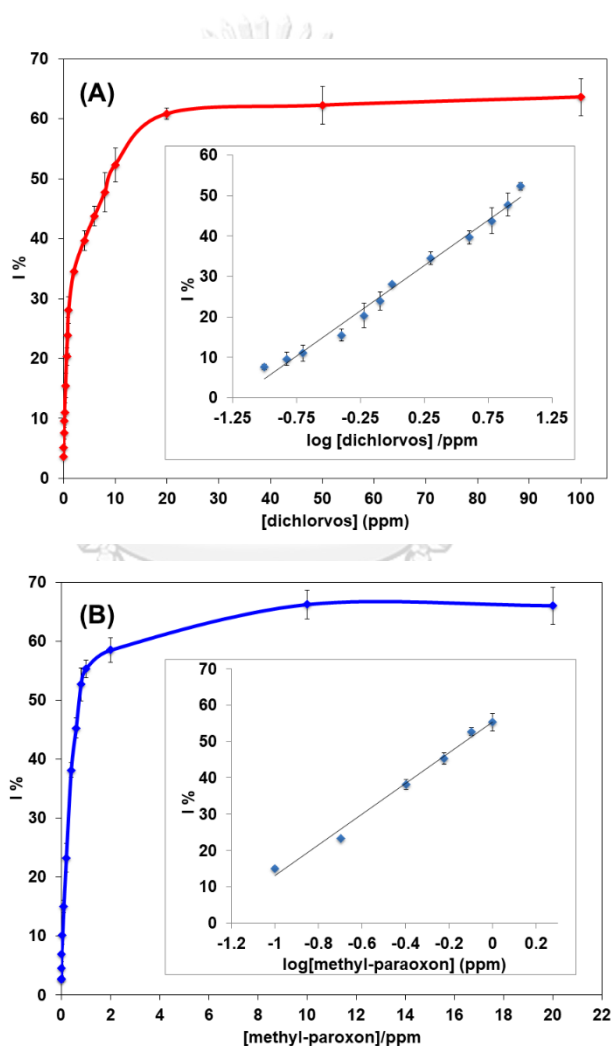


Figure 2.17 % Inhibition efficiency (I%) of GQDs/Enz biosensor after incubation with various concentration of dichlorvos from 0.025 to 100 ppm (A) and methyl-paraoxon from 1×10^{-5} to 20 ppm (B). The insets of (A) and (B) showed the linear range of dichlorvos detection from 0.1 to 10 ppm and methyl-paraoxon from 0.1 to 1 ppm, respectively.

Table 2.5 The analytical comparison between this work and other works.

Organophosphate	Sensing method	Analytical characterization				Ref.
		Enzyme concentration	Linear range (μM)	LOD (μM)	Real sample recovery	
dichlorvos	Potentiometric	15 μL of 1900 IU/ml of AChE	Not reported	1	Not reported	[11]
dichlorvos	Amperometric	25-120 U/ml of AChE	Not reported	3.62×10^3	Not reported	[12]
dichlorvos	Luminescence	No enzyme	0.56-5.7	1.96	Not reported	[74]
dichlorvos	Optical mode	50 U/ml of AChE	2.26-31.67	2.26	Not reported	[75]
dichlorvos	Luminescence	1 U/ml of AChE, 0.125 U/ml of ChOx	0.45-45.25	0.78	101.33- 111.59 %	This work
paraoxon	Luminescence	217.5 U/ml of AChE	Not reported	1.05×10^{-5}	104.6-115 %	[10]
methyl-paraoxon	Spectrophotometric AChE assay	10 μM of AChE, 1.2 mg/mL ChOx	Not reported	10×10^{-3}	Not reported	[2]
methyl-paraoxon	Spectrophotometric cutinase assay	Not reported conc. of cutinase	Not reported	6.18×10^3	Not reported	[76]
methyl-paraoxon	Conductometric biosensor	Not reported conc. of AChE	0.5-50	0.5	Not reported	[77]
methyl-paraoxon	Luminescence	1 U/ml of AChE, 0.125 U/ml of ChOx	0.40-4.05	0.342	Not reported	This work

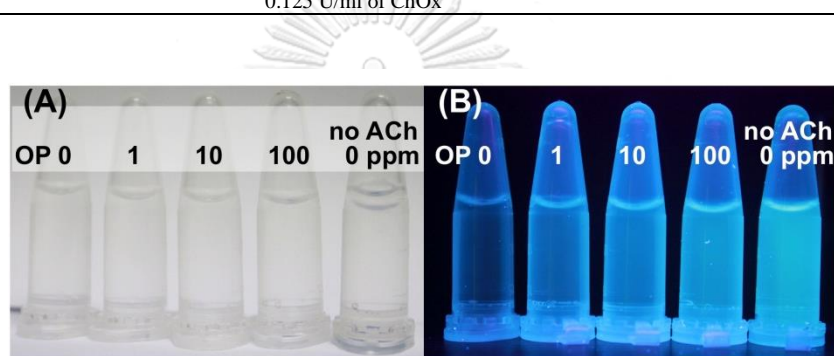


Figure 2.18 Colorimetric of **GQDs/Enz** biosensor in visible (A) and UV light (B) at various concentration of dichlorvos organophosphate (OP) at 0, 1, 10, 100 ppm and blank (no dichlorvos and ACh).

Extensive work for visual determination of this biosensor toward dichlorvos was carried out under visible and UV light. The naked-eye brightness upon the different concentration of dichlorvos at 1, 10 and 100 ppm with and without ACh under UV light has been exhibited in Figure 2.18. Under the UV light ($\lambda_{\text{ex}} = 365 \text{ nm}$), the sensing platform showed strong blue brightness (right tube of Figure 2.18B) and a non-bright solution was observed after adding ACh in the absence of OP, (left tube of Figure 2.18B). For the remaining solution in the middle tubes of Figure 2.18B, the tendency of blue brightness of this sensing platform has been raised in regarding to an increment of dichlorvos concentration. These results suggested that **GQDs/Enz** biosensor was capable of detecting dichlorvos by quantitative visual interpretation.

2.4.8 Effect of interfering ions

Due to the high abundance of metal ions in soil and water [74], the interference of metal ions for the OPs determination by this system was investigated. Figure 2.19 showed the inhibition efficiency (%) of AChE in the sensing platform without (black bar) and with (red bar) the interferences (1×10^{-5} M) upon incubation with dichlorvos at the concentration of 2 ppm (1×10^{-5} M). The results showed that most metal ions exhibited no interference to the dichlorvos detection. However, the **GQDs/Enz** biosensor exhibited a small quenching of PL response in the presence of Hg^{2+} . The previous work related to the GQDs optical properties also reported the influence of Hg^{2+} toward the fluorescence quenching of GQDs *via* electron or energy transfer from GQDs to Hg^{2+} [79, 80]. To test the effect of Hg^{2+} toward our sensor system, the free GQDs without enzymatic reaction has been further examined by adding the Hg^{2+} in the solution. It was found that Hg^{2+} affected directly to the PL quenching of GQDs as shown in Figure 2.20.

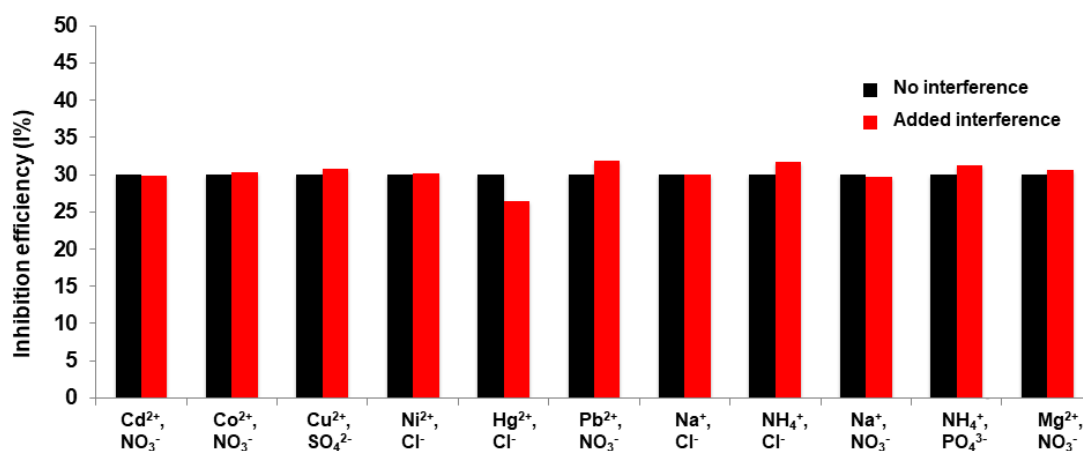


Figure 2.19 Effect of interference (1×10^{-5} M) to the inhibition efficiency (%) of AChE of **GQDs/Enz** biosensor in the presence of dichlorvos (1×10^{-5} M or 2 ppm) after incubation for 30 min.

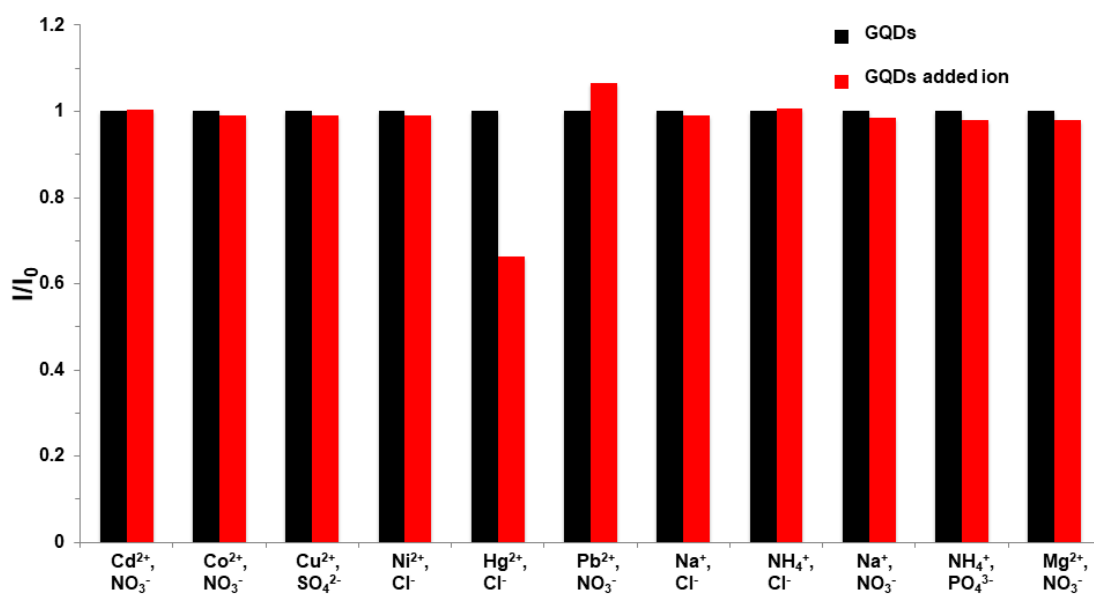
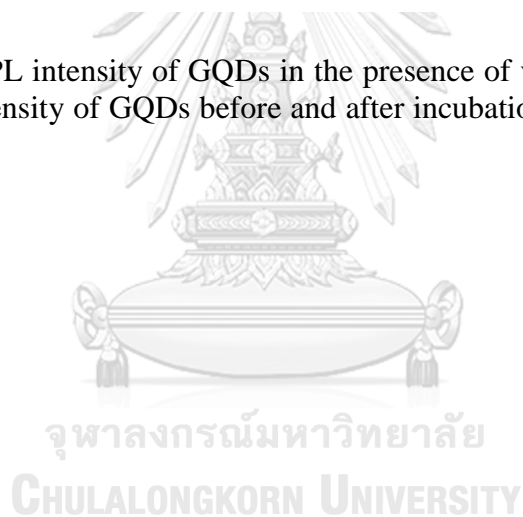


Figure 2.20 The PL intensity of GQDs in the presence of various ions (1×10^{-5} M). I_0 and I were the intensity of GQDs before and after incubation with various ions for 30 min.



2.4.9 Determination of organophosphate in real samples

In previous works, the determination of organophosphate has been carried out in MQ-water or DI water [2, 74]. Additionally, the LC-MS method required the complicated sample pretreatment to elude some interference [60, 81, 82]. Hence, this method showed the advantage of direct detection of dichlorvos in natural water under a small effect of interference. In order to determine dichlorvos in real samples, three samples of water (tap water from the laboratory, field water 1 from the lake at Chulalongkorn University and field water 2 from the lake at Roi Et province near agricultural land) were studied in this work. The water was collected a day prior to the experiment. The calibration curve of dichlorvos was achieved from the standard addition experiment.

Table 2.6 The determination of dichlorvos in real samples by using this biosensor and LC/MS.

Sample	Spiked dichlorvos (ppm)	This method			LC/MS		
		Measured (ppm)	%RSD	%Recovery	Measured (ppm)	%RSD	%Recovery
Tap water	0	-	-	-	-	-	-
	2	2.23	2.27	111.59	1.84	0.15	91.83
Field water 1	0	-	-	-	-	-	-
	2	2.03	5.87	101.33	1.83	0.16	91.67
Field water 2	0	-	-	-	-	-	-
	2	2.08	5.54	104.01	1.83	0.62	91.83

n = 3

- non-detectable

Table 2.6 demonstrates the correlation of concentration of organophosphate that was determined by **GQDs/Enz** biosensor and LC/MS method. According to the acceptable recovery of 80-110% for the analyte concentrations at 0.1-10 ppm, and their acceptable relative standard deviation (RSD) of 14% at 2.0 ppm [83], satisfactory accuracy in the amount of dichlorvos at 2.0 ppm spiked in the solution system was obtained with the recovery of 101-112% and 91.5-92.0% for the **GQDs/Enz** biosensor and UHPLC-MS/MS, respectively, along with the satisfactory precision with %RSD of 2.3-5.9% and 0.15-0.62% for the **GQDs/Enz** biosensor and UHPLC-MS/MS,

respectively. This indicates that, in comparison with the UHPLC-MS/MS method, our developed **GQDs/Enz** biosensor can be used with the acceptable accuracy and precision in quantitative analysis of dichlorvos in various water samples.

In summary of this part, we have successfully demonstrated the real time sensor of graphene quantum dots based enzymatic reaction (**GQDs/Enz**) for adaptive determination ability toward organophosphate pesticides (OPs) especially in real water samples with small effect of interference.



CHAPTER III

Hybrid hydrogels for organophosphate detection

3.1 Introduction

In this work, we constructed the sensing materials based on the hybrid hydrogels system to selectively detect organophosphate. Ongoing development of GQDs efficiency for OPs sensing by hybrid hydrogel has ignited remarkable research interest for us. Owing to intrinsic hydrophobic properties of hydrogel, we search for an effectively hydrophobic gelator for incorporation with GQDs and enzyme in buffer solution. The bolaamphiphile (two-headed amphiphiles) gelators based on bis(urea) and L-phenylalanine amino acid are considered as well-suited candidates for gel sensing due to its excellent structural design derived the hydrogelations encouragement *via* non-covalent interaction, such as, ionic, hydrogen bonding, hydrophobic interaction and π -stacking [41, 46, 84-86]. Furthermore, the peripheral substituents of carboxylate group would support the water solubility and act as a hosting for GQDs and bi-enzyme (AChE and ChOx) in phosphate buffer solution. The effectively quantitative analysis of OPs by these materials, **GQDs/Enz/Gels**, has been achieved by monitoring the turn-on PL response regarding to the inhibition of enzyme in the presence of OPs in hybrid hydrogels as shown in Figure 3.1.

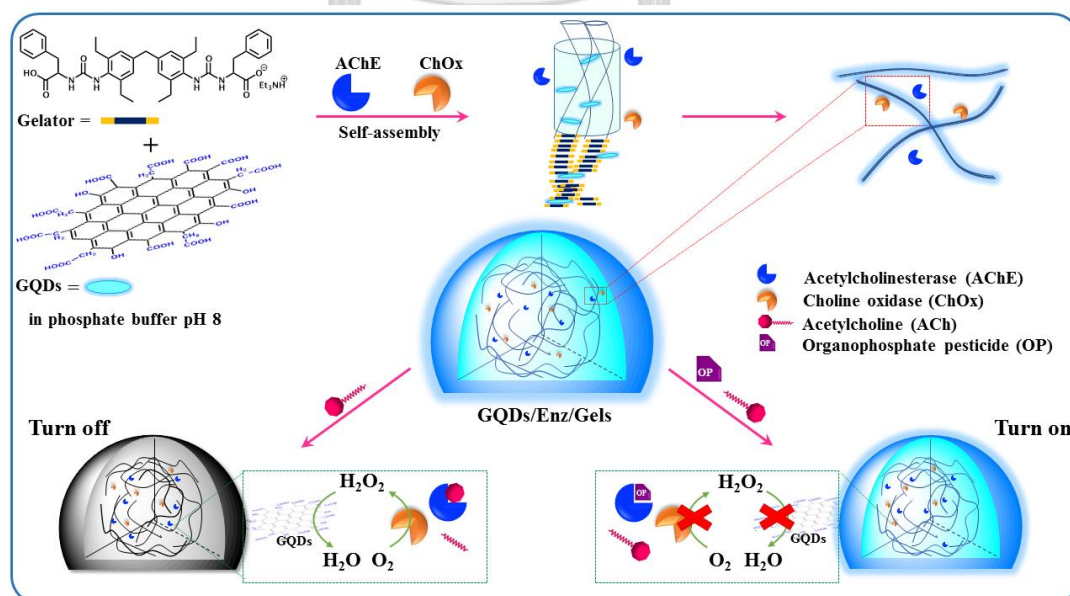


Figure 3.1 Hybrid hydrogels of **GQDs/Enz/Gels** and proposed mechanism of organophosphate pesticide detection.

3.2 Experimental

3.2.1 Materials

All materials, organophosphate pesticides, solvents and chemicals were purchased from Sigma-aldrich, Fluka and Merck. Phosphate buffer (PB) was prepared by using sodium phosphate monobasic (NaH_2PO_4) and sodium phosphate dibasic (Na_2HPO_4). Tris-HCl was obtained from Carlo Erba. Milli-Q (MQ) was obtained by ultra-pure water system.

3.2.2 Synthesis of compound 1 to 6b

In this work, the gelators were designed based on bis(urea) system, type of space group of methylene bis(diethyl phenyl) and bis(methyl ethyl) benzene and type of amino acid including aliphatic amino acid, aromatic amino acid and amino acid methyl ester as shown structure of compounds **1**, **2c**, **3**, **4a**, **4b**, **4c**, **5**, **6a** and **6b** (**a**, **b** and **c** represent 0, 1 and 2 Et_3NH^+ , respectively) in Figure 3.2. We expected that the bis(urea) system and methylene bis(diethyl phenyl) spacer will promote the gelation *via* hydrogen bonding and hydrophobic interaction, respectively. Furthermore, ionizable amino acid system possibly encourages water solubility and enzyme compatibility.

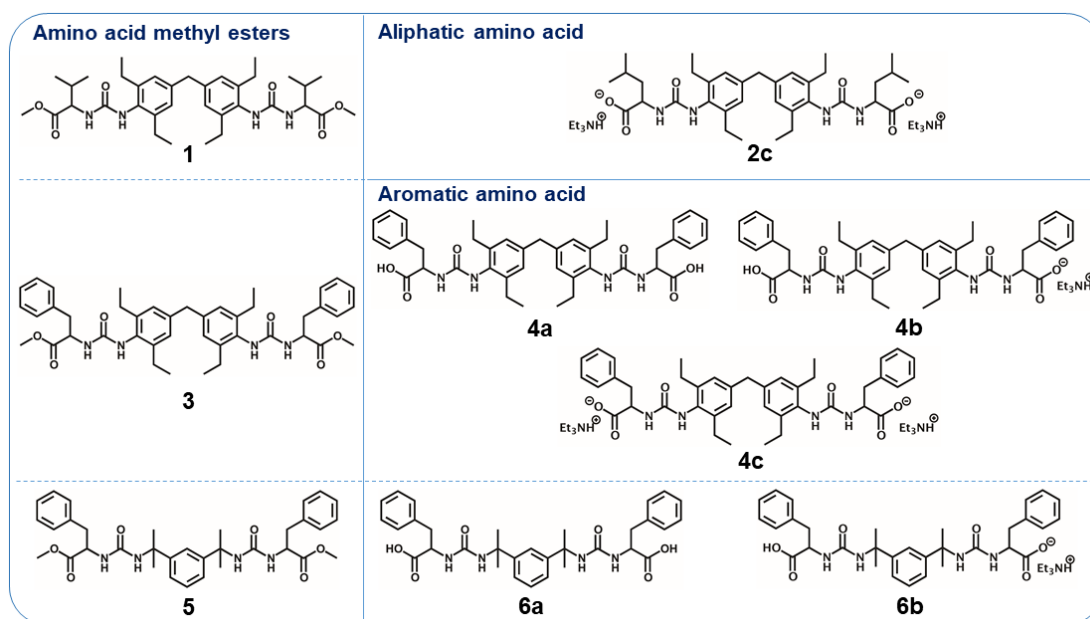


Figure 3.2 The molecular structures of compound **1-6b**.

3.2.2.1 4,4'-methylenebis(2,6-diethylphenyl isocyanate)

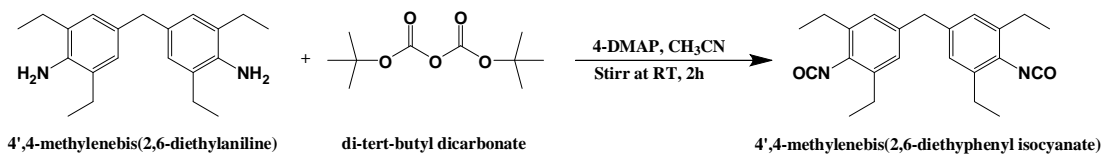


Figure 3.3 Synthetic pathway of 4,4'-methylenebis(2,6-diethylphenyl isocyanate).

A solution of dibutylcarbonate (6 g) in dry acetonitrile (20 ml) was slowly added to the solution of 4-DMAP (0.33 g) in dry acetonitrile. A solution of 4,4'-methylenebis(2,6-diethylaniline) (4g) in 20 ml dry acetonitrile was slowly added to solution of dibutylcarbonate. The clear solution was stirred for 2 h at room temperature under N_2 . H_2SO_4 (2 ml, 18 M) in 3 ml acetonitrile was added to the mixture solution. The mixture solution was stirred for 5 min and then, 65 ml of water was added to the mixture solution. The solution was slowly extracted by hexane 4 times (4x100 ml) and dried over anhydrous MgSO_4 . The solvent was evaporated under in vacuum to afford the white solid of 4,4'-methylenebis(2,6-diethylphenyl isocyanate) (4.11 g, 11.34 mmol, 89% yield) mol. wt. = 362.46.

3.2.2.2 Compound 1

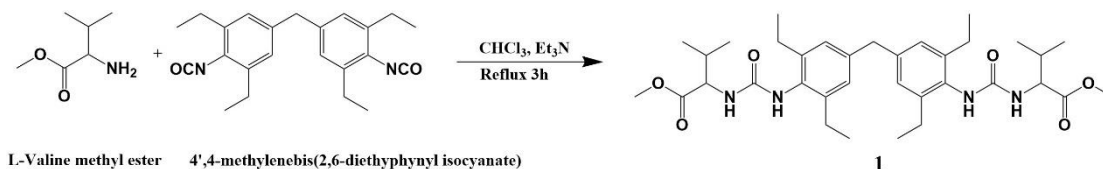


Figure 3.4 Synthetic pathway of compound **1**.

Triethylamine (0.78 ml, 5.59 mmol) was added to a suspension of L-valine methyl ester (0.44 g, 3.37 mmol) in CHCl_3 (15 ml). The solution of 4,4'-methylenebis(2,6-diethylphenyl isocyanate) (0.59 g, 1.63 mmol) in CHCl_3 (15 ml) was slowly added to the previous solution. The mixture solution was stirred under reflux for 3 h. The 20 ml of water was added to the solution. The solution was extracted by CHCl_3 (4x50 ml) and dried over anhydrous MgSO_4 . The solvent was evaporated under in vacuum. The solid was recrystallized by 20:30 ml of acetone: hexane. The suspension was then filtrated and washed with cold CHCl_3 to afford a white solid of compound **1** (0.653 g, 1.04 mmol, 64 % yield) mol. wt. = 624.81. $^1\text{H NMR}$ (400 MHz, DMSO-d_6) δ 7.46 (s, 2H, NH), 6.93 (s, 4H, ArH), 6.54 (s, 2H, NH), 4.14 (q, $^3J = 4$ Hz, NHCH), 3.81 (s, 2H, ArCH_2Ar), 3.65 (s, 6H, OCH_3), 2.47 (q, $^3J = 4$ Hz, 8H, ArCH_2CH_3), 1.07 (t, $^3J = 8$ Hz, 12H, ArCH_2CH_3), 0.90 (d, $^3J = 12$ Hz, 12H, CHCH_3); $^{13}\text{C}\{^1\text{H}\}$ NMR (400 MHz, DMSO-d_6) δ 173.46 (CO_2CH_3), 156.90 (C=O), 142.20 (ArC), 126.66 (ArC), 58.18 (CH), 52.09 (CH), 30.95 (CH_2), 24.90 (CH_2), 19.46 (CH_3), 18.25 (CH_3), 15.16 (CH_3); **ESI** (m/z): 648.64 m/z $[\text{M}+\text{Na}]^+$ (calc. 647.36 m/z), 625.19 m/z $[\text{M}+\text{H}]^+$ (calc. 625.38 m/z); **analysis calc.** for $\text{C}_{35}\text{H}_{52}\text{N}_4\text{O}_6$: C 67.28, H 8.39, N 8.97%; found: C 67.46, H 8.46, N 8.87%.

3.2.2.3 Compound 2c

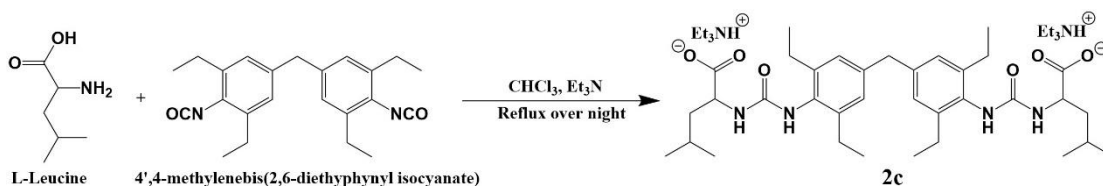


Figure 3.5 Synthetic pathway of compound 2c.

Triethylamine (0.78 ml, 5.59 mmol) was added to a suspension of L-leucine (0.428 g, 3.27 mmol) in EtOH:CHCl₃ (1:15 ml). The solution of 4,4'-methylenebis(2,6-diethylphenyl isocyanate) (0.59 g, 1.63 mmol) in CHCl₃ (15 ml) was slowly added to the solution. The mixture was stirred under reflux for overnight. The mixture was extracted by water and CHCl₃. (4x50 ml) and the organic phase was dried over MgSO₄. The solvent was evaporated under in vacuum. The solid was recrystallized by 20:30 ml of acetone: hexane for 3h. The suspension was then filtrated and washed with cold CHCl₃ (40 ml) to afford a light-yellow solid (0.643 g, 0.77 mmol, 48 % yield) mol. wt. = 827.19. ¹H NMR (400 MHz, DMSO-d₆) δ 7.77 (s, 2H, NH), 6.93 (s, 4H, ArH), 6.31 (s, 2H, NH), 4.06 (q, ³J = 8.0 Hz, 2H, CH₂CHNH), 3.81 (s, 2H, ArCH₂Ar), 2.56 (m, 12H, NCH₂CH₃), 2.46 (m, 8H, ArCH₂CH₃), 1.71 (m, 2H, CH(CH₃)₂), 1.47 (m, 4H, CH₂CH), 1.09 (t, 18H NCH₂CH₃), 0.88 (d, ³J = 8.0 Hz, 12H, CHCH₃) ESI (m/z): 625.39 m/z [M-2Et₃N+H]⁺ (calc. 625.39 m/z), [M+H]⁺ (calc. 827.63 m/z); **analysis calc.** for C₄₇H₈₂N₆O₆: C 68.24, H 9.99, N 10.16%; found: C 64.43, H 9.06, N 9.18%. The compound was found to strongly retain CHCl₃ **calc.** for C₄₇H₈₂N₆O₆·0.5CHCl₃: C 64.32, H 9.38, N 9.48%.

3.2.2.4 Compound 3

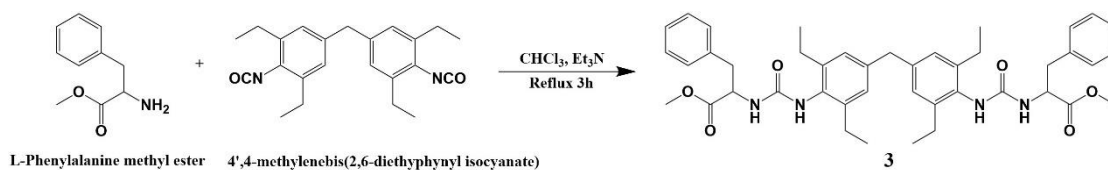


Figure 3.6 Synthetic pathway of compound 3.

Triethylamine (0.78 ml, 5.59 mmol) was added to a suspension of L-phenylalanine methyl ester (0.60 g, 3.37 mmol) in CHCl_3 (15 ml). The solution of 4,4'-methylenebis(2,6-diethylphenyl isocyanate) (0.59 g, 1.63 mmol) in CHCl_3 (15 ml) was slowly added to the mixture solution. The mixture was stirred under reflux for 3 h. The suspension was then filtrated and washed with cold CHCl_3 to afford a white solid (0.871 g, 1.21 mmol, 74 % yield) mol. wt. = 720.90. $^1\text{H NMR}$ (400 MHz, DMSO-d_6) δ 7.57 (s, 2H, NH), 7.30 (m, 10H, ArH), 6.91 (s, 4H, ArH), 6.76 (s, 2H, NH), 4.47 (q, $^3J=8.0$ Hz, 2H, CH_2CHNH), 3.80 (s, 2H, ArCH_2Ar), 3.62 (s, 6H, OCH_3), 3.04 (dd, $^3J=8.0$ Hz, 2H, $\text{CHCH}_x\text{H}_y\text{Ar}$), 2.98 (dd, $^3J=8.0$ Hz, 2H, $\text{CHCH}_x\text{H}_y\text{Ar}$), 2.42 (q, $^3J=8.0$ Hz, 8H, ArCH_2CH_3), 1.04 (t, $^3J=8.0$, 12H, ArCH_2CH_3); $^{13}\text{C}\{^1\text{H}\}$ NMR (400 MHz, DMSO-d_6) δ 173.20 (CO_2CH_3), 156.46 (C=O), 137.55 (ArC), 129.65 (ArC), 128.67 (ArC), 126.97 (ArC), 126.63 (ArC), 52.19 (CH), 24.83 (CH_2), 15.13 (CH_3); **ESI** (m/z): 721.67 m/z $[\text{M}+\text{Na}]^+$ (calc. 721.38 m/z); **analysis calc.** for $\text{C}_{43}\text{H}_{52}\text{N}_4\text{O}_6$: C 71.64, H 7.27, N 7.74%; found: C 71.39, H 7.32, N 7.80%.

3.2.2.5 Compound 4b

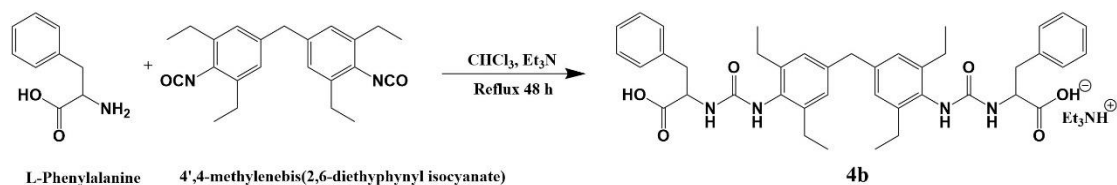


Figure 3.7 Synthetic pathway of compound 4b.

Triethylamine (0.78 ml, 5.59 mmol) was added to a suspension of L-phenylalanine (0.54 g, 3.27 mmol) in EtOH:CHCl₃ (1:15 ml). The solution of 4,4'-methylenebis(2,6-diethylphenyl isocyanate) (0.59 g, 1.63 mmol) in CHCl₃ (15 ml) was slowly added to the mixture solution. The mixture was stirred under reflux at 68 °C for 48 h. The 20 ml of water was added and extracted by CHCl₃ (4x50 ml) and then the organic part was evaporated under in vacuum. The solid was recrystallized by 20:30 ml of acetone: hexane. The suspension was then filtrated and washed with cold CHCl₃ (40 ml) to afford a light-yellow solid (0.995 g, 1.25 mmol, 77 % yield) mol. wt. = 794.03. **¹H NMR** (400 MHz, DMSO-d₆) δ 7.59 (s, 2H, NH), 7.23 (m, 10H, ArH), 6.90 (s, 4H, ArH), 6.28 (s, 2H, NH), 4.27 (q, ³J= 8 Hz, 2H, CH₂CHNH), 3.80 (s, 2H, ArCH₂Ar), 3.04-2.96 (m, 4H, CHCH₂Ar), 2.76 (q, ³J= 8 Hz, 6H, NCH₂CH₃), 2.45 (q, ³J= 4 Hz, 8H, ArCH₂CH₃), 1.05 (t, ³J= 8 Hz, 9H and 12H, NCH₂CH₃ and ArCH₂CH₃); **¹³C{¹H} NMR** (400 MHz, DMSO-d₆) δ 174.19 (C=O), 156.41 (C=O), 142.26 (ArC), 138.46 (ArC), 129.94 (ArC), 128.28 (ArC), 126.49 (ArC), 54.49 (CH), 45.76 (NCH₂CH₃), 41.15 (CH₂), 38.23 (CH₂), 24.85 (CH_{3x}), 15.14 (CH_{3y}), 10.34 (NCH₂CH₃); **ESI (m/z)**: 693.59 m/z [M-Et₃N+H]⁺ (calc. 693.36 m/z); **analysis calc.** for C₄₇H₆₃N₅O₆: C 71.09, H 8.00, N 8.82%; found: C 66.62, H 7.59, N 8.17%. The compound was found to strongly retain CHCl₃ **calc.** for C₄₇H₆₃N₅O₆·0.5CHCl₃: C 66.83, H 7.50, N 8.20%. The residual CHCl₃ can be observed by **¹H NMR** at δ 8.27 (s).

3.2.2.6 Compound 4a

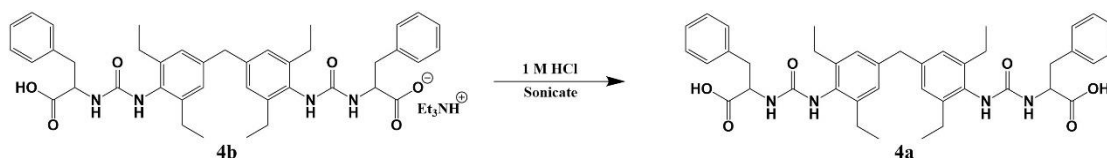


Figure 3.8 Synthetic pathway of compound 4a.

Compound **4b** was synthesized by the same amount as above data, after that suspended in 1 M aqueous HCl (250 ml), and then sonicated for 30 minutes. The suspension was filtrated and washed by water and cold CHCl_3 . Light-yellow solid was achieved (0.448 g, 0.65 mmol, 39.65 % yield) mol. wt. = 692.84. $^1\text{H NMR}$ (400 MHz, DMSO- d_6) δ 12.67 (s, 1H, OH), 7.53 (s, 2H, NH), 7.24 (m, 10H, ArH), 6.91 (s, 4H, ArH), 6.34 (s, 2H, NH), 4.44 (q, $^3J = 8.0$ Hz, 2H, CH_2CHNH), 3.82 (s, 2H, ArCH_2Ar), 3.08-2.93 (m, 4H, CHCH_2Ar), 2.40 (q, $^3J = 8.0$ Hz, 8H, ArCH_2CH_3), 1.09 (t, $^3J = 8.0$ Hz, 12H, ArCH_2CH_3); $^{13}\text{C}\{^1\text{H}\}$ NMR (400 MHz, DMSO- d_6) δ 174.08 (CO_2H), 156.43 ($\text{C}=\text{O}$), 142.21 (ArC), 137.77 (ArC), 129.74 (ArC), 128.54 (ArC), 126.84 (ArC), 54.16 (CH), 41.14 (CH_2), 38.06 (CH_2), 24.80 (CH_{3x}), 15.12 (CH_{3y}); **ESI** (m/z): 693.60 m/z $[\text{M}+\text{H}]^+$ (calc. 693.36 m/z); **analysis calc.** for $\text{C}_{41}\text{H}_{48}\text{N}_4\text{O}_6$: C 71.08, H 6.98, N 8.09%; found: C 69.66, H 7.00, N 7.88%. The compound was found to strongly retain HCl **calc.** for $\text{C}_{41}\text{H}_{48}\text{N}_4\text{O}_6 \cdot 0.3\text{HCl}$: C 69.97, H 6.92, N 7.96%. (second time, better than the first one)

3.2.2.7 Compound 4c

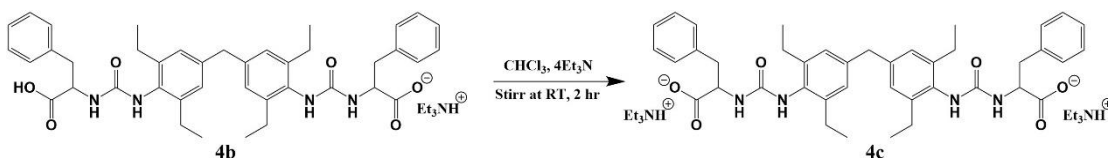


Figure 3.9 Synthetic pathway of compound 4c.

Compound **4b** (0.25 g, 0.35 mmol) was suspended in 10 ml CHCl_3 . Triethylamine (0.19 ml, 1.41 mmol) was added to a suspension to give yellow solution. Then the solution was stirred for 2 h at room temperature and evaporated to left behind the yellow oil. Hexane (25ml) was added to give the precipitate which was sonicated for 1 minute. The suspension was filtrated and washed by Hexane. Light-yellow solid was achieved (0.208 g, 0.23 mmol, 66 % yield) mol. wt. = 894.60. $^1\text{H NMR}$ (400 MHz, DMSO-d_6) δ 7.60 (s, 2H, NH), 7.19 (m, 10H, ArH), 6.90 (s, 4H, ArH), 6.29 (s, 2H, NH), 4.24 (q, $^3J = 8$ Hz, 2H, CH_2CHNH), 3.80 (s, 2H, ArCH_2Ar), 3.08-2.93 (m, 4H, CHCH_2Ar), 2.70 (q, $^3J = 8$ Hz, 12H, NCH_2CH_3), 2.45 (q, $^3J = 8$ Hz, 8H, ArCH_2CH_3), 1.05 (t, $^3J = 8$ Hz, 19H and 12H, NCH_2CH_3 and ArCH_2CH_3); **ESI** (m/z): 715.52 m/z $[\text{M}-2\text{Et}_3\text{N}+\text{Na}]^+$ (calc. 715.35 m/z), 693.55 m/z $[\text{M}-2\text{Et}_3\text{N}+\text{H}]^+$ (calc. 693.36 m/z); **analysis calc.** for $\text{C}_{53}\text{H}_{78}\text{N}_6\text{O}_6$: C 71.11, H 8.78, N 9.39%; found: C 65.20, H 8.90, N 8.21%. The compound was found to strongly retain CHCl_3 and Hexane **calc.** for $\text{C}_{53}\text{H}_{78}\text{N}_6\text{O}_6 \cdot 0.85\text{CHCl}_3 \cdot 0.5\text{Hexane}$: C 65.54, H 8.50, N 8.07%. The residual CHCl_3 and Hexane can be observed by $^1\text{H NMR}$ at δ 8.34 (s) and δ 1.25 (m).

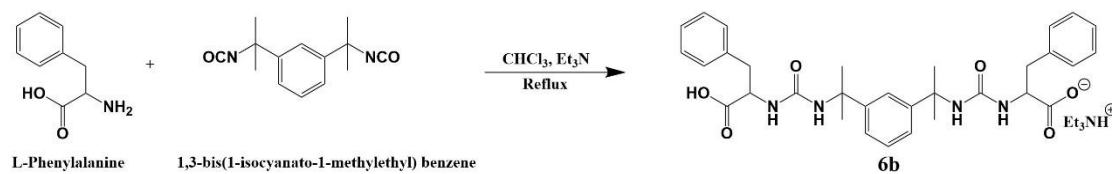
3.2.2.9 Compound **6b**

Figure 3.11 Synthetic pathway of compound **6b**.

Triethylamine (0.78 ml, 5.59 mmol) was added to a suspension of L-phenylalanine (0.54 g, 3.27 mmol) in EtOH:CHCl₃ (1:15 ml). The solution of 1,3-Bis(1-isocyanato-1-methylethyl)benzene (0.38 ml, 1.63 mmol) in CHCl₃ (15 ml) was slowly added to the mixture solution. The mixture was stirred under reflux for 48 h. The 20 ml of water was added and extracted by CHCl₃ (4x50 ml). Then CHCl₃ phase was evaporated under vacuum. The solid was recrystallized by 20:30 ml of acetone: hexane for 3h. The suspension was then filtrated and washed with cold CHCl₃ (40 ml) to afford a white solid (0.921g, 1.36 mmol, 84 % yield) mol. wt. = 675.40. ¹H NMR (400 MHz, DMSO-d₆) δ 7.33-7.06, (m, 14H, ArH), 6.55 (s, 1H, a-NH), 6.50 (s, 1H, b-NH), 6.19 (m, 1H, a-NH), 6.01 (d, ³J= 4.0 Hz, 1H, b-NH), 4.22 (q, ³J= 8.0 Hz, 2H, CH₂CHNH), 3.90 (m, 1H, CH₃CH₂NH⁺), 2.87-2.95 (m, 4H, CHCH_xH_yAr), 2.76 (q, ³J= 8 Hz, 6H, CH₃CH₂NH⁺), 1.49 (d, ³J= 4.0 Hz 6H, CCH_{3x}), 1.46 (d, ³J= 8.0 Hz 6H, CCH_y), 1.05 (t, 9H, ³J= 8.0 Hz, CH₃CH₂NH⁺); ¹³C{¹H} NMR (400 MHz, DMSO-d₆) δ 174.88 (a-CO₂⁻), 174.46 (b-CO₂H), 157.17 (a-C=O), 156.88 (b-C=O), 148.81 (ArC), 138.48 (a-ArC), 138.23 (b-ArC), 129.82 (a-ArC), 129.72 (b-ArC), 128.45 (a-ArC), 128.43, 127.66 (a-ArC), 127.58(b-ArC), 126.63 (a-ArC), 126.54(b-ArC), 122.84 (a-ArC), 122.68(b-ArC), 122.54 (a-ArC), 121.70 (b-ArC), 54.93 (a-CCH₃), 54.83 (b-CCH₃), 54.70 (a-CH), 54.63 (b-CH), 45.78 (NCH₂CH₃), 38.47 (a-CH₂), 38.39 (b-CH₂), 31.40 (a-CH_{3x}), 31.14 b-CH_{3x}), 30.86 (a-CH_{3y}), 30.80 (b-CH_{3y}), 10.36 (NCH₂CH₃); ESI (m/z): 575.56 m/z [M-Et₃N+H]⁺ (calc. 575.28 m/z), 597.49 m/z [M-Et₃N+Na]⁺ (calc. 597.49 m/z); **analysis calc.** for C₃₈H₅₃N₅O₆: C 67.53, H 7.90, N 10.36%; found: C 65.77, H 7.72, N 9.74%. The compound was found to strongly retain CHCl₃ **calc.** for C₄₇H₈₂N₆O₆·0.2CHCl₃: C 64.32, H 9.38, N 9.48%. The residual CHCl₃ can be observed by ¹H NMR at δ 8.34 (s).

3.2.2.10 Compound 6a

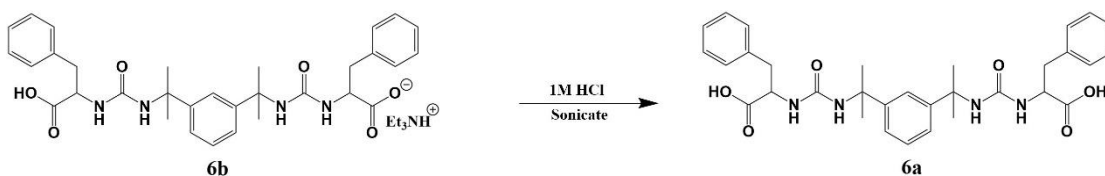


Figure 3.12 Synthetic pathway of compound **6a**.

Compound **6b** was suspended in 1 M aqueous HCl (250 ml), and then sonicated for 30 min. The suspension was filtrated and washed by water and cold CHCl_3 . White solid was achieved (0.594 g, 1.03 mmol, 63 % yield) mol. wt. = 574.28. $^1\text{H NMR}$ (400 MHz, DMSO- d_6) δ 12.57 (s, 2H, OH) 7.47-7.04 (m, 14H, ArH), 6.51 (s, 2H, NH), 6.04 (d, $^3J = 8$ Hz, 2H, NH), 4.31 (q, $^3J = 8$ Hz, 2H, CH_2CHNH), 2.98 (dd, $^3J = 4$ Hz, 2H, $\text{CH}_x\text{H}_y\text{Ar}$), 2.85 (dd, $^3J = 4$ Hz, 2H, $\text{CH}_x\text{H}_y\text{Ar}$), 1.47 (d, $^3J = 4$ Hz, 12H, ArCH_2CH_3); $^{13}\text{C}\{^1\text{H}\}$ NMR (400 MHz, DMSO- d_6) δ 174.35 (CO_2H), 156.85 (C=O), 148.64 (ArC), 137.81 (ArC), 129.71 (ArC), 128.59 (ArC), 127.60 (ArC), 126.84 (ArC), 122.71 (ArC), 121.71 (ArC), 54.81 (CCH_3), 53.87 (CH), 38.24 (CH_2), 30.69 (CH_{3x}), 30.56 (CH_{3y}); **ESI** (m/z): 575.48 m/z $[\text{M}+\text{H}]^+$ (calc. 575.28 m/z), 597.49 m/z $[\text{M}+\text{Na}]^+$ (calc. 597.49 m/z); **analysis calc.** for $\text{C}_{32}\text{H}_{38}\text{N}_4\text{O}_6$: C 66.88, H 6.67, N 9.75%; found: C 66.50, H 6.83, N 9.64%.

3.2.3 Gel screening test

The gelation behavior of gelator was examined in several solvents with different polarity, including, water, ethanol (EtOH), methanol (MeOH), 1-propanol, acetone, dimethyl sulfoxide (DMSO), chloroform, hexane, cyclohexane and cyclohexanone. The conditions of sample in each system were studied as shown in Table 3.1. 0.5 mL of each solvent was added to 5 mg (1% wt) of each gelator in a sealed vial. The mixture was sonicated for 30 seconds, and then heated by using heat gun for 30 seconds. The gel formation was carried out by turning vial upside down under ambient temperature.

Table 3.1 Various conditions used in gels screening test.

Exp.	Compound	wt%	Solvent	Time measurement
1.	1 – 6b	1	Water	5 min-7day
2.	1 – 6b	1	EtOH	5 min-7day
3.	1 – 6b	1	MeOH	5 min-7day
4.	1 – 6b	1	1-Propanol	5 min-7day
5.	1 – 6b	1	Acetone	5 min-7day
6.	1 – 6b	1	DMSO	5 min-7day
7.	1 – 6b	1	Chloroform	5 min-7day
8.	1 – 6b	1	Hexane	5 min-7day
9.	1 – 6b	1	Cyclohexane	5 min-7day
10.	1 – 6b	1	Cyclohexanone	5 min-7day
11.	1 – 6b	1	10% EtOH	5 min-7day
12.	1 – 6b	1	20% EtOH	5 min-7day
13.	1 – 6b	1	50% EtOH	5 min-7day

3.2.4 Preparation of hybrid GQDs/Gels

The **GQDs/Gels** were prepared by following method. GQDs solution and phosphate buffer (0.5 mL of mixture solution in various condition) was added to 0.25 mg of gelators (0.5% wt) in a sealed vial. The various conditions of samples were listed in Table 3.2. Then the suspension was sonicated for 30 seconds and heated for 30 seconds until the suspension was dissolved and ended up with sonicating for 10 seconds. The gel formation was monitored by turning vial upside down under ambient temperature.

Table 3.2 Various conditions used in **GQDs/Gels** preparation.

Exp.	Compound	wt%	Solvent	GQDs (mg/mL)	PB buffer	
					(mM)	(pH)
1.	1 – 6b	1	water	2	-	-
2.	4a, 4b, 4c	0.25, 0.5, 1	water	2	-	-
3.	4a, 4b, 4c	0.5	water	2	10	8
4.	4b	0.3, 0.5, 1, 2, 3	water	-	10	8
5.	4b	0.3, 0.5, 1, 2, 3	water	2	10	8
6.	4b	0.5	water	0, 0.5, 1, 2, 3	10	8
7.	4b	0.5	water	2	10	6,7,8,9
8.	4a, 4b, 4c	0.5	water	2	10, 25, 50	8

3.2.5 Impact of H₂O₂ toward the GQDs/Gels

The hybrid **GQDs/Gels** were screened to study the H₂O₂-responsive by monitoring the naked-eyed fluorescence changing after addition of H₂O₂ under UV lamp (λ_{ex} 365 nm). Initially, 0.2 mL of 1M H₂O₂ was added to 0.5 mL of **GQDs/Gels** (0.5 wt% and 1 wt% of **4b** with 2 mg/mL of GQDs in 10 mM phosphate buffer pH 8) in sealed vial at room temperature.

The hybrid **GQDs/Gels** were reasonably utilized to study the H₂O₂-responsive by following their photoluminescence intensity after adding H₂O₂. Initially, 0.2 mL of H₂O₂ with various concentration and 0.2 mL of water were added to 1.2 mL of **GQDs/Gels** in sealed vial and incubated at 37 °C for 20 min. After that, the sample was heated and transferred to a cuvette and left for 15 min under ambient condition before measuring the photoluminescence intensity. The **GQDs/Gels** were studied upon the final concentration of 1.25 mg/ml of GQDs and 0.3125 %wt of **4b** in 12.5 mM phosphate buffer.

3.2.6 Preparation of hybrid GQDs/Enz/Gels

The 2 mg/mL GQDs solution and 10 mM pH 8 of phosphate buffer was added to 0.5 mg of **4b** (0.5 wt% of gelator in 1 mL of mixture solution) in a sealed vial. Then the suspension was sonicated for 30 seconds followed by heating for 30 seconds until the suspension was dissolved and ended up with sonicating for 10 seconds. After 5 min, 0.1 mL of acetylcholinesterase (AChE) and 0.1 mL choline oxidase (ChOx) in 10 mM

phosphate buffer were added to the partial gels and the mixture was left under 5 °C for 24 h to form hybrid hydrogels of **GQDs/Enz/Gels** biosensor.

The enzyme activity of **GQDs/Enz/Gels** was carried out by addition of acetylcholine (ACh). Parameters such as temperature, pH, concentration of enzyme and acetylcholine were studied to improve the signal of sensor or signal amplification which were collected in Table 3.3.

Table 3.3 Parameters used in signal amplification of **GQDs/Enz/Gels**.

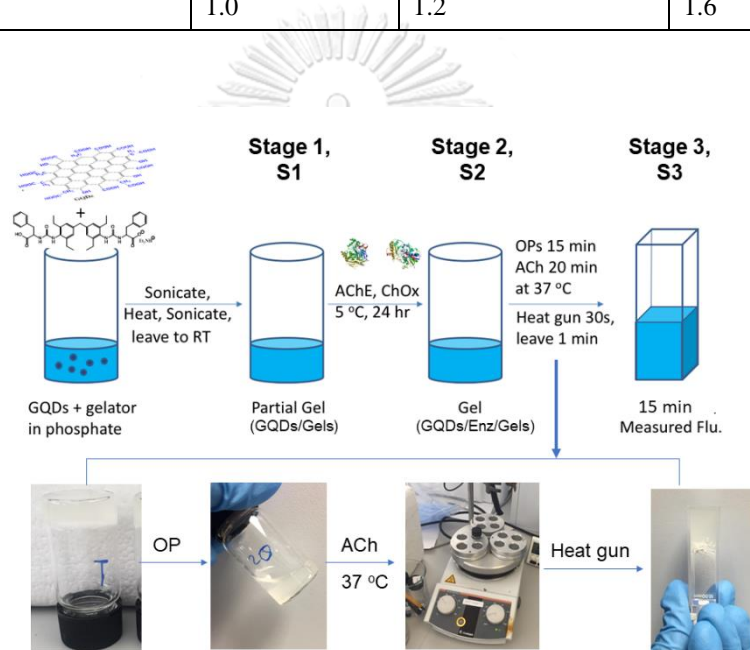
Exp.	Parameter	Studied range	unit
1.	Temperature	25 and 37	°C
2.	pH	7-9	-
3.	Concentration of AChE	0.625-2.5	U/mL
4.	Concentration of ChOx	0.15625-0.625	U/mL
5	Concentration of ACh	2.5-10	mM

3.2.7 The determination of organophosphate pesticides

The hybrid **GQDs/Enz/Gels** were utilized to determine the organophosphate pesticides (OPs) by monitoring their photoluminescence intensity after adding OPs. Firstly, 0.2 mL OPs with various concentrations were added to 1.2 mL of **GQDs/Enz/Gels** in sealed vial and incubated at 37 °C for 15 min. After that, 0.2 mL of 40 mM of acetylcholine (ACh) was added to the sample solution and the mixture was continuously incubated at 37 °C for 20 min. Then the mixture was re-heated by heat gun. After 1 min cooling down, the mixture was transferred to a cuvette and left to form gel for 15 min. The PL intensity was measured with the same method as H₂O₂-responsive study. Each experiment was repeated 3 times. The **GQDs/Enz/Gels** were studied under the final concentration of 1.25 mg/ml of GQDs, 1.25 U/mL of AChE, 0.3125 U/mL of ChOx and 0.3125 %wt of **4b** in 12.5 mM phosphate buffer pH 8. The concentration of each component and the preparation of hybrid biosensor before and after OPs detection were defined in stage 1-3 and shown in Table 3.4 and Figure 3.13.

Table 3.4 Final concentration of component in **GQDs/Enz/Gels** for organophosphate detection.

Component	Stage 1 (GQDs/Gels)	Stage 2 (GQDs/Enz/Gels)	Stage 3 OPs detection
GQDs (mg/mL)	2.00	1.67	1.25
Gelator 4b (wt%)	0.50	0.4167	0.3125
Phosphate buffer pH 8 (mM)	10.00	16.67	12.50
AChE (U/mL)	-	1.67	1.25
ChOx (U/mL)	-	0.4167	0.3125
OPs (M)	-	-	$1.25 \times 10^{-9} - 1.25 \times 10^{-4}$
ACh (mM)	-	-	5.00
V_{final} (mL)	1.0	1.2	1.6

**Figure 3.13** Preparation of **GQDs/Enz/Gels** for organophosphate pesticides (OPs) detection.

The photoluminescence spectra of **GQDs/Enz/Gels** were recorded *via* PTI QuantaMasterTM spectrofluorometer at room temperature as a function of time under following condition.

<i>Parameter</i>	
<i>Start (nm)</i>	368
<i>End (nm)</i>	700
<i>Excitation (nm)</i>	360
<i>Excitation Slit</i>	2.5
<i>Emission Slit</i>	1.5
<i>Emission (nm)</i>	465

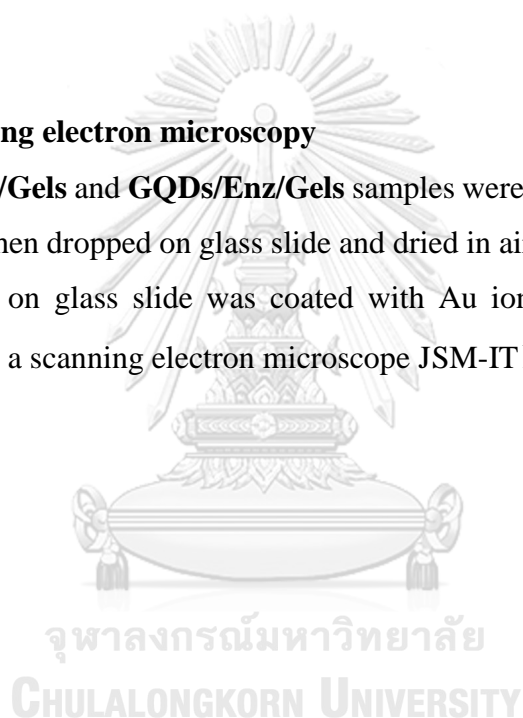
The percentage of enzyme inhibition (I%) was plotted as a function of the concentration of organophosphate pesticide to obtain calibration curve.

3.2.8 Rheology

Rheological measurements were carried out with an AR2000 rheometer at 10 °C. Frequency sweep experiments were performed at a constant oscillation stress of 0.5 Pa for the angular frequency of 0.1–100 rad/sec. The stress sweep was performed at a constant angular frequency of 1 Pa for the oscillation stress of 0.1–1000.

3.2.9 Scanning electron microscopy

The **GQDs/Gels** and **GQDs/Enz/Gels** samples were prepared for 1 and 30 min, respectively, and then dropped on glass slide and dried in air at room temperature for 2 days. The sample on glass slide was coated with Au ions and SEM images were measured by using a scanning electron microscope JSM-IT100.



3.3 Result and discussions

In this work, we attempt to explore the novel supramolecular hydrogels which can encapsulate small molecules such as graphene quantum dots and especially enzymes. This hybrid enables to retain their activity. In our previous work [56], the hydrogels based urea and ionisable salicylic acid system have established the key of gel formation depending on the carboxyl-terminal group of salicylic acids and the non-steric hindrance around the urea carbonyl group of gelator.

Predictable gelators based on bis(urea) system have been studied by varying two hydrophobic central spacers including methylenebis(diethylphenyl) (compound **1-4**) and bis(methylethyl)benzene (compound **5-6**) conjugated to the end group of biocompatible amino acid derivatives, including amino acid methyl ester based L-valine methyl ester (**1**) and L-phenylalanine methyl ester (**3** and **5**); aliphatic amino acid based L-leucine (**2c**); and aromatic amino acid based L-phenylalanine (**4a-c** and **6a-b**; the **a**, **b** and **c** are composed of 0, 1 and 2 of triethylammonium cations in structure, respectively). As we expect, the bis(urea) system and methylene bis(diethyl phenyl) spacer could promote the gelation *via* hydrogen bonding and hydrophobic interaction, respectively. Furthermore, ionizable amino acid system possibly encourages water solubility and enzyme compatibility.

3.3.1 Characterization of compound 1-6b

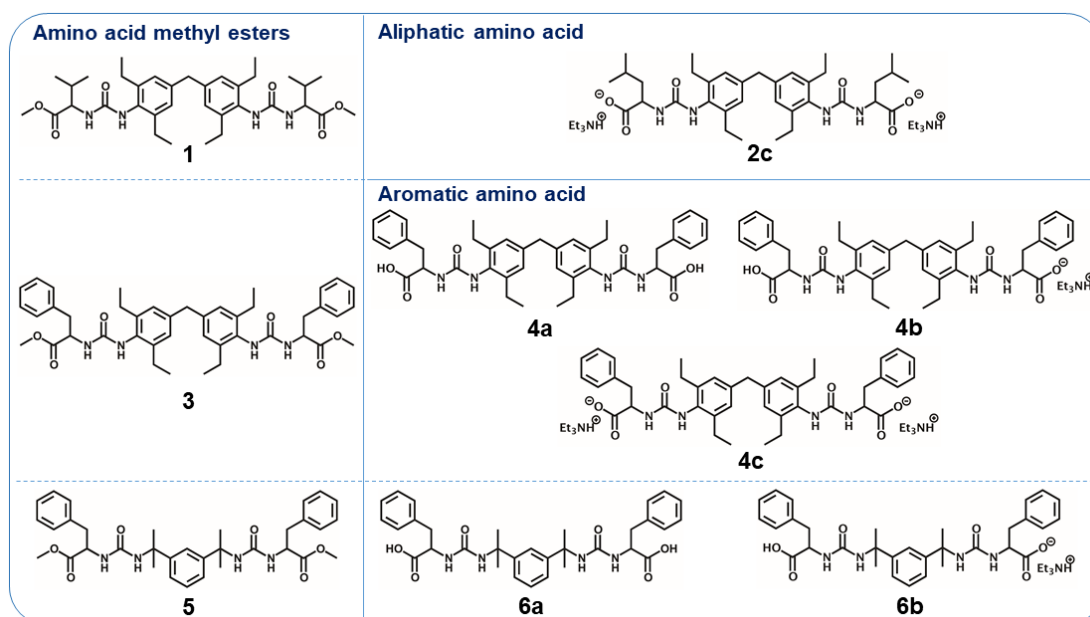


Figure 3.14 The molecular structures of compound 1-6b.

All molecular structures of attractive gelators were showed in Figure 3.14. The synthesis of all compounds was achieved from one-step reaction of isocyanate and amino acid derivatives in the presence of triethylamine base. Then, the characterization of all compounds was investigated by ^1H NMR, $^{13}\text{C}\{^1\text{H}\}$ NMR, mass spectrometry and elemental analysis. The ^1H NMR spectra and analytical data can confirm the presence of carboxylic acid at the C-terminal or the carboxylate moiety with different number of triethylammonium cations 0, 1 and 2 Et_3NH^+ (characteristic peak at δ 2.70 and 1.05 ppm) in compounds **4a**, **4b** and **4c**, respectively, as shown in Figure 3.15. To confirm the conjugation between hydrophobic central spacer and amino acid, D_2O exchanged experiment was carried out by monitoring the decrease of NH-bis(urea) protons at δ 7.59 and 6.28 ppm upon the increment of D_2O . The ^1H -NMR spectra of 4,4'-methylenebis(2,6-diethylphenyl isocyanate), **1**, **2c**, **3**, **5**, **6a** and **6b** were displayed in Figure A1 to A7 (in Appendix). Mass spectra of all compounds revealed in Figure A8 to A16. The mass spectra of **4a**, **4b** and **4c** showed 693.36 m/z, regarding to $[\text{M}+\text{H}]^+$ without Et_3NH^+ counter ion in molecular structure (Figure A11 to A13 in Appendix).

Fortunately, $^1\text{H-NMR}$ and elemental analysis can prove the existence of Et_3NH^+ in structure.

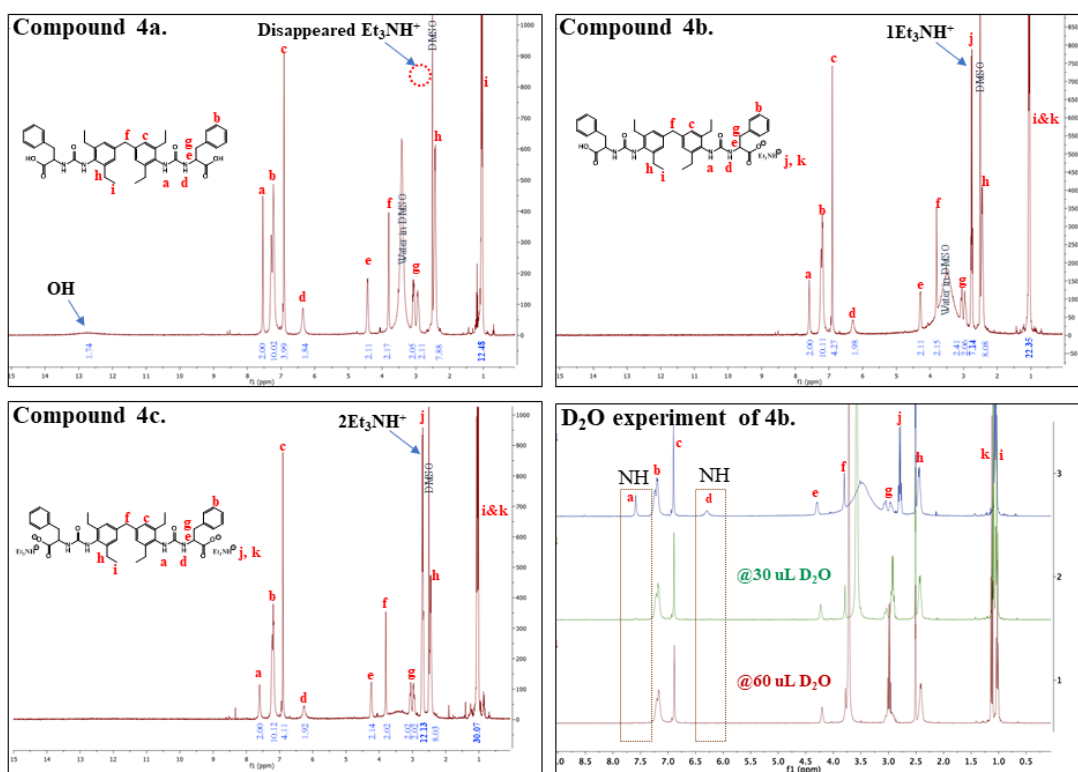


Figure 3.15 NMR spectra of compounds 4a-4c and D_2O experiment of compound 4b.

3.3.2 Gel screening

Owing to a well-constructed hydrogel property, the gelation behavior of all synthesized compounds was tested in several solvents and recoded in Table 3.5. The behavior of solution (S), insoluble (I), rapid precipitate formed from solution (P), partial gel (PG), gel (G) and collapsed gel (CG) were observed upon the assigned picture in Figure 3.16



Figure 3.16 The assigned behavior of solution (S), insoluble (I), rapid precipitate formed from solution (P), partial gel (PG), gel (G) and collapsed gel (CG).

Table 3.5 Gel formation studies of compounds **1-6b**.

Compound	wt%	Solvent	Time							comment
			1 min	5 min	30 min	4 h	24 h	48 h	7 days	
1	1.0	Water	I	I	I	I	I	I	I	
1	1.0	EtOH	S	P	P	P	P	G	G	
1	1.0	MeOH	S	P	P	P	P	P	P	
1	1.0	1-Propanol	S	P	P	P	P	P	G	
1	1.0	Acetone	S	G	G	G	G	G	G	
1	1.0	DMSO	S	S	S	S	P	P	P	
1	1.0	Chloroform	S	P	P	P	P	P	P	
1	1.0	Hexane	I	I	I	I	I	P	P	
1	1.0	Cyclohexane	I	I	I	I	I	P	P	
1	1.0	Cyclohexanone	S	G	G	G	G	G	G	
1	1.0	10% EtOH/Water	P	P	P	P	P	P	P	
1	1.0	20% EtOH/Water	P	P	P	P	P	P	P	
1	1.0	50% EtOH/Water	S	P	P	P	P	P	P	
2c	1.0	Water	I	I	I	I	I	I	I	
2c	1.0	EtOH	I	I	I	I	I	I	I	
2c	1.0	MeOH	I	I	I	I	I	I	I	
2c	1.0	1-Propanol	P	P	P	P	P	P	P	
2c	1.0	Acetone	I	I	I	I	I	I	I	
2c	1.0	DMSO	S	S	P	P	P	P	P	
2c	1.0	Chloroform	P	P	P	P	P	P	P	
2c	1.0	Hexane	I	I	I	I	I	I	I	
2c	1.0	Cyclohexane	P	P	P	P	P	P	P	
2c	1.0	Cyclohexanone	S	S	S	S	S	S	S	
2c	1.0	10% EtOH/Water	I	I	I	I	I	I	P	
2c	1.0	20% EtOH/Water	I	I	I	I	I	I	P	
2c	1.0	50% EtOH/Water	S	P	P	P	P	P	P	

G = gel, PG = partial gel, CG = collapsed gel, S = Solution, I = insoluble, P = rapid precipitate formed from solution

Table 3.5 Gel formation studies of compounds 1-6b (continued).

Compound	wt%	Solvent	Time							comment
			1 min	5 min	30 min	4 h	24 h	48 h	7 days	
3	1.0	Water	I	I	I	I	I	I	I	
3	1.0	EtOH	G	G	G	G	G	G	G	
3	1.0	MeOH	G	G	G	G	G	G	G	
3	1.0	1-Propanol	G	G	G	G	G	G	G	
3	1.0	Acetone	G	G	G	G	G	G	G	
3	1.0	DMSO	S	S	S	S	S	S	S	
3	1.0	Chloroform	S	S	S	S	PG	G	G	
3	1.0	Hexane	P	P	P	P	P	P	P	
3	1.0	Cyclohexane	P	P	P	P	P	P	P	
3	1.0	Cyclohexanone	S	G	G	G	G	G	G	
3	1.0	10% EtOH/Water	I	P	P	P	P	P	P	
3	1.0	20% EtOH/Water	P	P	P	P	P	P	P	
3	1.0	50% EtOH/Water	P	P	P	P	P	P	G	
4a	1.0	Water	I	I	I	I	I	I	I	
4a	1.0	EtOH	S	P	P	P	P	P	P	
4a	1.0	MeOH	S	P	P	P	P	P	P	
4a	1.0	1-Propanol	S	P	P	G	G	G	G	
4a	1.0	Acetone	P	G	G	G	G	G	G	
4a	1.0	DMSO	S	S	S	S	S	S	S	
4a	1.0	Chloroform	P	P	P	P	P	P	P	
4a	1.0	Hexane	P	P	P	P	P	P	P	
4a	1.0	Cyclohexane	P	P	P	P	P	P	P	
4a	1.0	Cyclohexanone	S	G	G	G	G	G	G	
4a	1.0	10% EtOH/Water	P	P	P	P	P	P	P	
4a	1.0	20% EtOH/Water	P	P	P	P	P	P	P	
4a	1.0	50% EtOH/Water	S	G	G	G	G	G	G	
4b	1.0	Water	S	PG	PG	PG	PG	PG	PG	
4b	1.0	EtOH	S	P	P	P	P	P	P	
4b	1.0	MeOH	P	P	P	P	P	PG	PG	
4b	1.0	1-Propanol	S	P	P	P	P	P	P	
4b	1.0	Acetone	P	P	P	P	P	P	P	
4b	1.0	DMSO	S	S	S	S	S	S	S	
4b	1.0	Chloroform	S	PG	PG	G	G	G	G	
4b	1.0	Hexane	I	I	I	I	I	I	I	
4b	1.0	Cyclohexane	I	I	P	P	P	P	P	
4b	1.0	Cyclohexanone	S	G	G	G	G	G	G	
4b	1.0	10% EtOH/Water	S	S	S	S	PG	PG	PG	
4b	1.0	20% EtOH/Water	G	G	G	G	G	G	G	
4b	1.0	50% EtOH/Water	G	G	G	G	G	G	G	
4c	1.0	Water	S	S	S	S	PG	PG	PG	Clear PG
4c	1.0	EtOH	S	S	S	S	P	P	P	
4c	1.0	MeOH	S	S	S	S	P	P	P	
4c	1.0	1-Propanol	S	S	S	S	P	P	P	
4c	1.0	Acetone	S	G	G	G	G	G	G	
4c	1.0	DMSO	S	S	S	S	S	S	S	
4c	1.0	Chloroform	S	G	G	G	G	G	G	
4c	1.0	Hexane	I	I	P	P	P	P	P	
4c	1.0	Cyclohexane	I	I	P	P	P	P	P	
4c	1.0	Cyclohexanone	S	G	G	G	G	G	G	
4c	1.0	10% EtOH/Water	S	S	S	S	PG	PG	G	
4c	1.0	20% EtOH/Water	S	S	S	S	PG	PG	G	
4c	1.0	50% EtOH/Water	S	S	S	S	P	P	P	

G = gel, PG = partial gel, CG = collapsed gel, S = Solution, I = insoluble, P = rapid precipitate formed from solution

Table 3.5 Gel formation studies of compounds **1-6b** (continued).

Compound	wt%	Solvent	Time							comment
			1 min	5 min	30 min	4 h	24 h	48 h	7 days	
5	1.0	Water	I	I	I	I	I	I	I	
5	1.0	EtOH	S	S	S	S	S	S	S	
5	1.0	MeOH	S	S	S	S	S	S	S	
5	1.0	1-Propanol	S	S	S	S	S	S	S	
5	1.0	Acetone	S	S	S	S	S	S	S	
5	1.0	DMSO	S	S	S	S	S	S	S	
5	1.0	Chloroform	S	S	S	S	S	S	S	
5	1.0	Hexane	P	P	P	P	P	P	P	
5	1.0	Cyclohexane	P	P	P	P	P	P	P	
5	1.0	Cyclohexanone	S	S	S	S	S	S	S	
5	1.0	10% EtOH/Water	S	I	I	I	I	I	I	
5	1.0	20% EtOH/Water	S	I	I	I	I	I	I	
5	1.0	50% EtOH/Water	S	S	S	S	S	S	P	
6a	1.0	Water	I	I	I	I	P	P	P	
6a	1.0	EtOH	S	S	S	P	P	P	P	
6a	1.0	MeOH	S	S	S	P	P	P	S	
6a	1.0	1-Propanol	S	S	S	P	P	P	P	
6a	1.0	Acetone	I	I	P	P	P	P	P	
6a	1.0	DMSO	S	S	S	S	S	S	S	
6a	1.0	Chloroform	I	I	I	I	I	I	I	
6a	1.0	Hexane	I	P	P	P	P	P	P	
6a	1.0	Cyclohexane	I	P	P	P	P	P	P	
6a	1.0	Cyclohexanone	S	S	PG	PG	PG	PG	PG	
6a	1.0	10% EtOH/Water	I	P	P	P	P	P	P	
6a	1.0	20% EtOH/Water	I	P	P	P	P	P	P	
6a	1.0	50% EtOH/Water	S	P	P	P	P	P	P	
6b	1.0	Water	S	I	I	I	I	I	I	
6b	1.0	EtOH	S	S	S	S	S	S	S	
6b	1.0	MeOH	S	S	S	S	S	S	S	
6b	1.0	1-Propanol	S	S	S	S	S	S	S	
6b	1.0	Acetone	S	S	S	S	S	S	S	
6b	1.0	DMSO	S	S	S	S	S	S	S	
6b	1.0	Chloroform	S	S	S	P	P	P	P	
6b	1.0	Hexane	I	I	P	P	P	P	P	
6b	1.0	Cyclohexane	S	I	I	P	P	P	P	
6b	1.0	Cyclohexanone	S	S	S	S	S	S	S	
6b	1.0	10% EtOH/Water	S	I	I	P	P	P	P	
6b	1.0	20% EtOH/Water	S	I	I	P	P	P	P	
6b	1.0	50% EtOH/Water	S	S	S	S	S	S	S	

G = gel, PG = partial gel, CG = collapsed gel, S = Solution, I = insoluble, P = rapid precipitate formed from solution

The gel formation studies in various solvent under varying time were carried out by turning the vials upside down under ambient temperature. The results listed in Table 3.5 showed the different properties of each gelator for gel formation in various solvents. As a result, 1%wt of compounds with bis(methylethyl)benzene space group (**5**, **6a** and **6b**) cannot form gel in any solvents due to an interruption of hydrogen bonding formation from steric hindrance around urea carbonyl group [56]. In case of 1%wt of compounds with methylenebis(diethylphenyl) space group (**1**, **3**, **4a**, **4b** and **4c**, except **2c**), they showed a good gelation behavior in many solvents, for example

EtOH, 50%EtOH, MeOH, acetone, chloroform and cyclohexanone. Deeply considering, the gelators containing the aromatic amino acid in carboxylic form as the end group of molecules including **4b** and **4c** exhibited the potential soluble and form partial gel in water. The gelation studied for only compound **4b** was illustrated in Figure 3.17.

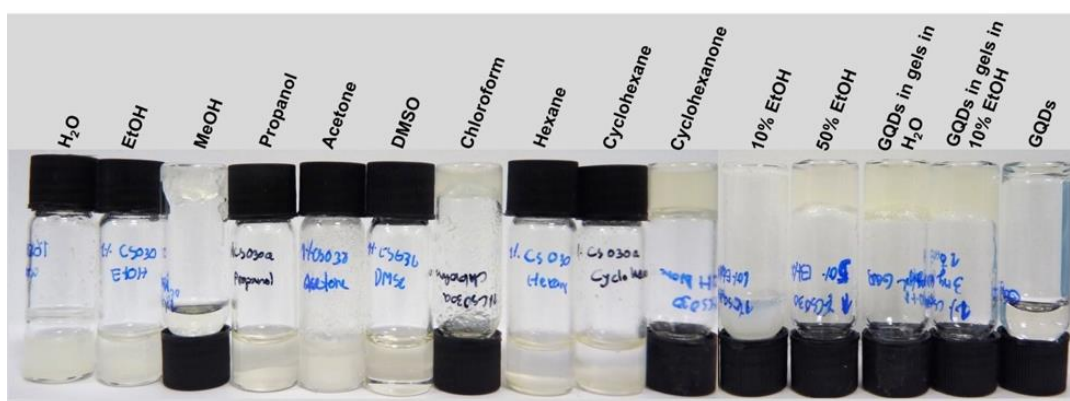


Figure 3.17 Gel formations of 1wt% of compounds **4b** in various solvents.

3.3.3 Preparation of hybrid GQDs/Gels

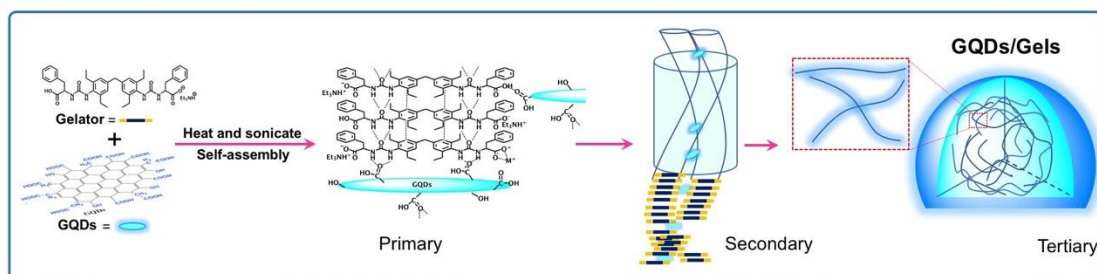


Figure 3.18 Proposed primary, secondary and tertiary structures of hybrid GQDs hydrogel materials (GQDs/Gels).

Taking on a broad of sensing application, most of numerous sensing system has demonstrated in water since most target analyte is soluble in water. Regarding to gelator formation study, no gel formation was observed in water. Previous work by our group [56], GQDs enable to encourage the gel formation of gelator in water. We, thus, investigated the hybrid hydrogel formation of each gelator integrated with GQDs in water. The preparation was divided into two pathways; (i) sample was sonicated for 30 seconds followed by heating for 30 seconds, called M1; (ii) sample was sonicated for 30 seconds followed by heating for 30 seconds and ended up with sonicating for 10 seconds, called M2. In Figure 3.19, method 2 (M2) with a good dispersion of GQDs in gels was selected for further studies.

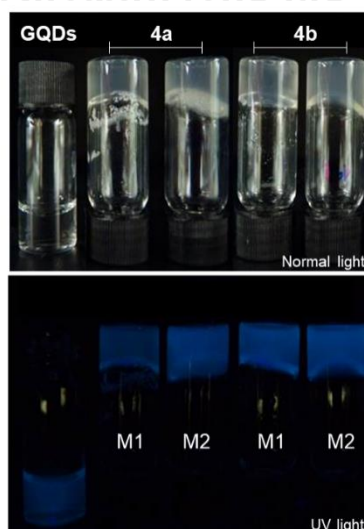


Figure 3.19 Comparison between hybrid GQDs/Gels from 4a and 4b that formed by method 1 (M1) and method 2 (M2).

Table 3.6 GQDs/Gels formation studies of compounds 1-6b.

Compound	wt%	Solvent	GQDs (mg/ml)	Time							Comment
				1 min	5 min	30 min	4 h	24 h	48 h	7 days	
1	1.0	water	2	I	I	I	I	I	I	I	
2c	1.0	water	2	I	I	I	I	I	I	I	
3	1.0	water	2	I	I	I	I	I	I	I	
4a	1.0	water	2	S	G	G	G	G	G	G	
4a	0.5	water	2	S	PG	PG	G	G	G	G	
4a	0.25	water	2	S	PG	PG	PG	PG	PG	PG	
4b	1.0	water	2	G	G	G	G	G	G	G	
4b	0.5	water	2	PG	PG	G	G	G	G	G	
4b	0.25	water	2	S	PG	PG	PG	PG	PG	PG	
4c	1.0	water	2	S	PG	PG	G	G	G	G	
4c	0.5	water	2	S	S	S	PG	PG	PG	PG	
4c	0.25	water	2	S	S	S	S	S	PG	PG	
5	1.0	water	2	S	P	P	P	P	P	P	
6a	1.0	water	2	S	P	P	P	P	P	P	
6b	1.0	water	2	S	I	I	I	I	P	P	

G = gel, PG = partial gel, CG = collapsed gel, S = Solution, I = insoluble, P = rapid precipitate formed from solution

The hybrid hydrogel formation of each gelator integrated with GQDs in water was illustrated in Table 3.6. Surprisingly, the gel formation in water was observed for compounds **4a** and **4b** within 5 min. Of particular interest in the organophosphate detection based on enzymatic reaction is the fact that the enzyme would be immobilized in the hybrid hydrogel. Therefore, we attempt to retard the hydrogel formation to facilitate the penetration of enzyme in the hydrogel. Presumably, decrease of amount of gelators at 0.5% wt and 0.25 %wt would retard the hydrogel formation time. From Table 3.6, the hybrid hydrogels formation by **4b** (0.5 wt%) in water was found to be retarded within 30 min. In contrast to other gelators, the gel formation has not been success except **4c** (0.5 wt%) with a gel formation time in 4 h.

3.3.3.1 The effect of GQDs toward GQDs/Gels formation

To the best of our knowledge, supramolecular gels were spontaneously formed primary structure in solution by interactions between each low molecular weight hydrogelators (LMWGs) *via* non-covalent interactions such as hydrogen bonding, van der Waals interaction and hydrophobic forces. The secondary and tertiary structures were further arisen from the aggregation of primary strand into α -helix/ β -sheet and fibrous network[52, 53]. Conversely, in water, the hydrogen bonding between gelators in primary structure was interrupted. Undoubtedly, the dominant force of a self-assembled hydrogels was the hydrophobic interaction[87]. The GQDs in this work have the sp^2 -hybridized carbon network surrounded by $-COOH$ - and $-OH$ - functional groups at the edge of graphene. They might easily interact with the gelators using π - π stacking between the hydrophobic spacer or aromatic of phenylalanine, and hydrogen bonding between carboxylate terminal of amino acid resulting in the water gel formations [36, 53, 84, 88]. The proposed primary, secondary and tertiary structures of hybrid GQDs hydrogel materials (**GQDs/Gels**) was illustrated in Figure 3.18. It was confirmed by the increment of the concentration of GQDs from 0-3 mg/ml as shown in Table 3.7. The data showed that the gelator preferred to form the hybrid hydrogels upon the increment of GQDs. It suggested that the gelation process was gradually observed within 30 minutes in the presence of 2 and 3 mg/ml of GQDs and **4b** at 0.5 wt%.

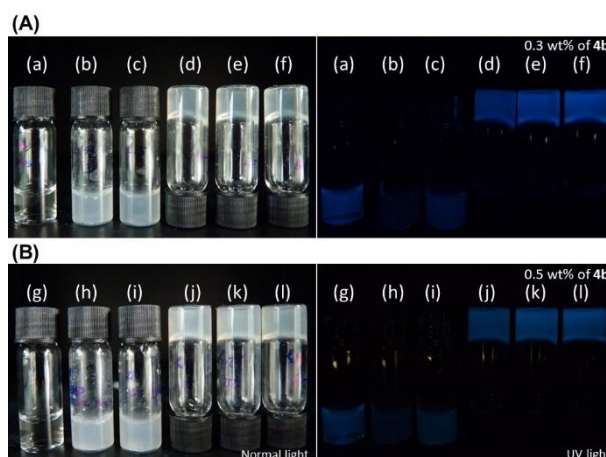


Figure 3.20 The gelation behavior by 0.3%wt of **4b** (A) and 0.5%wt of **4b** (B) at various amount of GQDs at 0 (b, h), 0.5 (c, i), 1 (d, j), 2 (e, k) and 3 mg/mL (f, l). For GQDs solution at 2 mg/mL (a, g) in 10 mM phosphate buffer pH 8 for 24 h. The left picture was taken in normal light and right picture was taken under 365 nm UV light.

Table 3.7 GQDs/Gels formation studies in various concentration of gelator **4b** and GQDs.

Gelator 4b (wt%)	Solvent	GQDs (mg/ml)	Time							Comment
			1 min	5 min	30 min	4 h	24 h	48 h	7 days	
0.3	10 mM Phosphate pH 8	-	S	PG	PG	PG	PG	PG	PG	
0.5	10 mM Phosphate pH 8	-	S	PG	PG	PG	PG	PG	PG	
1	10 mM Phosphate pH 8	-	S	PG	PG	PG	PG	PG	PG	
2	10 mM Phosphate pH 8	-	S	PG	G	G	G	G	G	Opaque
3	10 mM Phosphate pH 8	-	S	G	G	G	G	G	G	Opaque
0.3	10 mM Phosphate pH 8	2	S	PG	PG	G	G	G	G	
0.5	10 mM Phosphate pH 8	2	S	PG	G	G	G	G	G	
1	10 mM Phosphate pH 8	2	S	G	G	G	G	G	G	Robust
2	10 mM Phosphate pH 8	2	S	G	G	G	G	G	G	Opaque
3	10 mM Phosphate pH 8	2	S	G	G	G	G	G	G	Opaque
0.3	10 mM Phosphate pH 8	0	S	PG	PG	PG	PG	PG	PG	
0.3	10 mM Phosphate pH 8	0.5	S	PG	PG	PG	PG	PG	G	
0.3	10 mM Phosphate pH 8	1	S	PG	PG	PG	G	G	G	
0.3	10 mM Phosphate pH 8	2	S	PG	PG	G	G	G	G	
0.3	10 mM Phosphate pH 8	3	S	PG	PG	G	G	G	G	
0.5	10 mM Phosphate pH 8	0	S	PG	PG	PG	PG	PG	PG	
0.5	10 mM Phosphate pH 8	0.5	S	PG	PG	PG	PG	G	G	
0.5	10 mM Phosphate pH 8	1	S	PG	PG	G	G	G	G	
0.5	10 mM Phosphate pH 8	2	S	PG	G	G	G	G	G	
0.5	10 mM Phosphate pH 8	3	S	PG	G	G	G	G	G	
1	10 mM Phosphate pH 8	0	S	PG	PG	PG	PG	PG	PG	
1	10 mM Phosphate pH 8	0.5	S	PG	PG	PG	PG	G	G	
1	10 mM Phosphate pH 8	1	S	PG	G	G	G	G	G	Robust
1	10 mM Phosphate pH 8	2	S	G	G	G	G	G	G	Robust
1	10 mM Phosphate pH 8	3	S	G	G	G	G	G	G	Robust

G = gel, PG = partial gel, CG = collapsed gel, S = Solution, I = insoluble, P = rapid precipitate formed from solution

3.3.3.2 The effect of pH toward GQDs/Gels formation

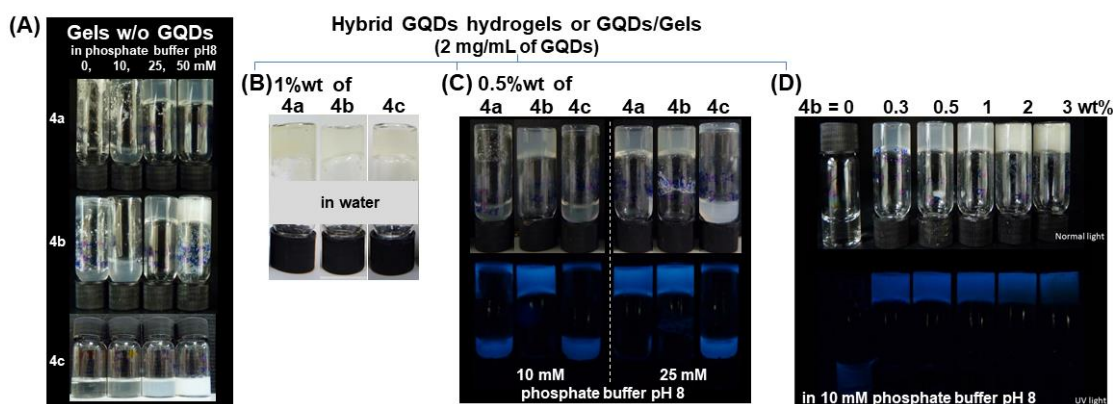


Figure 3.21 Photographs of gel behavior at 30 min (A) gel formation studies of gelators **4a**, **4b** and **4c** without GQDs in various concentration of phosphate buffer pH 8; the **GQDs/Gels** from 1wt% gelators **4a**, **4b** and **4c** in water (B); and 0.5% wt gelator under different concentration of phosphate buffer (C) and different wt% of gelator **4b**, in 10 mM phosphate buffer pH 8 (D) respectively.

The pH effect is one crucial factor which might impact on enzymatic activities. Thus the gelation behavior of **4a-4c** integrated with GQDs in different pH of 6-9 at 10 mM buffer solution was investigated and the results were collected in Table 3.8 and pointed out the similarly efficient gelation behavior in case of water and phosphate buffer solution pH 8. Furthermore, the study on the different concentration ranged 10-50 mM of buffer solution pH 8 surprisingly revealed the complete hydrogel formation at the concentration of buffer at 25 and 50 mM with and without GQDs incorporation (as shown in Table 3.9). For visual study in gelation behavior, Figure 3.21A-D demonstrated the gelation behavior in the different concentration of phosphate buffer pH 8 from 10 to 50 mM with and without GQDs. Surprisingly, the good gel formation without GQDs was observed by 0.5wt% of **4a** and **4b** in phosphate buffer pH 8.0 at the concentration of 25-50 mM for gelation time of 30 min (Figure 3.21A). Deeply considering Figure 3.21C and Figure 3.21D, gelator **4b** at concentration of 0.5 wt% incorporated GQDs can form a potential hybrid hydrogel and high brightness in 10 mM phosphate buffer solution pH 8.0. The results show that the neutral compound of **4b** (pH 7.52) bearing one Et_3NH^+ can form hydrogels better than compounds **4a** (pH 4.87) and **4c** (pH 9.98) containing 0 and 2 of Et_3NH^+ , respectively, owing to the easy

adjustment to equilibrium between carboxylic acid and carboxylate forms at amino group[49].

Accordingly, we assumed that the GQDs and phosphate buffer (pH) are the important roles for the formation of hybrid hydrogels by acting as the cooperative species in this work. Hence, the concentration of the bis(urea-phenylalanine) based compound **4b** in 10 mM phosphate buffer pH 8 was carried out in the range of 0-3 wt% as displayed in Figure 3.21D. Interestingly, the transparent hybrid **GQDs/Gels** at the concentration of 0.5 and 1 wt% of **4b** in a presence of 2 mg/ml of GQDs in 10 mM of phosphate buffer pH 8 were chosen for further photoluminescent (PL) applications.



Table 3.8 Gel formation studies of gelators **4a-4c** in a range of pH between 6-9.

Gelator	%	Solvent	GQDs (mg/ml)	Time					Comment
				1 min	5 min	30 min	24 h	7 days	
4a	0.5	Water	-	I	I	I	I	I	
4a	0.5	Water	2	S	PG	PG	G	G	
4a	0.5	10 mM Phosphate pH6	2	S	PG	PG	G	G	
4a	0.5	10 mM Phosphate pH7	2	S	PG	PG	G	G	
4a	0.5	10 mM Phosphate pH8	2	S	PG	PG	G	G	
4a	0.5	10 mM Tris pH8	2	S	PG	PG	PG	G	4a is not all dissolved
4a	0.5	10 mM Tris pH9	2	S	PG	PG	PG	G	
4b	0.5	Water	-	PG	PG	PG	PG	PG	
4b	0.5	Water	2	PG	PG	G	G	G	
4b	0.5	10 mM Phosphate pH6	2	S	PG	PG	G	G	
4b	0.5	10 mM Phosphate pH7	2	S	PG	PG	G	G	
4b	0.5	10 mM Phosphate pH8	2	S	PG	G	G	G	
4b	0.5	10 mM Tris pH8	2	S	PG	G	G	G	4b is not all dissolved
4b	0.5	10 mM Tris pH9	2	S	PG	PG	PG	G	
4c	0.5	Water	-	S	S	S	S	PG	
4c	0.5	Water	2	S	S	PG	PG	PG	
4c	0.5	10 mM Phosphate pH8	2	S	S	PG	G	G	

Table 3.9 Gel formation studies of gelators **4a-4c** in different concentration of phosphate buffer pH 8.

Gelator	%wt	Phosphate buffer pH 8 (mM)	GQDs (mg/ml)	pH (measured)	Time			comment
					1 min	5 min	30 min	
4a	0.5	-	-	4.87	I	I	I	
4b	0.5	-	-	7.52	S	PG	PG	
4c	0.5	-	-	9.98	S	S	S	
4a	0.5	10	-	7.71	S	PG	PG	
4b	0.5	10	-	7.80	S	PG	PG	
4c	0.5	10	-	8.78	S	S	S	
4a	0.5	25	-	7.89	S	PG	G	
4b	0.5	25	-	7.97	S	G	G	Robust
4c	0.5	25	-	8.62	S	S	PG	
4a	0.5	50	-	7.86	S	G	G	
4b	0.5	50	-	7.93	S	G	G	Opaque
4c	0.5	50	-	8.41	S	PG	PG	Opaque
-	0.0	-	4	7.70	-	-	-	
4a	0.5	10	2	7.76	S	PG	PG	
4b	0.5	10	2	7.84	S	PG	G	Robust
4c	0.5	10	2	8.68	S	S	PG	
4a	0.5	25	2	7.83	S	G	G	Robust
4b	0.5	25	2	7.90	S	G	G	Robust
4c	0.5	25	2	8.42	S	PG	PG	
4a	0.3125	12.5	1.25	7.84	S	PG	PG	
4b	0.3125	12.5	1.25	7.93	S	PG	G	
4c	0.3125	12.5	1.25	8.17	S	S	S	

G = gel, PG = partial gel, CG = collapsed gel, S = Solution, I = insoluble, P = rapid precipitate formed from solution

3.3.3.3 The rheological properties

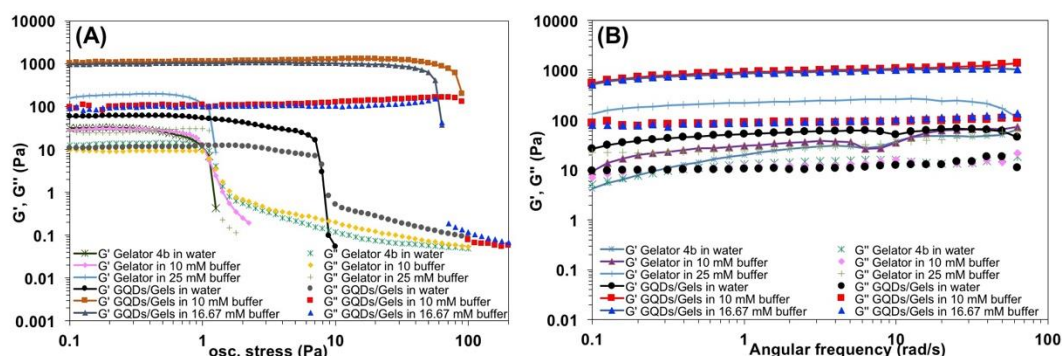


Figure 3.22 (A) Stress sweep and (B) frequency-sweep rheology of gelator **4b** and **GQDs/Gels** from **4b** in different conditions.

Table 3.10 Summarized values of storage modulus and loss modulus of **GQDs/Gels** in various condition

Gelator	wt%	GQDs (mg/ml)	PB buffer (mM)	Storage modulus, G' (Pa)	Loss modulus, G'' (Pa)
4b	0.5	-	0	30±2	14±1
4b	0.5	-	10	28±1	9±0.2
4b	0.5	-	25	187±12	26±2
4b	0.5	2	0	60±1	11±0.3
4b	0.5	2	10	1160±75	112±14
4b	0.5	2	16.7	1011±28	100±5

To gain more informative gelation properties, the studies of frequency and stress sweep rheometry were examined. The rheological properties of salt-compound **4b** and **GQDs/Gels** in water and phosphate buffer pH 8 were shown in Figure 3.22A-B. The storage modulus (G') and loss modulus (G''), which represent the solid and liquid-like behavior, respectively, were summarized in Table 3.10. The salt-compound **4b** exposed some very weak partial gels in water with low G' value. The gelator integrated with GQDs and phosphate buffer enhanced the G' value for gel formation. Interestingly, the gel formation under optimized condition by **4b** is relatively weak with G' values of 30-1100 Pa and yield stress around 10-100 Pa which are accepted for effective hydrogel. Concerning the G' value of gelation properties, the results are consistent with the gelation behavior by visual studies suggesting the strong hybrid hydrogel obtained by the incorporating **4b** with GQDs and phosphate buffer, which can support the proposed structure of **GQDs/Gels** as in Figure 3.18 at the primary stage.

3.3.4 Preparation of hybrid GQDs/Enz/Gels materials

In this work, the hybrid hydrogel for sensing application was prepared in 3 stages. For stage 1 (S1), the adaptive partial gels of the integrated gelator and GQDs were performed. After that, AChE and ChOx in phosphate buffer were added to the partial gels and the as-prepared materials were left for 24 h until the complete gels formation, defined as stage 2 (S2). The final stage (S3) was carried out in the sensing step.

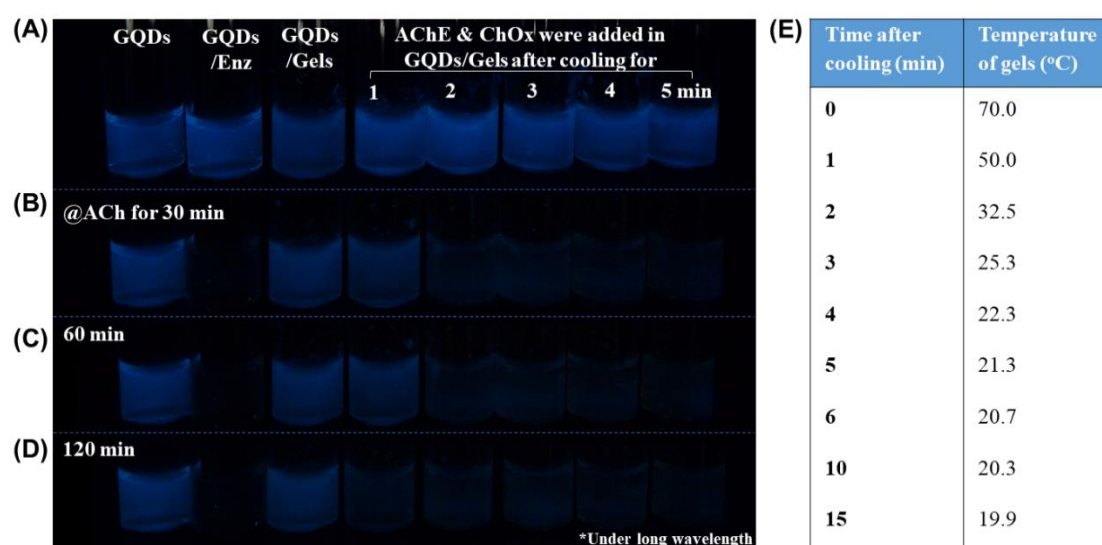


Figure 3.23 The fluorescent images of **GQDs**, **GQDs/Enz**, **GQDs/Gels** and **GQDs/Enz/Gels** before (A) and after incubation in acetylcholine for 30 (B), 60 (C) and 120 min (D). The **GQDs/Enz/Gels** were prepared by cooling down of **GQDs/Gels** from 1 to 5 min, and then, enzymes were added and kept at 5 °C for 24 h prior activity tests. (E) The temperature of **GQDs/Gel** after cooling at room temperature from 0-15 min.

To prepared **GQDs/Enz/Gels** (stage 2), the cooling time of **GQDs/Gels** (stage 1) before addition of bi-enzyme was considerably studied for enzyme activity. The 0.5 mL of each **GQDs/Gels** was prepared and cooled between 1 to 5 min at ambient condition (20 °C in UK), then, 0.1 mL of AChE and ChOx was added and kept at 5 °C for 24 h (see Figure 3.23).

The 0.1 mL of 10 mg/mL (55 mM) acetylcholine (ACh) was added to the **GQDs/Enz/Gels**. The observation of the enzyme activity by naked-eyed under UV-light (λ_{ex} 365 nm) was realized at 30, 60 and 120 min, respectively, (Figure 3.23B-D).

From Figure 3.23B, the PL response of sensing platform reacted with ACh for 30 min exhibited a large PL quenching in the system by cooling time in a range of 2 to 5 min. The high efficiency of enzymatic reaction was address under the proper temperature about 32-20 °C regarding to the cooling time of 2 to 15 min, respectively, (Figure 3.23E). These results proved that the enzyme activity was destroyed at high temperature with a respect of cooling time of 1 min. The cooling time over 2 min can retain the enzyme activity. The addition of enzyme during the partial gel formation process at 5 min was well suited for further experiments.

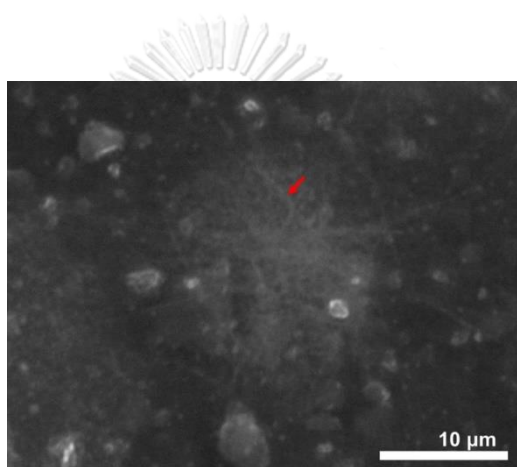


Figure 3.24 SEM image of gelator **4b** in 10 mM phosphate buffer.

To study the formation of hybrid hydrogels with enzymes, SEM images were expected to gain more informative network structure of **GQDs/Gels (S1)** and **GQDs/Enz/Gels (S2)**. The gelator **4b** in 10 mM phosphate buffer solution showed SEM image of nucleated dots and few fibrous networks with average diameter of 200 nm as shown in Figure 3.24. In case of **GQDs/Gels (S1)**, SEM image of xerogel in Figure 3.25B exhibited several short and small nanofiber or fibrous gel with average diameter of 290 nm (calculated 100 particles from SEM by using ImageJ software) ascribing by the initially self-assembling cooperative GQDs and amino acid gelators after heating for 1 min. The well-constructed supramolecular networks of **GQDs/Enz/Gels (S2)** have been found after 30 min of the gelation with enzyme and the inset showed longer fibrous network, which was additionally surrounded by many small fibres with average diameter of 50 nm (blue arrow). It was assumed that the small

fibers gradually self-assembled formed with GQDs to be hydrophobic hybrid supramolecular networks via hydrophobic interaction (π - π interaction) and hydrogen bonding[41, 46, 84-86]. Particularly, the hydrophilic enzymes could be entrapped inside the aqueous cavity or the surface of hydrophobic nano/microfiber of hydrogel as shown in Figure 3.25A to retain their activity [50, 89]. Unfortunately, the GQDs with size distribution less than 10 nm could not be observed in SEM image of this hybrid material[58].

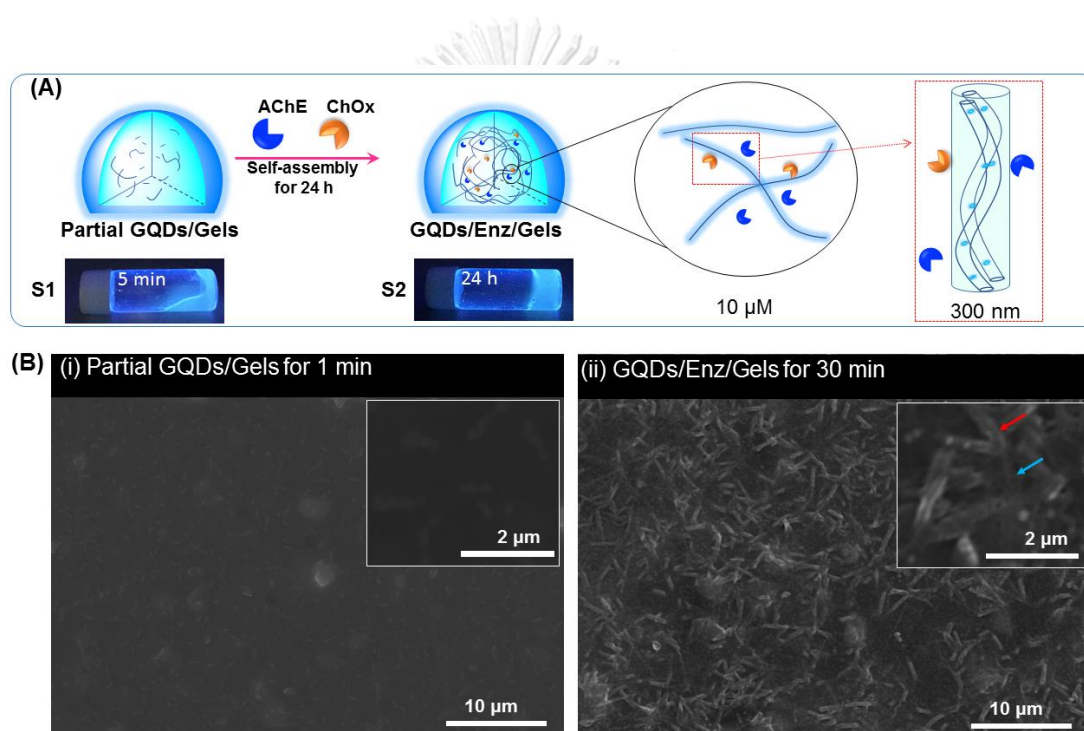
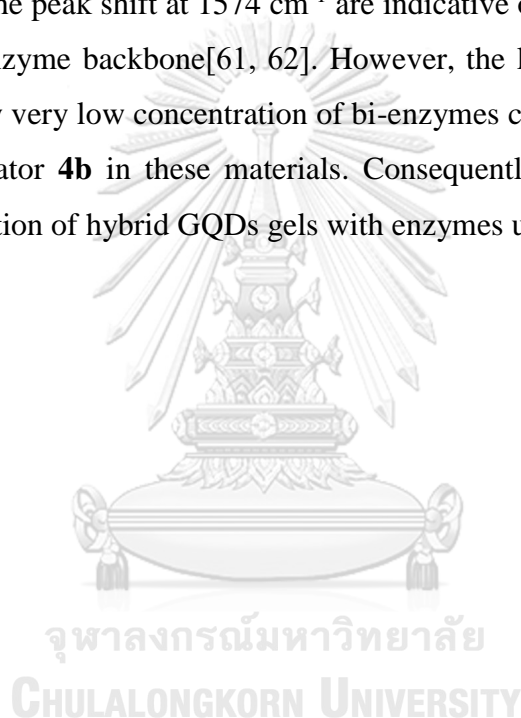


Figure 3.25 (A) Preparation of partial **GQDs/Gels** (stage 1) and **GQDs/Enz/Gels** hybrid hydrogels (stage 2). (B) SEM images of the partial gels in stage 1 that was prepared for 1 min and the hybrid hydrogels in stage 2 that was prepared for 30 min before dropping on stuff and dried for 2 days.

The FT-IR spectra of xerogel of hybrid **GQDs/Enz/Gels** materials were represented the combination of GQDs, enzymes and gelator **4b** as illustrated in Figure 3.26. Spectrum of these hybrid materials showed a broad absorption band at 3000-3500 cm^{-1} ($\nu_{\text{O-H}}$), shifted peaks at 1633-1645 cm^{-1} (ν_{asCOO} and ν_{CN} of amide I of enzymes), 1574 cm^{-1} ($\nu_{\text{asCOO-}}$ of GQDs), 1574-1496 (δ_{NH} and ν_{CN} of urea in gelator **4b** and amide II of enzymes) in both of both of gelator **4b** and enzymes[61, 62] as well as 1386 cm^{-1} ($\nu_{\text{sCOO-}}$) and 1077 cm^{-1} ($\nu_{\text{C-OH}}$), belonging to the characteristic peak of -COOH and -OH group of the edge of GQDs, respectively. Additionally, the appearance of a small peak at 1641 cm^{-1} and the peak shift at 1574 cm^{-1} are indicative of an amide I and amide II, respectively, of enzyme backbone[61, 62]. However, the low intensity of enzyme is possibly caused by very low concentration of bi-enzymes compared to a large amount of GQDs and gelator **4b** in these materials. Consequently, these results reveal the cooperative formation of hybrid GQDs gels with enzymes upon cooling down to room temperature.



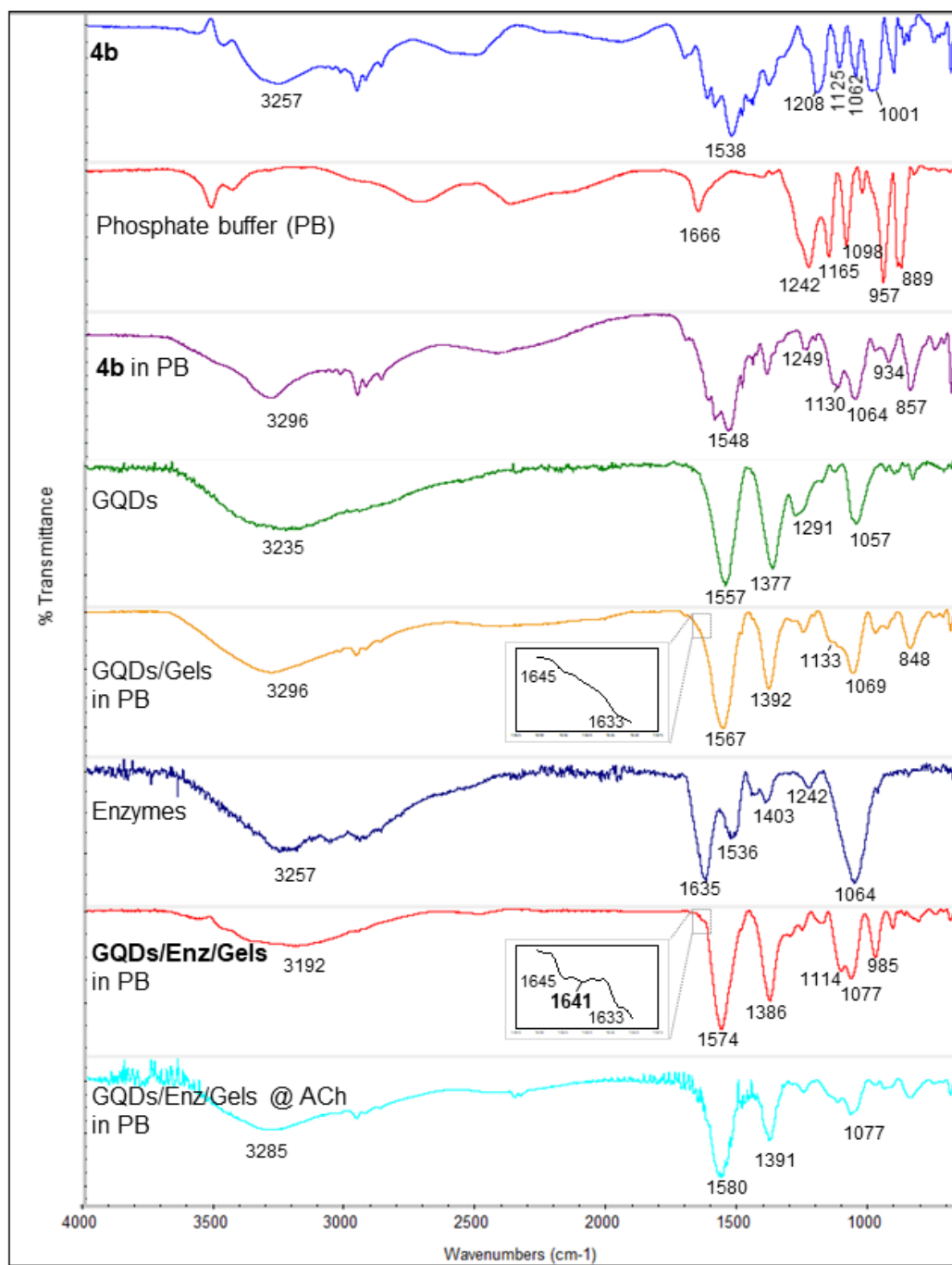


Figure 3.26 FT-IR spectra of starting materials and xerogel of the hybrid hydrogels.

3.3.5 Impact of H₂O₂ toward GQDs/Gels

Nowadays, the detection of H₂O₂ is widely utilized for many clinical diagnostics because it is an important by-product in many bio-reactions, for example, the catalytic reaction of glucose and choline by glucose oxidase and choline oxidase, respectively[49]. Carbon quantum dots species (CQDs) were reported as the peroxide-responsive materials, which exhibited the catalytic properties toward the oxidation of 3,3,5,5,-tetramethylbenzidine (TMB) in a reaction with H₂O₂ for detecting glucose[20, 21]. Likewise, GQDs themselves demonstrated a good capability to catalyze H₂O₂ to be H₂O [26, 58].

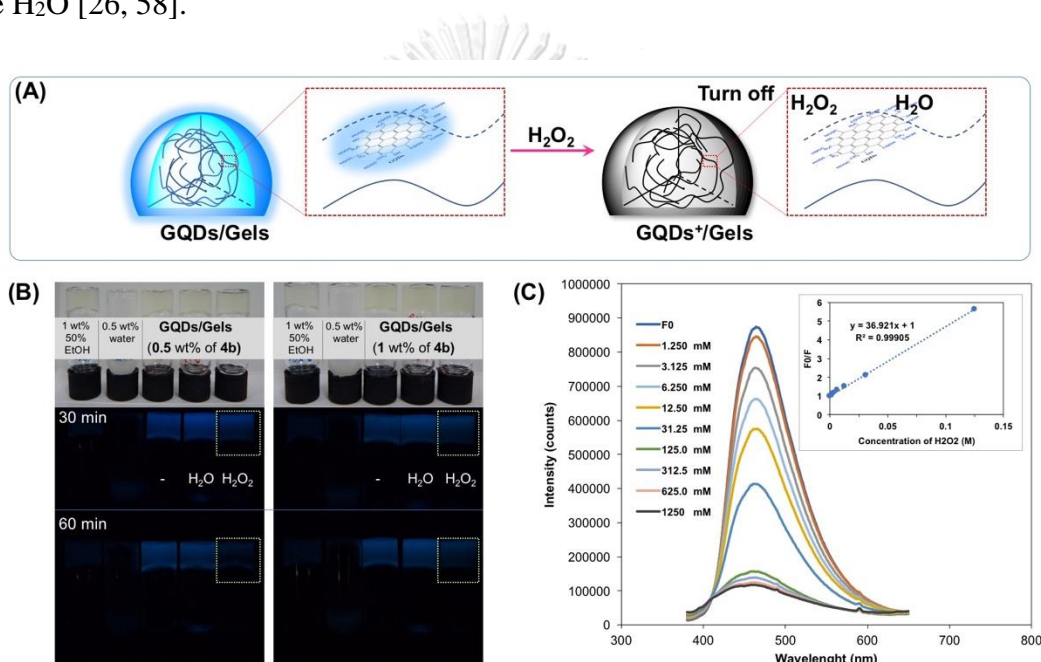


Figure 3.27 (A) Illustration of peroxidase-catalytic reaction of **GQDs/Gels**. (B) Comparison between concentration of **4b** (0.5 and 1 wt%) toward naked-eyed brightness quenching by slow passing of H₂O₂ from top to bottom of vials at room temperature. (C) Concentration-dependent PL changes of **GQDs/Gels** after interaction with H₂O₂ between 0 and 1250 mM at 37 °C for 20 min. Inset of C is Stern-Volmer plots from PL of **GQDs/Gels** after interaction with H₂O₂ at concentration ranging from 0 to 125 mM.

According to the good photoluminescent (PL) properties of our hybrid **GQDs/Gels**, we attempt to utilize these hybrid materials for study on the H₂O₂-responsive ability *via* the PL quenching upon interaction with H₂O₂. The concentration of **4b** at 0.5 and 1 wt% was used to prepare the hybrid GQDs hydrogels in 10 mM

phosphate buffer pH 8. The time-dependent naked-eyed brightness of hybrid **GQDs/Gels** upon the addition of 200 μL of 1 M H_2O_2 was monitored in Figure 3.27B. At 60 min, the brightness quenching of hybrid **GQDs/Gels** by 0.5 wt% of **4b** was higher than 1 wt% of **4b**. It was implied that the 0.5 wt% of gelator **4b** might form the weak gels resulting in an easier penetration of H_2O_2 through the weak gels than a strong one. The 0.5 wt% of **4b** was selected to further study on the H_2O_2 -reponsive ability. The intensity of PL spectra of **GQDs/Gels** was gradually decreased upon an increment of H_2O_2 from 0 to 1250 mM as shown in Figure 3.27C. The Stern-Volmer equation[66, 67] ($I_0/I = 1.0 + K_{sv}[\text{Analytes}]$) of the relative PL quenching of **GQDs/Gels** was plotted in Figure 3.27C-inset. This reveals the quenching effect relied on the concentration of H_2O_2 with the Stern-Volmer constant, K_{sv} of 36.92 L/mol. Notably, the GQDs-quenched mechanism has not been clearly identified. However, the peroxidase-like catalytic activity by graphene oxide and graphene dots was anticipated *via* an electron transfer process[20, 26]. It was implied that the abundant electrons on the surface of small particles of GQDs in hybrid hydrogels could transfer to the LUMO of H_2O_2 , then, generating GQDs^+ species[26] with low PL intensity and releasing H_2O as following the proposed mechanism in Figure 3.27A.



3.3.6 Responsibility of H₂O₂-generated *in situ* by the hybrid GQDs/Enz/Gels

As mentioned above, the encapsulated enzymes on materials have been remarkably served their sensitivity and stability[14, 37]. If the entrapment of enzymes in this hybrid hydrogels was successfully performed, H₂O₂ generated *in situ* by active AChE and ChOx could encourage the PL quenching of this material.

The **GQDs/Enz/Gels** were incubated with analyte (this case was acetylcholine) under 37 °C for 20 min, called stage 3 (S3). Moreover, the rheological studies were used to verify the gel properties as illustrated in Figure 3.28. Decrease of gel strength assumedly depended on the dilution effect of hybrid material (S1) and in the presence of enzymes (S2) as well as acetylcholine solution (S3), respectively. However, all stages exhibited an elastic modulus G' higher than the viscous modulus G'' (the G' value of S1 to S3 is 1100 to 50 Pa and yield stress of 100 to 10 Pa), which gave a potential gel state [90] for the sensing application in further sections.

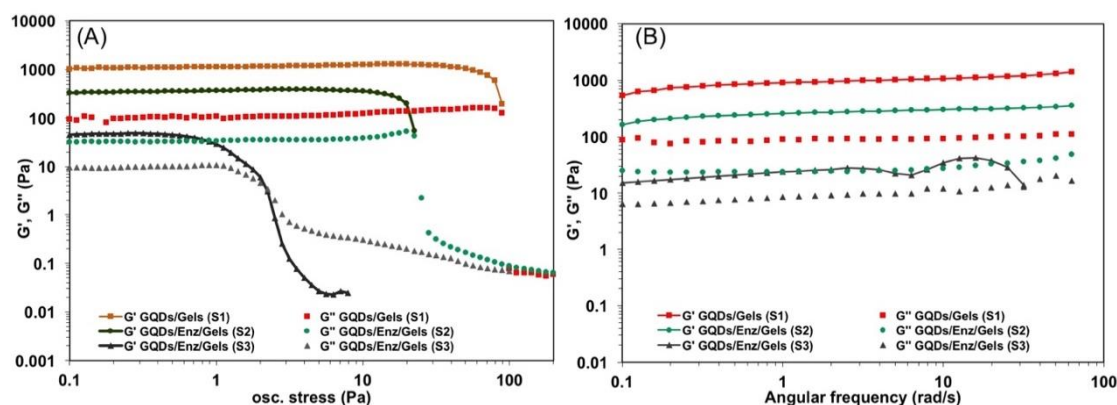


Figure 3.28 Stress sweep and (A) frequency-sweep(B) rheology of **GQDs/Gels** before (S1) and after (S2) adding enzyme, and **GQDs/Enz/Gels** after reacting with acetylcholine (S3).

Fluorescent spectrometry was further used for gelation and *in situ* studies. All hybrid hydrogel samples were prepared and kept at 5 °C for 24 h prior to use. Firstly, the **GQDs/Gels** hybrid materials were re-heated and then transferred to cuvette for PL measurement from 1 min until 20 min. The PL intensity at 465 nm as a function of time was remained unchange after cooling down for 15 min as shown in Figure 3.29

demonstrating an effective gel-reforming of this hybrid materials. Additionally, the concentration range of acetylcholine and organophosphate pesticide did not influence on the PL response of **GQDs/Gels** (Figure 3.30).

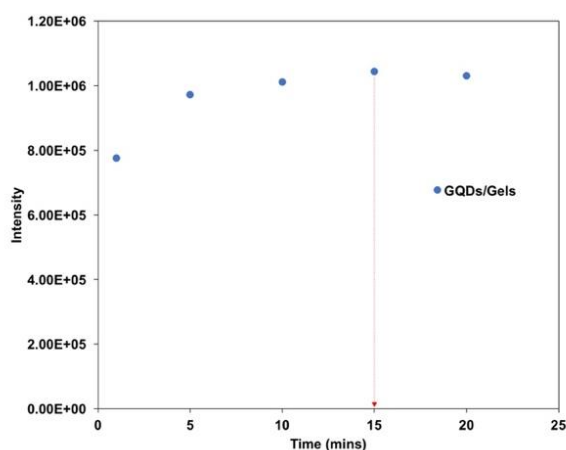


Figure 3.29 Fluorescent intensity of **GQDs/Gels** from gelator **4b** showed stable intensity after re-heating and forming gel again in a cuvette for 15 minutes. The **GQDs/Gels** was prepared under condition of 1.25 mg/ml of GQDs with 0.3125 wt% of **4b** in 12.5 mM phosphate buffer pH 8.

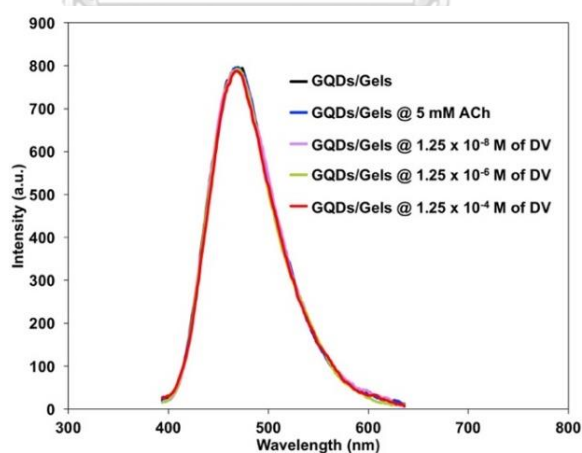


Figure 3.30 Fluorescent intensity of **GQDs/Gels** after addition of ACh and dichlorvos (DV) in a range of 1.25×10^{-8} to 1.25×10^{-4} M.

Incorporation of the GQDs and bi-enzymes in the gels arised the PL intensity compared to the GQDs without gels as displayed in Figure 3.31B. It is noticed that the PL intensity depended on the quantum confinement with regarding to the size, surface and edge of GQDs [24, 27-29]. However, the GQDs solution significantly aggregates at high temperature resulting in the continuous change of PL intensity. Hence, the enhanced PL intensity of this hybrid hydrogels stemmed from the interaction between gelators and GQDs. It was implied that the gelator **4b** with two carboxylic groups would stabilize the single sheet of GQDs resulting in the aggregated prevention[56, 91].

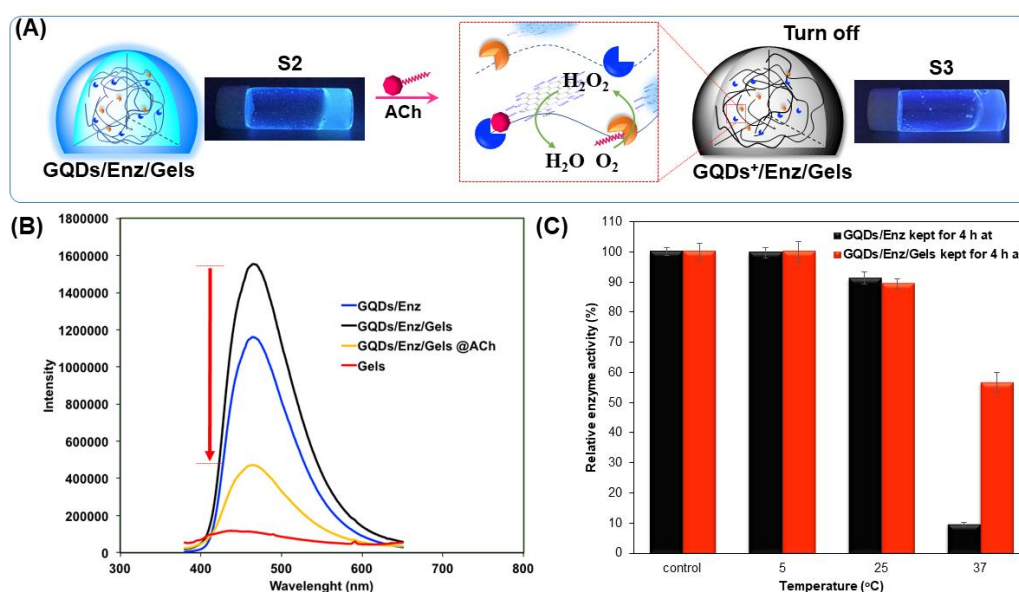
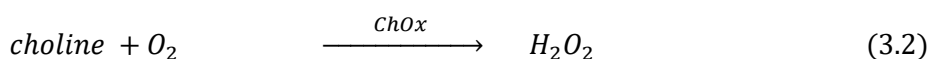
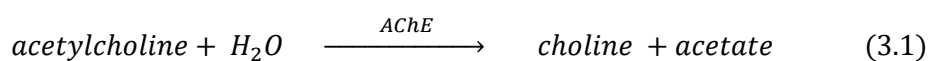


Figure 3.31 (A) Scheme of H₂O₂-responsive in situ of GQDs/Enz/Gels biosensor (stage 3; S3). (B) The PL quenching of biosensor after adding acetylcholine. (C) In comparison of relative enzyme activity between in aqueous solution and gel phase after incubated in 5, 25 and 37 °C for 4 h.

To the best our knowledge, the enzymatic reaction of AChE and ChOx in the presence of acetylcholine was hydrolyzed to be choline and acetate by AChE, and then choline was further oxidized by ChOx to generate H₂O₂.



The **GQDs/Enz/Gels** were incubated with acetylcholine under 37 °C for 20 min (stage3 in Figure 3.31A) and their PL intensity was measured by a spectrofluorometer. From Figure 3.31B, the PL quenching of **GQDs/Enz/Gels** stemmed from H₂O₂ generated from enzymatic reaction as shown in equation 3.1 and 3.2. This material is reliably constructive for further clinical diagnosis as a biomarker or effective organophosphate pesticide sensing.

The immobilization of enzyme in hydrogels for increasing of their thermal stability in industrial and agricultural application has been considerably studied[37, 92]. Generally, average temperature in Thailand is about 19-38 °C, thereby the stability of hybrid material at mild condition from 5-37 °C was reliably concerned. The comparison of relative enzyme activity in aqueous solution and in gel phase was monitored by PL quenching as showed in Figure 3.31C. At 5 °C for 4 h, the relative enzyme activity (%) in both systems showed a similar to the same condition at the initial time (control). The activity of materials stored at room temperature (25 °C) was slightly decreased. Remarkably, the activity of materials was significantly reduced under the storage temperature at 37 °C. Interestingly, the relative enzyme activity after incubated in 37 °C for 4 h in gel phase (more than 50%) were much greater than those in aqueous solution (less than 10%). The results suggested that hydrogels obtained from gelator **4b** based on bis urea spacer and phenylalanine amino acid as end group can stabilize an enzyme. This property is suitable for industrial and agricultural applications in term of a mild temperature using. Furthermore, the activity of **GQDs/Enz/Gels** is more than 90 % upon storing at 5 °C for 15 days as shown in Figure 3.32.

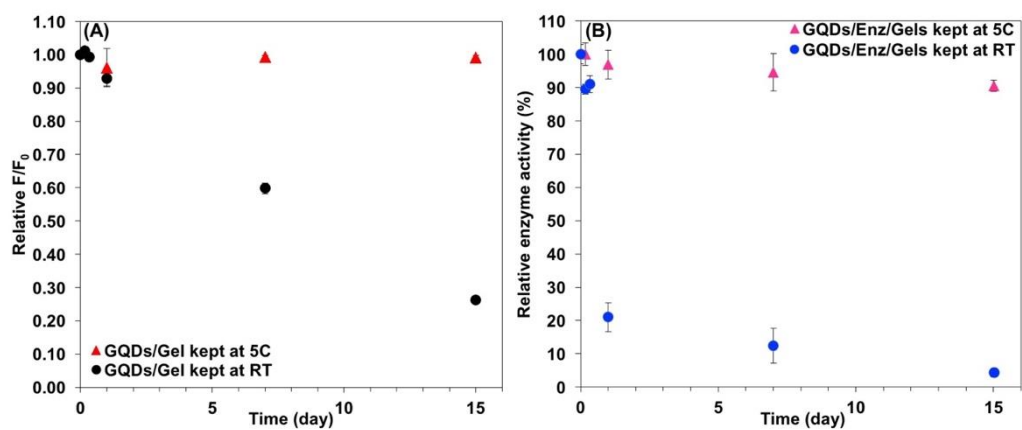


Figure 3.32 (A) Relative F/F_0 of GQDs/Gels. (B) Relative enzyme activity (%) of GQDs/Enz/Gels that were kept in 5 °C and room temperature from 4h to 15 days.



3.3.7 Signal amplification for increasing responsive sensing of GQDs/Enz/Gels

Base on the organophosphate pesticide detection, the optimized conditions such as temperature, pH and concentration of enzymes and acetylcholine are necessary requirement.

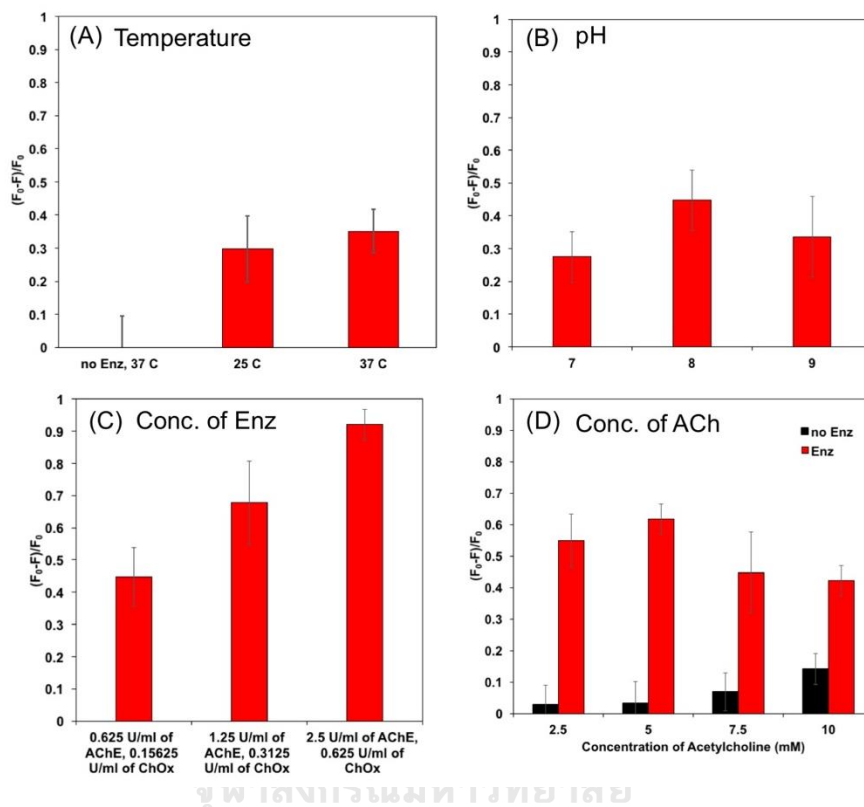
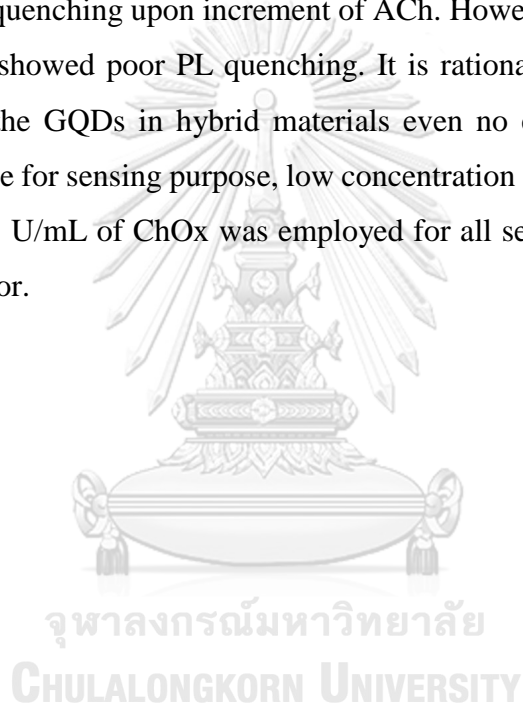


Figure 3.33 Optimized condition such as temperature (A), pH (B), concentration of two enzymes (C) and acetylcholine (D) for sensing application.

For all manipulation, the hybrid hydrogel (**GQDs/Gel**) in the partial state was incubated in ACh for 20 min, then heated and transferred to a cuvette. The mixture was left for 15 min prior to PL measurement. The comparison of normalized PL quenching $(F_0-F)/F_0$ was exhibited in Figure 3.33, where F_0 and F are PL intensity of **GQDs/Gels** and **GQDs/Enz/Gels**, respectively, after incubation with ACh for 20 min. Figure 3.33A and B showed that the normalized PL quenching of **GQDs/Enz/Gels** was increased upon the increment of temperature from 25 °C to 37 °C and pH from 7 to 8, after that the PL quenching were slightly decreased at pH 9. The proper condition for sensing of this materials is 12.5 mM phosphate buffer pH 8 at 37 °C which is an effective condition

of AChE and ChOx for acetylcholine hydrolyzing with a consistent of the previous researches [70-72].

The large photoluminescent quenching of **GQDs/Enz/Gels** was discovered upon the introduction of the enzymes AChE and ChOx at 2.5 U/mL and 0.625 U/mL, respectively, (Figure 3.33C). Interestingly, the PL quenching of **GQDs/Enz/Gels** was increased upon the increment of the concentration of both enzymes. However, the proper concentration of ACh at 5 mM provided the largest PL quenching (Figure 3.33D). Compared to the PL quenching of **GQDs/Enz/Gel**, the **GQDs** in gel showed an increase of PL quenching upon increment of ACh. However, a high amount of ACh (7.5 and 10 mM) showed poor PL quenching. It is rationalized that ACh enabled to directly interfere the GQDs in hybrid materials even no enzyme. Based on a cost-effective alternative for sensing purpose, low concentration of enzyme at 1.25 U/mL of AChE, and 0.3125 U/mL of ChOx was employed for all sensing manipulation of this enzymatic biosensor.



3.3.8 Study on the detection of GQDs/Enz/Gel toward organophosphate

Typically, the organophosphate pesticides (OPs) are widely used in agricultural industry that can generate a serious problem for animal and human health[6]. Consequently, an easy, fast and highly effective detection of OPs are the crucial challenges. In this work, the hybrid **GQDs/Enz/Gels** is an alternative material to expectedly serve as a high potential sensing approach. The proposed mechanism for OPs detection were illuminated in Figure 3.34A. To the best knowledge, the AChE and ChOx can catalyze acetylcholine (ACh) to generate H₂O₂. OPs preferred to bind the covalent bond with the active site of AChE [7], thereby, leading the inactive AChE and a consequent inhibition of H₂O₂-generation in the presence of ACh addition. Consequently, the turned-on PL response was observed. Moreover, it was found that the PL intensity of **GQDs/Enz/Gels** depended on the concentration of dichlorvos which inhibited the activity of AChE in this hybrid hydrogels (Figure 3.34B). Other organophosphate pesticide including, parathion, malathion, and methyl-paraoxon at the concentration of 1.25 and 12.5 μM were further examined in the inhibition efficiency (I%) towards AChE, which was calculated via equation 3.3, where K_{20without} and K_{20withOP} are the photoluminescent quenching with and without OP after incubation in ACh for 20 min (K₂₀ = F₀-F₂₀/20, where F₀ and F are PL intensity of **GQDs/Enz/Gels** in the presence and absence of ACh followed by incubation time for 20 min)[10].

$$I(\%) = \left(\frac{K_{20without} - K_{20withOP}}{K_{20without}} \right) \times 100 \quad (3.3)$$

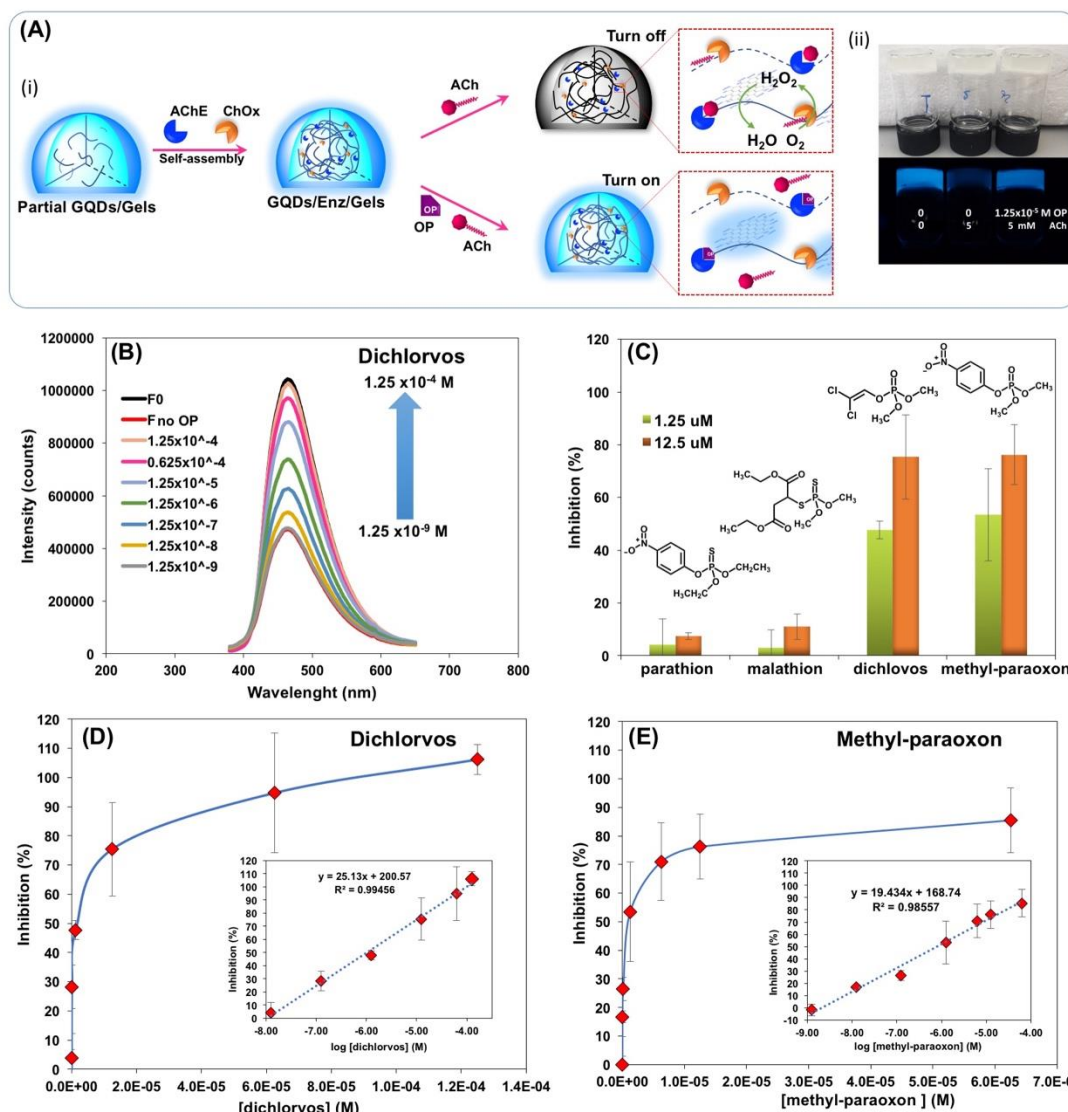


Figure 3.34 (A) Proposed mechanism of hybrid **GQDs/Enz/Gels** for organophosphate pesticide detection. (B) PL intensity of **GQDs/Enz/Gels** upon increment of dichlorvos concentration between 1.25×10^{-9} to 1.25×10^{-4} M (λ_{ex} 360 nm). (C) Comparison of inhibition efficiency (%) of AChE in hybrid hydrogels after incubated in 1.25×10^{-6} and 12.5×10^{-6} M of four OPs. (D) and (E) Inhibition efficiency (%) of AChE in this material after incubation in various concentration of dichlorvos and methyl-paraoxon. Insets of D and E showed linear range of dichlorvos and methyl-paraoxon detections in log concentration of 1.25×10^{-8} to 1.25×10^{-4} M and 1.25×10^{-9} to 0.625×10^{-4} M, respectively.

From Figure 3.34C, the inhibition efficiency (I%) in two concentrations showed the similar trend of the I% for both methyl-paraoxon and dichlorvos which are higher than malathion and parathion, respectively. The inhibition efficiency of AChE by OPs in the oxo-form (P=O) proved to be higher inhibition efficiency (I%) than that of OPs

in thio-form (P=S) possibly caused by the effect of more electrophile phosphorus atom in oxo-form of methyl-paraoxon and dichlorvos than the thio-form of malathion and parathion resulting in the favorable covalent formation between oxygen based enzyme and phosphorus atom of OPs [13, 19]. Therefore, we further studied the sensing ability of **GQDs/Enz/Gel** toward the oxo-form of dichlorvos and methyl-paraoxon in phosphate buffer solution pH 8.0. In particular of quantitative analysis of **GQDs/Enz/Gel**, the PL titration in term of the correlation between an inhibition efficiency (I%) and concentration of OPs was demonstrated, and the calibration curve was plotted in Figure 3.34D and E. The inhibition efficiency (%I) of AChE towards dichlorvos (DV) and methyl-paraoxon (MP) in linear range of 1.25×10^{-8} to 1.25×10^{-4} M and 1.25×10^{-9} to 0.625×10^{-4} M, respectively, that are better linearity than our previous work in the range of 0.45×10^{-6} to 0.45×10^{-4} M for DV and 0.4×10^{-6} to 0.4×10^{-5} for MP, respectively, as shown in Table 3.11. Most sensory system based on enzymatic reaction showed the detection limit of pesticide at 10% inhibition of AChE [73]. Fascinatingly, the LOD of this hybrid material towards DV and MP are 2.61×10^{-8} M and 6.79×10^{-9} M, which are more effective than our previous work providing the LOD of DV and MP of 0.78×10^{-6} M and 0.34×10^{-6} M, respectively.

Table 3.11 The comparison of linear range and LOD between **GQDs/Enz** and **GQDs/Enz/Gels**.

Organophosphate	Method	Linear range	LOD	LOD
		(μ M)	(μ M)	(ppm)
dichlorvos	aqueous	0.45-45	0.78	0.172
	hydrogel	0.0125-125	0.0261	5.76×10^{-3}
methyl-paraoxon	aqueous	0.40-4.05	0.34	0.084
	hydrogel	0.00125-62.5	0.00679	1.67×10^{-3}

3.3.9 Comparison of the GQDs/Enz in aqueous and in hydrogel state

As previous works, the small molecule detection using hydrogel based biosensor in both electrochemical and optical transduction have been reported such that the responsive sensor and linearity would be improved by signal amplification, particularly by optimum enzyme loading and concentrations, hydrogel networks, optimum buffer strength and pH [93-101]. Generally, in electrochemically methods, the enzyme needs to be deposited on the electrode by using hydrogels for analysis detection such as glucose, glutamase and lactase in electrochemical method. In comparison, increasing amount of immobilized enzyme can generate a highly sensitive sensor (or the detection limit is very low), but the linearity is limited. Interestingly, the linear range can be extended by a thicker membrane or using selective membrane such as polyurethane due to diffusion-limiting membrane. Then, the sensitivity must be sacrificed [96, 97, 99, 101].

According to our previous work, the different concentration of enzyme in the **GQDs/Enz** platform without gels was for OPs sensing approach. To compare the sensing affinity of **GQDs/Enz** and **GQDs/Enz/Gel** under same condition, methyl-paraoxon was chosen as a model for investigation as shown in Figure 3.35A and B. Our hypothesis in the enhancement of the sensitivity and linearity of this biosensor was reasonably addressed.

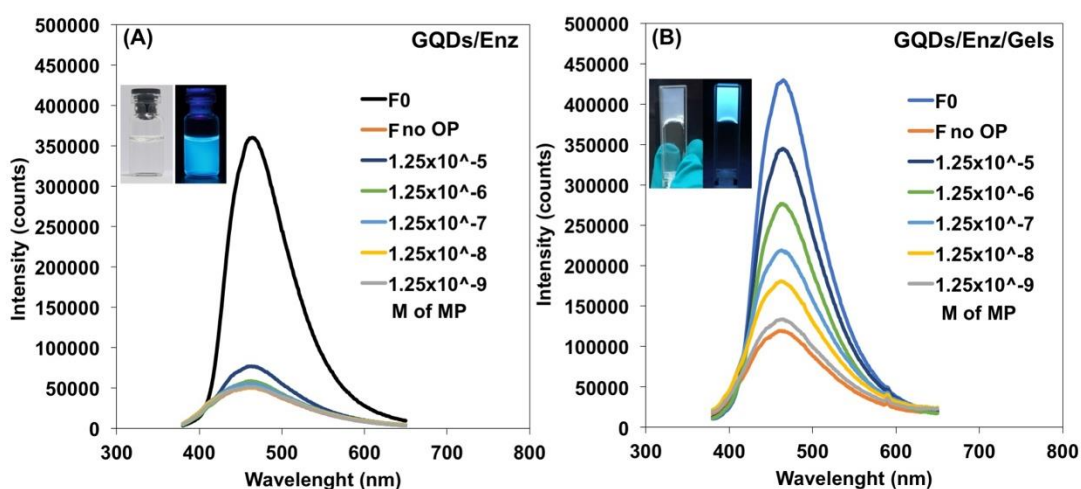


Figure 3.35 PL emission spectra of **GQDs/Enz** (A) and **GQDs/Enz/Gels** (B) upon the increasing of methyl-paraoxon (MP) at concentration between 1.25×10^{-9} to 1.25×10^{-5} M (λ_{ex} 360 nm).

As comparison of this work with the previous work without gels, the **GQDs/Enz** in aqueous phase at higher concentration of enzyme gives lower response to methyl-paraoxon. It is indicated that this concentration of enzyme is not suitable for aqueous phase (overloaded enzyme). Deeply considering, the rate of fluorescent change for **GQDs/Enz/Gel** in the presence of the same amount of OPs is higher than that of **GQDs/Enz** in solution possibly caused by the diffusion-limiting role of hydrogels[96, 97, 99, 101] which can extend the linear range of detection.

An effective detection limit should be reliably realized. By careful adjustment of parameter, such increasing of enzyme concentration and the higher PL intensity of GQDs signal in hybrid materials may encourage the sensitivity of sensing aspect. Moreover, the hydrophobic molecule of OPs might be well compatible with hydrophobic nano/microfibers of hybrid hydrogel media and consequently, it takes high impact interaction with enzyme incorporated in gel resulting in a large turn-on PL even in the presence of small amount of OPs [10, 50, 91]. Hence, we supposed that the properties of the diffusion-limiting role, the PL enhancing, and the stabilization of the hydrophobic-induced interaction of OPs-AChE hold out tremendous promise for improving the linear range and detection limit for sensing approach by this hydrogel system.

3.3.10 Lab on chips

Furthermore, the development of small scale of rapid, convenient and high-throughput sensing system is currently of increasing interest. Portable lab of small scale of hybrid hydrogels on glass slide was prepared to screen the amount of dichlorvos (DV) illustrated in Figure 3.36. The naked eye fluorescence image obtained by smart phone for a sensing of **GQDs/Enz/Gels** with DV under UV-light at 365 nm displayed a significant brightness change upon the increment of DV from 1×10^{-3} to 1×10^{-6} M. After adding ACh for 20 min, the RGB values were evaluated by using imageJ software[18], which showed an increase of green value as a function of DV concentration (Figure 3.37). This result suggested that **GQDs/Enz/Gels** enable to be developed for the fundamental sensor with rapid and convenient system and applied to be a portable OPs sensor in food, water and environment.

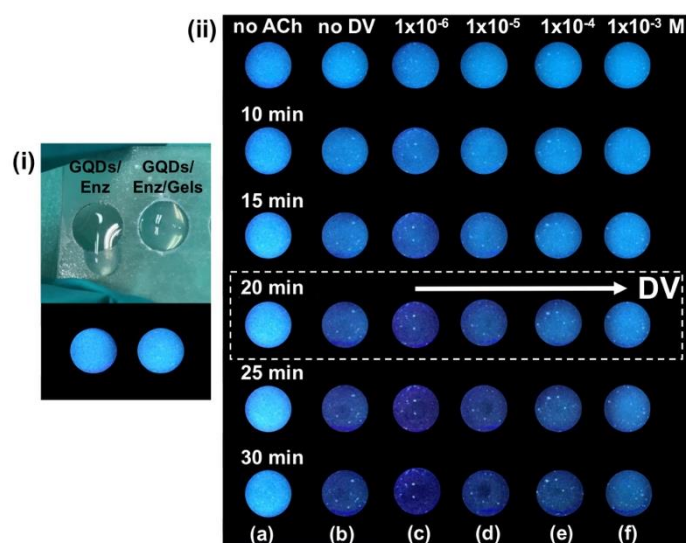


Figure 3.36 Photographs of hybrid **GQDs/Enz/Gels** sensory chips in the presence of various concentration of dichlorvos (DV) and time of measurement.

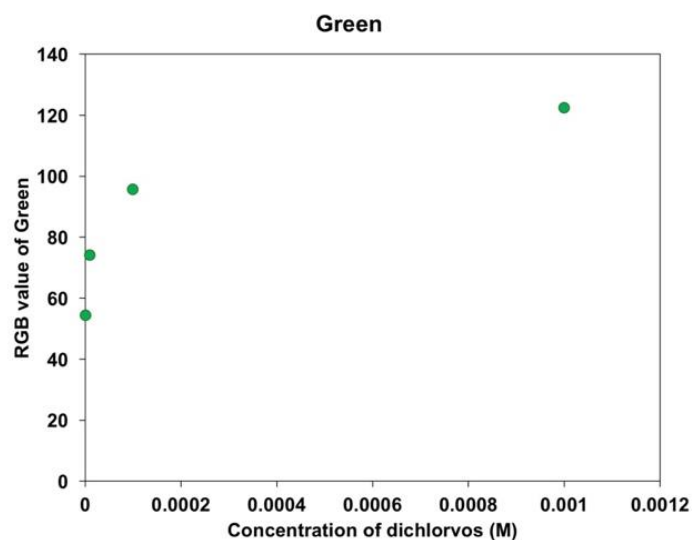
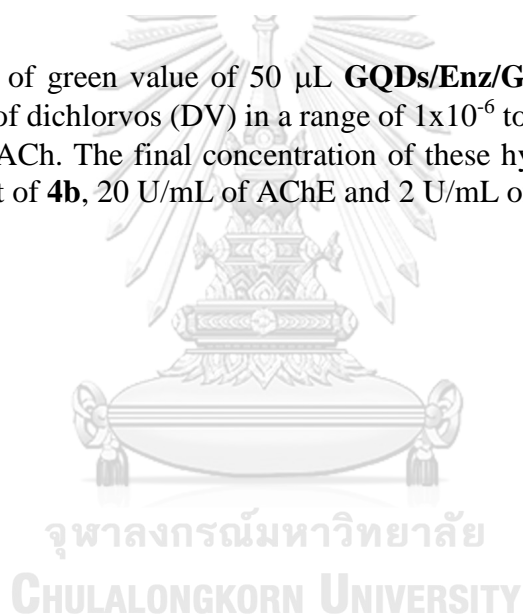


Figure 3.37 RGB of green value of 50 μL **GQDs/Enz/Gels** on glass slide 2h after addition of 10 μL of dichlorvos (DV) in a range of 1×10^{-6} to 1×10^{-3} M and followed by 10 μL of 80 mM ACh. The final concentration of these hydrogels is 1.25 mg/mL of GQDs, 0.3125% wt of **4b**, 20 U/mL of AChE and 2 U/mL of ChOx.



CHAPTER IV

4.1 Conclusion

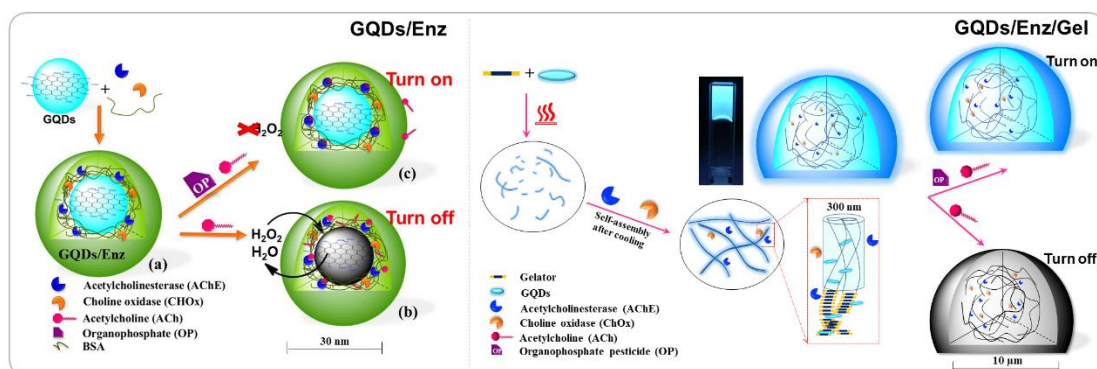


Figure 4.1 Proposed **GQDs/Enz** and **GQDs/Enz/Gels** biosensor systems for detection of organophosphate pesticide

In summary, we have successfully demonstrated the real time sensor of graphene quantum dots based enzymatic reaction (**GQDs/Enz**) for adaptive determination ability toward organophosphate pesticides (OPs) as shown in Figure 4.1. Taking an advantage, **GQDs/Enz** biosensor would be easily oxidized by H_2O_2 at pH 8 condition inducing the fluorescence quenching. Upon the addition of dichlorvos and methyl-paraoxon, it will react with acetylcholinesterase (AChE) to inhibit the generation of H_2O_2 in the system resulting in a strong fluorescence response. This biosensor highlighted sensitive and rapid detection of dichlorvos with detection limit of 0.172 ppm (0.778 μM). Additionally, this approach offered the benefit for determination of the dichlorvos in real samples.

Furthermore, a new low molecular weight gelator (LMWG) based on methylenebis(diethylphenyl) spacer conjugated to bis-urea and phenylalanine amino acid as end group which performed an excellent gelation by integrating with graphene quantum dot (GQDs) and phosphate buffer. The advantage of this gelator formation is its preparation in phosphate buffer which offers a benefit for compatibly biological system and easy accessibility. Moreover, enzymes AChE and ChOx were incorporated in hydrogel containing GQDs as signaling unit. Therefore, the sensing affinity of

GQDs/Enz/Gel material for detection of organophosphate (OPs) have been investigated and found that **GQDs/Enz/Gel** is exploited to significantly improve the performance of OPs sensing. This hybrid hydrogel material showed 10-100 folds improvement in the limit of detection (LOD of dichlorvos is 0.0261 μM) and linearity range compared to the analogue enzymatic reaction by **GQDs/Enz** material in solution. The linear ranges of dichlorvos detection are in 1.25×10^{-8} to 1.25×10^{-4} M and 0.45×10^{-6} to 0.45×10^{-4} M for gels and solution phase, respectively. To develop an easily-visualized sensing approach, the small scale or lab on chips has been screened to improve the fundamental sensor in future. This work also provides new insight into improving the performance of hybrid hydrogel properties by low molecular weight gelator with an assist of GQDs and phosphate buffer and taking an advantage of sensing application with a highly potential sensitivity and stability.

4.2 Suggestions for future works

Future work will focus on:

- i) development of small scale or lab on chips sensing system for easy to use
- ii) development of another type of GQDs such as boronic graphene quantum dots that show high PL intensity for H_2O_2 and organophosphate detection.

REFERENCES

- [1] He, Y., Sun, J., Feng, D., Chen, H., Gao, F., and Wang, L. Graphene quantum dots: Highly active bifunctional nanoprobe for nonenzymatic photoluminescence detection of hydroquinone. Biosensors and Bioelectronics 74 (2015): 418-422.
- [2] Liang, M., et al. Fe₃O₄ magnetic nanoparticle peroxidase mimetic-based colorimetric assay for the rapid detection of organophosphorus pesticide and nerve agent. Anal Chem 85(1) (2013): 308-312.
- [3] The U.S. Environmental Protection Agency (EPA). Pesticides: topical & chemical fact sheets [Online]. 2012. Available from: <http://www.epa.gov/pesticides/factsheets/securety.htm> [February 17, 2015]
- [4] The United States Department of Agriculture (USDA). The pesticide data program annual summary calendar year 2005. Washington, DC, 2005.
- [5] The Official of Agricultural Economic of Thailand (OAE). Importation data of toxic compound for agricultural industry year 2011-2017 [Online]. 2017. Available from: <http://oldweb.oae.go.th/economicdata/pesticides.html> [August 01, 2018]
- [6] Quinn, D.M. Acetylcholinesterase: enzyme structure, reaction dynamics, and virtual transition states. Chemical Reviews 87(5) (1987): 955-979.
- [7] Robert B. Raffa, S.M.R., and Elena Portyansky Beyzarov. Netter's Illustrated Pharmacology Elsevier, 2014.
- [8] The UK Health and Safety Executive (HSE). Pesticide maximum residue levels for trade in or to the UK or other EU countries [Online]. 2008. Available from: <https://secure.pesticides.gov.uk/mrls/main.asp> [October 1, 2018]
- [9] Blesa, J., Soriano, J.M., Moltó, J.C., Marín, R., and Mañes, J. Determination of aflatoxins in peanuts by matrix solid-phase dispersion and liquid chromatography. Journal of Chromatography A 1011(1-2) (2003): 49-54.
- [10] Zheng, Z., Zhou, Y., Li, X., Liu, S., and Tang, Z. Highly-sensitive organophosphorous pesticide biosensors based on nanostructured films of acetylcholinesterase and CdTe quantum dots. Biosens Bioelectron 26(6) (2011): 3081-3085.
- [11] Ivnitskii, D.M. and Rishpon, J. A potentiometric biosensor for pesticides based on the thiocholine hexacyanoferrate (III) reaction. Biosensors and Bioelectronics 9(8) (1994): 569-576.
- [12] Lawal, A.T. and Adeloju, S.B. Comparison of enzyme immobilisation methods for potentiometric phosphate biosensors. Biosensors and Bioelectronics 25(2) (2009): 406-410.
- [13] Lazarević-Pašti, T.D., Bondžić, A.M., Pašti, I.A., and Vasić, V.M. Indirect electrochemical oxidation of organophosphorous pesticides for efficient detection via acetylcholinesterase test. Pesticide Biochemistry and Physiology 104(3) (2012): 236-242.

- [14] Lee, S.R., Lee, H.E., Kang, Y.O., Hwang, W.S., and Choi, S.H. Bionzymatic acetylcholinesterase and choline oxidase immobilized biosensor based on a phenyl carboxylic acid-grafted multiwalled carbon nanotube. Advances in Materials Science and Engineering 2014 (2014): 1-12.
- [15] Zhang, S.-W. and Swager, T.M. Fluorescent detection of chemical warfare agents: functional group specific ratiometric chemosensors. Journal of the American Chemical Society 125(12) (2003): 3420-3421.
- [16] Jin, S., Xu, Z., Chen, J., Liang, X., Wu, Y., and Qian, X. Determination of organophosphate and carbamate pesticides based on enzyme inhibition using a pH-sensitive fluorescence probe. Analytica Chimica Acta 523(1) (2004): 117-123.
- [17] Badawy, M.E. and El-Aswad, A.F. Bioactive paper sensor based on the acetylcholinesterase for the rapid detection of organophosphate and carbamate pesticides. Int J Anal Chem 2014 (2014): 536823.
- [18] Sicard, C., et al. Tools for water quality monitoring and mapping using paper-based sensors and cell phones. Water Res 70 (2015): 360-9.
- [19] Pimsen, R., Khumsri, A., Wacharasindhu, S., Tumcharern, G., and Sukwattanasinitt, M. Colorimetric detection of dichlorvos using polydiacetylene vesicles with acetylcholinesterase and cationic surfactants. Biosens Bioelectron 62 (2014): 8-12.
- [20] Song, Y., Qu, K., Zhao, C., Ren, J., and Qu, X. Graphene oxide: intrinsic peroxidase catalytic activity and its application to glucose detection. Adv Mater 22(19) (2010): 2206-2210.
- [21] Zheng, A.X., Cong, Z.X., Wang, J.R., Li, J., Yang, H.H., and Chen, G.N. Highly-efficient peroxidase-like catalytic activity of graphene dots for biosensing. Biosens Bioelectron 49 (2013): 519-524.
- [22] Kim, J.-H., et al. The rational design of nitric oxide selectivity in single-walled carbon nanotube near-infrared fluorescence sensors for biological detection. Nat Chem 1(6) (2009): 473-481.
- [23] Li, X., Wang, X., Zhang, L., Lee, S., and Dai, H. Chemically derived, ultrasMOOTH graphene nanoribbon semiconductors. Science 319(5867) (2008): 1229-1232.
- [24] Dong, Y., et al. Blue luminescent graphene quantum dots and graphene oxide prepared by tuning the carbonization degree of citric acid. Carbon 50(12) (2012): 4738-4743.
- [25] Zhu, S., et al. Investigation of photoluminescence mechanism of graphene quantum dots and evaluation of their assembly into polymer dots. Carbon 77 (2014): 462-472.
- [26] Umrao, S., et al. Microwave bottom-up route for size-tunable and switchable photoluminescent graphene quantum dots using acetylacetone: New platform for enzyme-free detection of hydrogen peroxide. Carbon 81 (2015): 514-524.

- [27] Ju, J. and Chen, W. Synthesis of highly fluorescent nitrogen-doped graphene quantum dots for sensitive, label-free detection of Fe (III) in aqueous media. Biosens Bioelectron 58 (2014): 219-25.
- [28] Li, Y., et al. Nitrogen-doped graphene quantum dots with oxygen-rich functional groups. J Am Chem Soc 134(1) (2012): 15-8.
- [29] Qu, Z.B., et al. Boronic acid functionalized graphene quantum dots as a fluorescent probe for selective and sensitive glucose determination in microdialysate. Chem Commun (Camb) 49(84) (2013): 9830-9832.
- [30] Yan, Z., Qu, X., Niu, Q., Tian, C., Fan, C., and Ye, B. A green synthesis of highly fluorescent nitrogen-doped graphene quantum dots for the highly sensitive and selective detection of mercury (ii) ions and biothiols. Anal. Methods 8(7) (2016): 1565-1571.
- [31] Lee, S.R., Lee, H.E., Kang, Y.O., Hwang, W.S., and Choi, S.H. Bionzymatic Acetylcholinesterase and Choline Oxidase Immobilized Biosensor Based on a Phenyl Carboxylic Acid-Grafted Multiwalled Carbon Nanotube. Advances in Materials Science and Engineering 2014 (2014): 1-12.
- [32] Garcia-Galan, C., Barbosa, O., and Fernandez-Lafuente, R. Stabilization of the hexameric glutamate dehydrogenase from *Escherichia coli* by cations and polyethyleneimine. Enzyme Microb Technol 52(4-5) (2013): 211-217.
- [33] Nery, E.W. and Kubota, L.T. Evaluation of enzyme immobilization methods for paper-based devices--A glucose oxidase study. J Pharm Biomed Anal 117 (2016): 551-559.
- [34] Li, Y., Wang, F., and Cui, H. Peptide-Based Supramolecular Hydrogels for Delivery of Biologics. Bioeng Transl Med 1(3) (2016): 306-322.
- [35] Ravichandran, R., Griffith, M., and Phopase, J. Applications of self-assembling peptide scaffolds in regenerative medicine: the way to the clinic. Journal of Materials Chemistry B 2(48) (2014): 8466-8478.
- [36] Hirst, A.R., et al. Biocatalytic induction of supramolecular order. Nat Chem 2(12) (2010): 1089-94.
- [37] Lee, J., Ko, J.H., Lin, E.-W., Wallace, P., Ruch, F., and Maynard, H.D. Trehalose hydrogels for stabilization of enzymes to heat. Polymer Chemistry 6(18) (2015): 3443-3448.
- [38] Liang, H., et al. Co-immobilization of multiple enzymes by metal coordinated nucleotide hydrogel nanofibers: improved stability and an enzyme cascade for glucose detection. Nanoscale 8(11) (2016): 6071-6078.
- [39] Moreira Teixeira, L.S., Feijen, J., van Blitterswijk, C.A., Dijkstra, P.J., and Karperien, M. Enzyme-catalyzed crosslinkable hydrogels: Emerging strategies for tissue engineering. Biomaterials 33(5) (2012): 1281-1290.
- [40] Shigemitsu, H., Fujisaku, T., Onogi, S., Yoshii, T., Ikeda, M., and Hamachi, I. Preparation of supramolecular hydrogel-enzyme hybrids exhibiting biomolecule-responsive gel degradation. Nature Protocols 11 (2016): 1744.

- [41] Foster, J.A., et al. Pharmaceutical polymorph control in a drug-mimetic supramolecular gel. Chem Sci 8(1) (2017): 78-84.
- [42] Kaufmann, L., Kennedy, S.R., Jones, C.D., and Steed, J.W. Cavity-containing supramolecular gels as a crystallization tool for hydrophobic pharmaceuticals. Chem Commun (Camb) 52(66) (2016): 10113-6.
- [43] Ruiz-Palomero, C., Kennedy, S.R., Soriano, M.L., Jones, C.D., Valcarcel, M., and Steed, J.W. Pharmaceutical crystallization with nanocellulose organogels. Chem Commun (Camb) 52(50) (2016): 7782-5.
- [44] Foster, J.A., et al. Blending Gelators to Tune Gel Structure and Probe Anion-Induced Disassembly. Chemistry - A European Journal 20(1) (2014): 279-291.
- [45] Foster, J.A., Piepenbrock, M.O., Lloyd, G.O., Clarke, N., Howard, J.A., and Steed, J.W. Anion-switchable supramolecular gels for controlling pharmaceutical crystal growth. Nat Chem 2(12) (2010): 1037-43.
- [46] Meazza, L., Foster, J.A., Fucke, K., Metrangolo, P., Resnati, G., and Steed, J.W. Halogen-bonding-triggered supramolecular gel formation. Nat Chem 5(1) (2013): 42-7.
- [47] Offiler, C.A., Jones, C.D., and Steed, J.W. Metal 'turn-off', anion 'turn-on' gelation cascade in pyridinylmethyl ureas. Chem Commun (Camb) 53(12) (2017): 2024-2027.
- [48] Piepenbrock, M.O., Lloyd, G.O., Clarke, N., and Steed, J.W. Metal- and anion-binding supramolecular gels. Chem Rev 110(4) (2010): 1960-2004.
- [49] Ikeda, M., et al. Installing logic-gate responses to a variety of biological substances in supramolecular hydrogel-enzyme hybrids. Nat Chem 6(6) (2014): 511-8.
- [50] Wada, A., Tamaru, S.-i., Ikeda, M., and Hamachi, I. MCM-Enzyme-Supramolecular Hydrogel Hybrid as a Fluorescence Sensing Material for Polyanions of Biological Significance. Journal of the American Chemical Society 131(14) (2009): 5321-5330.
- [51] Yoshii, T., Onogi, S., Shigemitsu, H., and Hamachi, I. Chemically Reactive Supramolecular Hydrogel Coupled with a Signal Amplification System for Enhanced Analyte Sensitivity. Journal of the American Chemical Society 137(9) (2015): 3360-3365.
- [52] Estroff, L.A. and Hamilton, A.D. Water Gelation by Small Organic Molecules. Chemical Reviews 104(3) (2004): 1201-1218.
- [53] Ulijn, R.V. and Smith, A.M. Designing peptide based nanomaterials. Chem Soc Rev 37(4) (2008): 664-75.
- [54] Weiss, R.G. The past, present, and future of molecular gels. What is the status of the field, and where is it going? J Am Chem Soc 136(21) (2014): 7519-30.
- [55] Terech, P. and Weiss, R.G. Low Molecular Mass Gelators of Organic Liquids and the Properties of Their Gels. Chemical Reviews 97(8) (1997): 3133-3160.

- [56] Cayuela, A., Kennedy, S.R., Soriano, M.L., Jones, C.D., Valcárcel, M., and Steed, J.W. Fluorescent carbon dot–molecular salt hydrogels. Chemical Science 6(11) (2015): 6139-6146.
- [57] Cvjetko, M., Radosevic, K., Tomica, A., Slivac, I., Vorkapic-Furac, J., and Sreck, V.G. Cytotoxic effects of imidazolium ionic liquids on fish and human cell lines. Arh Hig Rada Toksikol 63(1) (2012): 15-20.
- [58] Sahub, C., Tuntulani, T., Nhujak, T., and Tomapatanaget, B. Effective biosensor based on graphene quantum dots via enzymatic reaction for directly photoluminescence detection of organophosphate pesticide. Sensors and Actuators B: Chemical 258 (2018): 88-97.
- [59] Inoue, S., et al. Rapid simultaneous determination for organophosphorus pesticides in human serum by LC-MS. J Pharm Biomed Anal 44(1) (2007): 258-64.
- [60] Yang, L., Hong Liu, Y., Zhe An, L., and Li, Y.b. Rapid and accurate determination of dichlorvos in water by liquid chromatography-electrospray ionization-tandem mass spectrometry. Journal of Liquid Chromatography & Related Technologies 29(20) (2006): 2943-2955.
- [61] Chai, F., et al. Fluorescent gold nanoprobe for the sensitive and selective detection for Hg. Nanoscale Res Lett 5(11) (2010): 1856-1860.
- [62] Xie, J., Zheng, Y., and Ying, J.Y. Protein-directed synthesis of highly fluorescent gold nanoclusters. Journal of the American Chemical Society 131(3) (2009): 888-889.
- [63] Zhao, X., Liu, R., Chi, Z., Teng, Y., and Qin, P. New insights into the behavior of bovine serum albumin adsorbed onto carbon nanotubes: comprehensive spectroscopic studies. The Journal of Physical Chemistry B 114(16) (2010): 5625-5631.
- [64] Sun, Y.-P., et al. Quantum-sized carbon dots for bright and colorful photoluminescence. Journal of the American Chemical Society 128(24) (2006): 7756-7757.
- [65] Wilson, W.L., Szajowski, P.F., and Brus, L.E. Quantum confinement in size-selected, surface-oxidized silicon nanocrystals. Science 262(5137) (1993): 1242-1244.
- [66] Chu, C.-S. and Su, C.-J. Optical fiber sensor for dual sensing of H₂O₂ and DO based on CdSe/ZnS QDs and Ru(dpp)₃²⁺ embedded in EC matrix. Sensors and Actuators B: Chemical 255 (2017): 1079-1086.
- [67] Kaur, M., Mehta, S.K., and Kansal, S.K. Nitrogen doped graphene quantum dots: Efficient fluorescent chemosensor for the selective and sensitive detection of 2,4,6-trinitrophenol. Sensors and Actuators B: Chemical 245 (2017): 938-945.
- [68] Ageda, S., Fuke, C., Ihama, Y., and Miyazaki, T. The stability of organophosphorus insecticides in fresh blood. Leg Med (Tokyo) 8(3) (2006): 144-9.

- [69] Chapman, R.A. and Cole, C.M. Observations on the influence of water and soil pH on the persistence of insecticides. Journal of Environmental Science and Health, Part B 17(5) (1982): 487-504.
- [70] Ikuta, S., Imamura, S., Misaki, H., and Horiuti, Y. Purification and characterization of choline oxidase from arthrobacter globiformis. Journal of Biochemistry 82(6) (1977): 1741-1749.
- [71] Zhang, Z., Wang, X., and Yang, X. A sensitive choline biosensor using Fe₃O₄ magnetic nanoparticles as peroxidase mimics. Analyst 136(23) (2011): 4960-5.
- [72] Yotova, L. and Medhat, N. Coimmobilization of acetylcholinesterase and choline oxidase on new nanohybrid membranes obtained by sol gel technology. Biotechnology & Biotechnological Equipment 26(3) (2014): 3039-3043.
- [73] Skládal, P., Nunes, G.S., Yamanaka, H., and Ribeiro, M.L. Detection of carbamate pesticides in vegetable samples using cholinesterase-based biosensors. Electroanalysis 9(14) (1997): 1083-1087.
- [74] Azab, H.A., Orabi, A.S., and Abbas, A.M. New polymerizable luminescence probe for detection of chlorfenvinphos and dichlorvos pesticides. Journal of Luminescence 167 (2015): 360-370.
- [75] Wong, F.C., Ahmad, M., Heng, L.Y., and Peng, L.B. An optical biosensor for dichlorvos using stacked sol-gel films containing acetylcholinesterase and a lipophilic chromoionophore. Talanta 69(4) (2006): 888-93.
- [76] Walz, I. and Schwack, W. Cutinase inhibition by means of insecticidal organophosphates and carbamates Part 2: screening of representative insecticides on cutinase activity. European Food Research and Technology 226(5) (2007): 1135-1143.
- [77] Dzyadevych, S.V., et al. Early-warning electrochemical biosensor system for environmental monitoring based on enzyme inhibition. Sensors and Actuators B: Chemical 105(1) (2005): 81-87.
- [78] Panuwet, P., et al. Agricultural Pesticide Management in Thailand: Situation and Population Health Risk. Environmental science & policy 17 (2012): 72-81.
- [79] Lu, W., et al. Economical, green synthesis of fluorescent carbon nanoparticles and their use as probes for sensitive and selective detection of mercury(II) ions. Anal Chem 84(12) (2012): 5351-7.
- [80] Wu, Z., Li, W., Chen, J., and Yu, C. A graphene quantum dot-based method for the highly sensitive and selective fluorescence turn on detection of biothiols. Talanta 119 (2014): 538-43.
- [81] Mukdasai, S., Thomas, C., and Srijaranai, S. Two-step microextraction combined with high performance liquid chromatographic analysis of pyrethroids in water and vegetable samples. Talanta 120 (2014): 289-96.
- [82] Wang, G.M., et al. Simultaneous determination of residues of trichlorfon and dichlorvos in animal tissues by LC-MS/MS. Food Addit Contam Part A Chem Anal Control Expo Risk Assess 27(7) (2010): 983-8.

- [83] Gustavo González, A. and Ángeles Herrador, M. A practical guide to analytical method validation, including measurement uncertainty and accuracy profiles. TrAC Trends in Analytical Chemistry 26(3) (2007): 227-238.
- [84] Ikeda, M., Tanida, T., Yoshii, T., and Hamachi, I. Rational molecular design of stimulus-responsive supramolecular hydrogels based on dipeptides. Adv Mater 23(25) (2011): 2819-22.
- [85] Mahler, A., Reches, M., Rechter, M., Cohen, S., and Gazit, E. Rigid, Self-Assembled Hydrogel Composed of a Modified Aromatic Dipeptide. Advanced Materials 18(11) (2006): 1365-1370.
- [86] Ulijn, R.V. and Smith, A.M. Designing peptide based nanomaterials. Chemical Society Reviews 37(4) (2008): 664-675.
- [87] Sangeetha, N.M. and Maitra, U. Supramolecular gels: functions and uses. Chem Soc Rev 34(10) (2005): 821-36.
- [88] Chen, L., Revel, S., Morris, K., L., C.S., and Adams, D.J. Effect of molecular structure on the properties of naphthalene-dipeptide hydrogelators. Langmuir 26(16) (2010): 13466-71.
- [89] Kondyurin, A., et al. Hybrid graphite film–carbon nanotube platform for enzyme immobilization and protection. Carbon 65 (2013): 287-295.
- [90] Piepenbrock, M.-O.M., Lloyd, G.O., Clarke, N., and Steed, J.W. Metal- and Anion-Binding Supramolecular Gels. Chemical Reviews 110(4) (2010): 1960-2004.
- [91] Ruiz-Palomero, C., Soriano, M.L., Benítez-Martínez, S., and Valcárcel, M. Photoluminescent sensing hydrogel platform based on the combination of nanocellulose and S,N-codoped graphene quantum dots. Sensors and Actuators B: Chemical 245 (2017): 946-953.
- [92] Wang, Q., Yang, Z., Gao, Y., Ge, W., Wang, L., and Xu, B. Enzymatic hydrogelation to immobilize an enzyme for high activity and stability. Soft Matter 4(3) (2008): 550-553.
- [93] Korpan, Y.I., Raushel, F.M., Nazarenko, E.A., Soldatkin, A.P., Jaffrezic-Renault, N., and Martelet, C. Sensitivity and Specificity Improvement of an Ion Sensitive Field Effect Transistors-Based Biosensor for Potato Glycoalkaloids Detection. Journal of Agricultural and Food Chemistry 54(3) (2006): 707-712.
- [94] Russell, R.J., Pishko, M.V., Gefrides, C.C., McShane, M.J., and Coté, G.L. A Fluorescence-Based Glucose Biosensor Using Concanavalin A and Dextran Encapsulated in a Poly(ethylene glycol) Hydrogel. Analytical Chemistry 71(15) (1999): 3126-3132.
- [95] Russell, R.J., Pishko, M.V., Simonian, A.L., and Wild, J.R. Poly(ethylene glycol) Hydrogel-Encapsulated Fluorophore–Enzyme Conjugates for Direct Detection of Organophosphorus Neurotoxins. Analytical Chemistry 71(21) (1999): 4909-4912.
- [96] Tavakoli, J. and Tang, Y. Hydrogel Based Sensors for Biomedical Applications: An Updated Review. Polymers 9(12) (2017): 364.

- [97] Vaddiraju, S., Singh, H., Burgess, D.J., Jain, F.C., and Papadimitrakopoulos, F. Enhanced Glucose Sensor Linearity Using Poly(Vinyl Alcohol) Hydrogels. Journal of diabetes science and technology (Online) 3(4) (2009): 863-874.
- [98] Weltin, A., Enderle, B., Kieninger, J., and Urban, G.A. Multiparametric, Flexible Microsensor Platform for Metabolic Monitoring In Vivo. IEEE Sensors Journal 14(10) (2014): 3345-3351.
- [99] Weltin, A., Kieninger, J., and Urban, G.A. Microfabricated, amperometric, enzyme-based biosensors for in vivo applications. Anal Bioanal Chem 408(17) (2016): 4503-21.
- [100] Yadavalli, V.K., Koh, W.-G., Lazur, G.J., and Pishko, M.V. Microfabricated protein-containing poly(ethylene glycol) hydrogel arrays for biosensing. Sensors and Actuators B: Chemical 97(2-3) (2004): 290-297.
- [101] Yu, B., et al. Use of hydrogel coating to improve the performance of implanted glucose sensors. Biosensors and Bioelectronics 23(8) (2008): 1278-1284.





APPENDIX

จุฬาลงกรณ์มหาวิทยาลัย
CHULALONGKORN UNIVERSITY

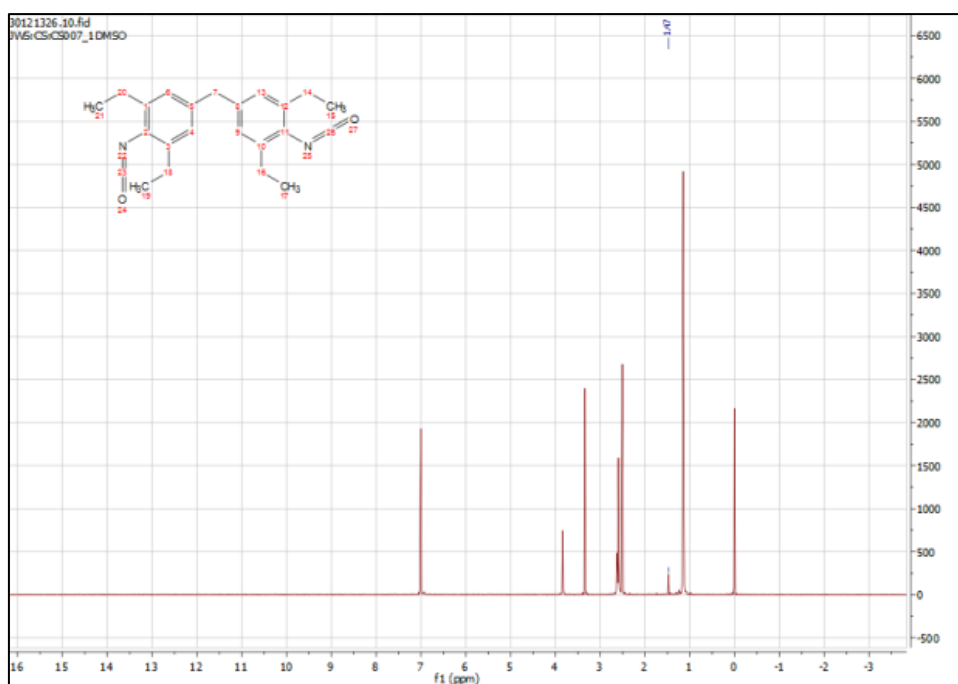


Figure A1. The $^1\text{H-NMR}$ of 4,4'-methylenebis(2,6-diethylphenyl isocyanate) in DMSO-d_6 .

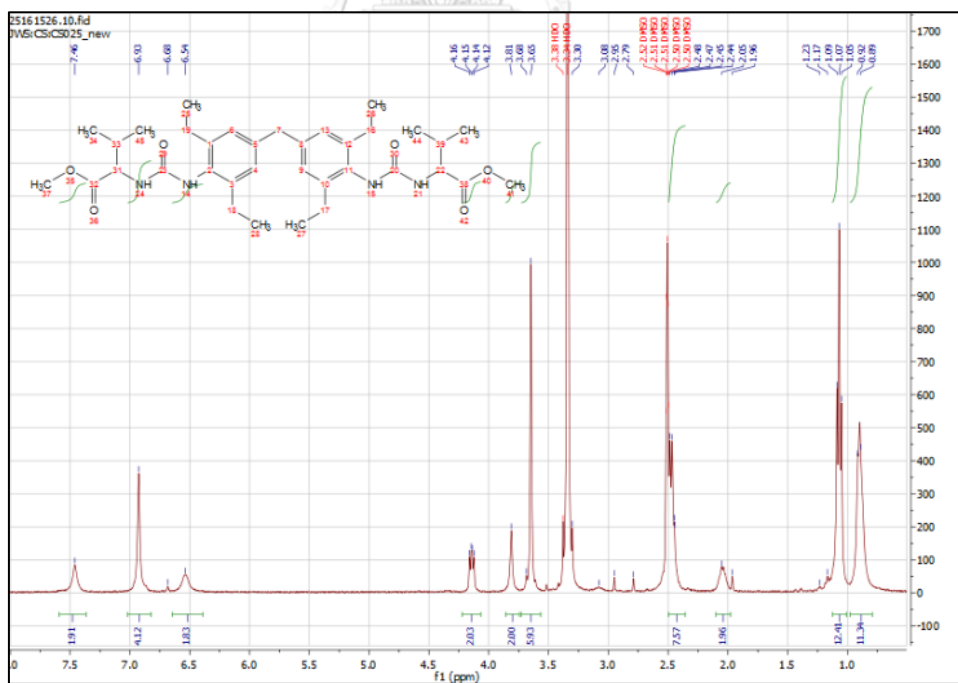


Figure A2. The $^1\text{H-NMR}$ of compound 1

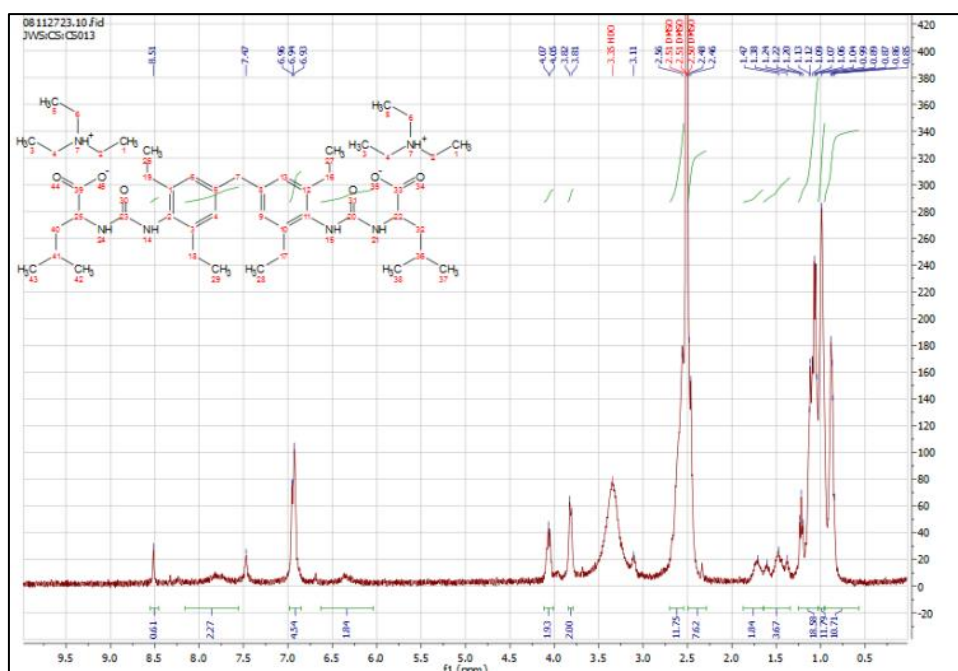


Figure A3. The ^1H -NMR of compound 2c

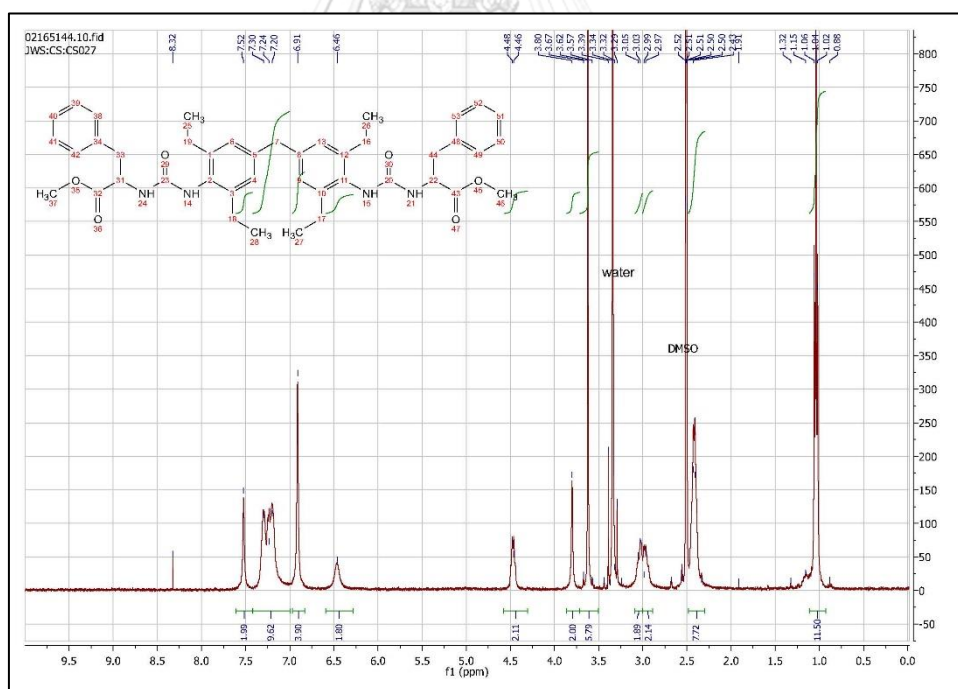


Figure A4. The ^1H -NMR of compound 3

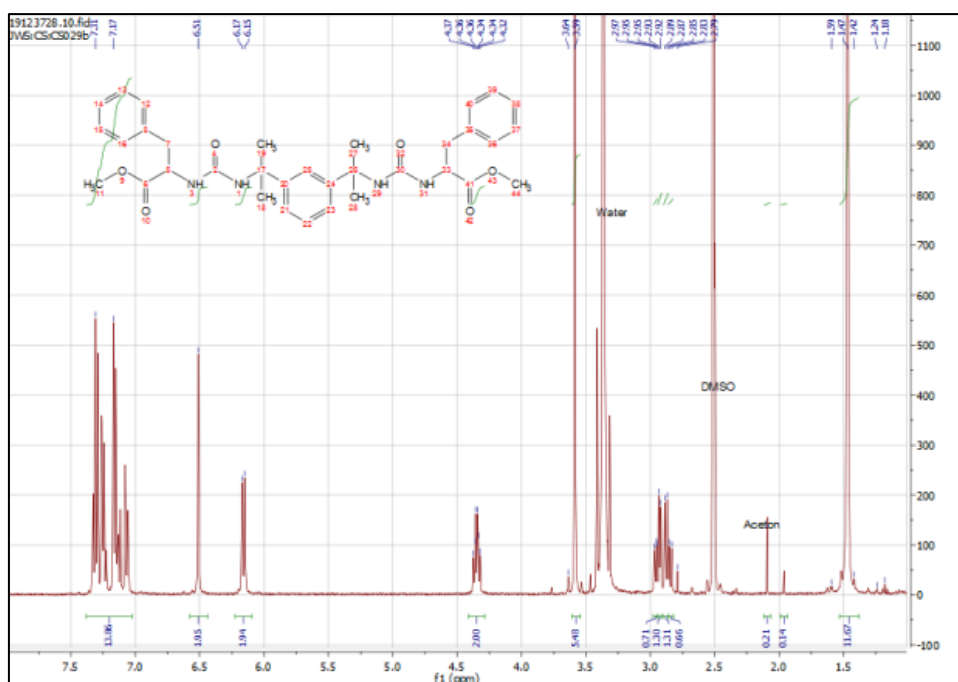


Figure A5. The $^1\text{H-NMR}$ of compound 5

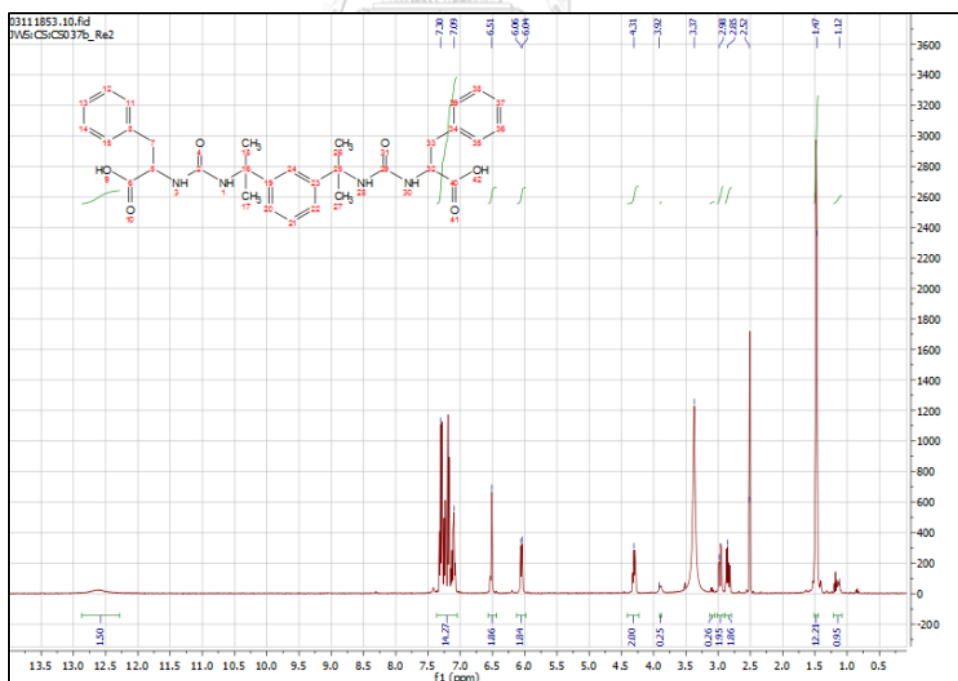


Figure A6. The $^1\text{H-NMR}$ of compound 6a

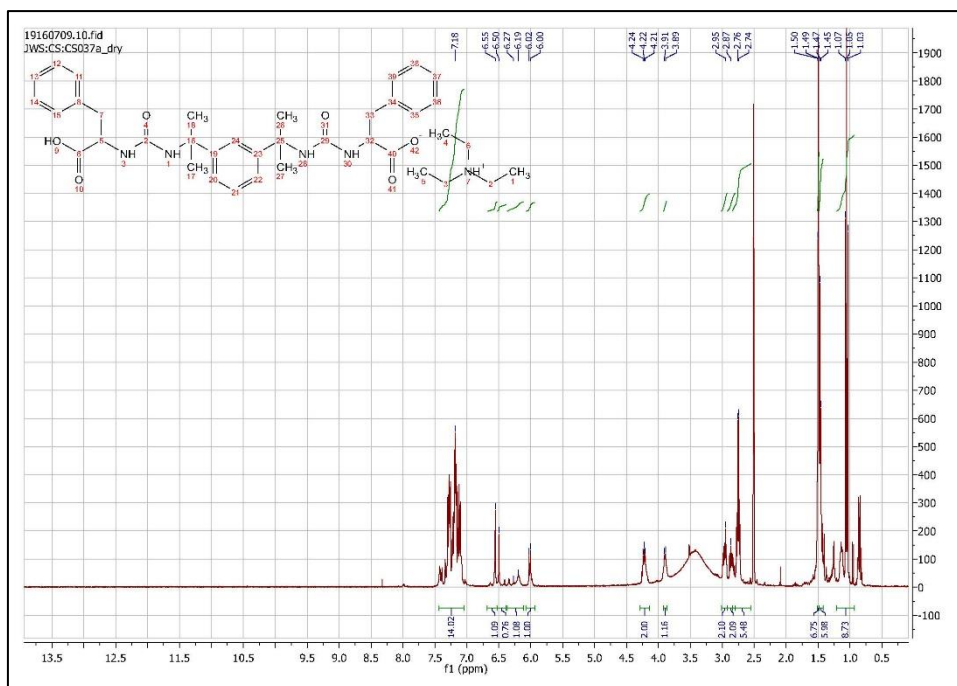


Figure A7. The $^1\text{H-NMR}$ of compound **6b**

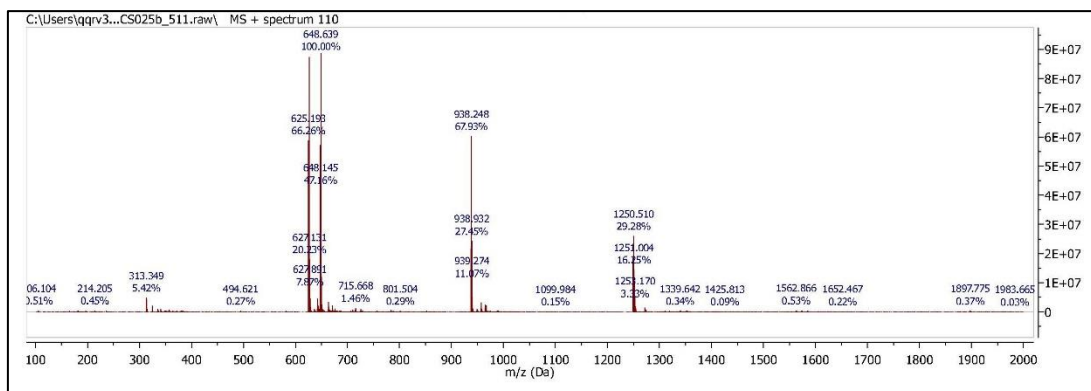


Figure A8. ESI mass spectrum of compound 1.

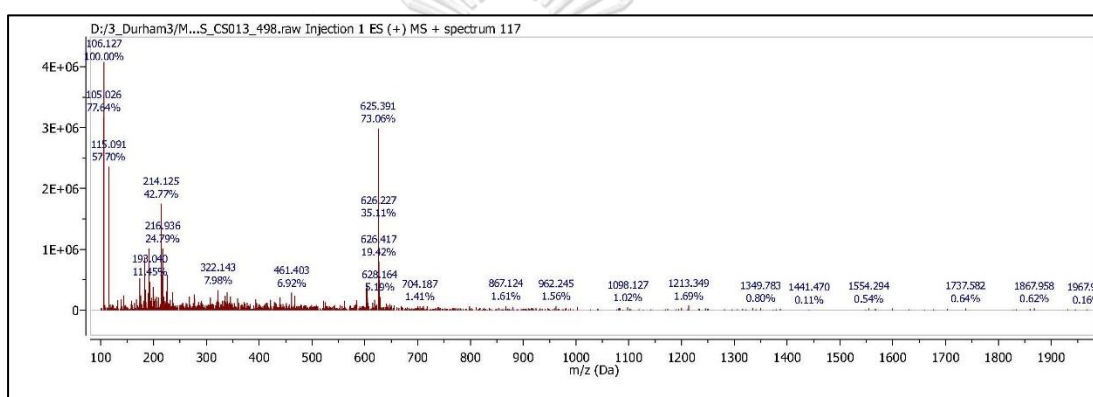


Figure A9. ESI mass spectrum of compound 2c.

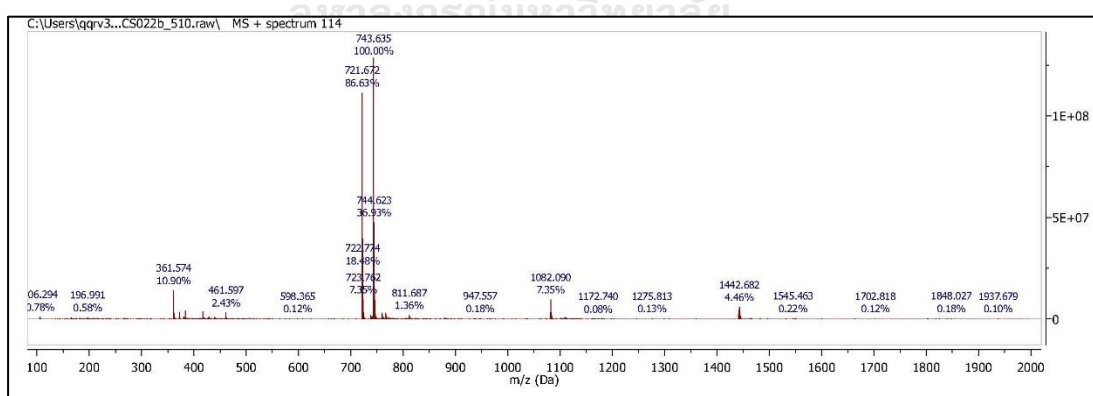


Figure A10. ESI mass spectrum of compound 3.

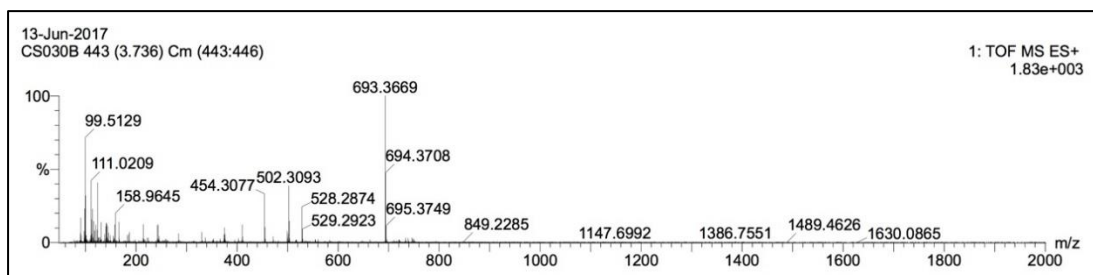


Figure A11. Accurate mass spectrum of compound **4a**

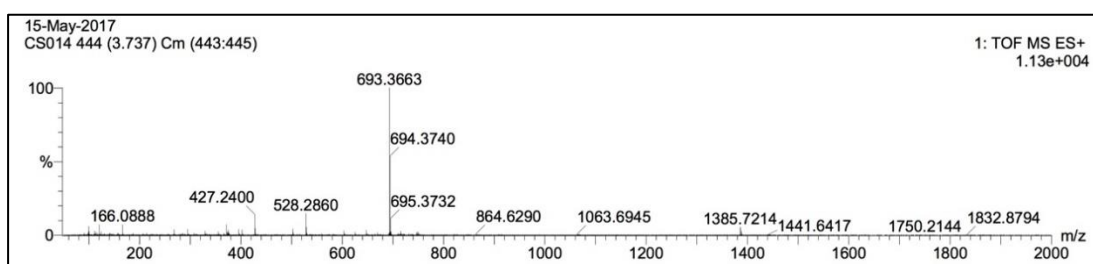


Figure A12. Accurate mass spectrum of compound **4b**

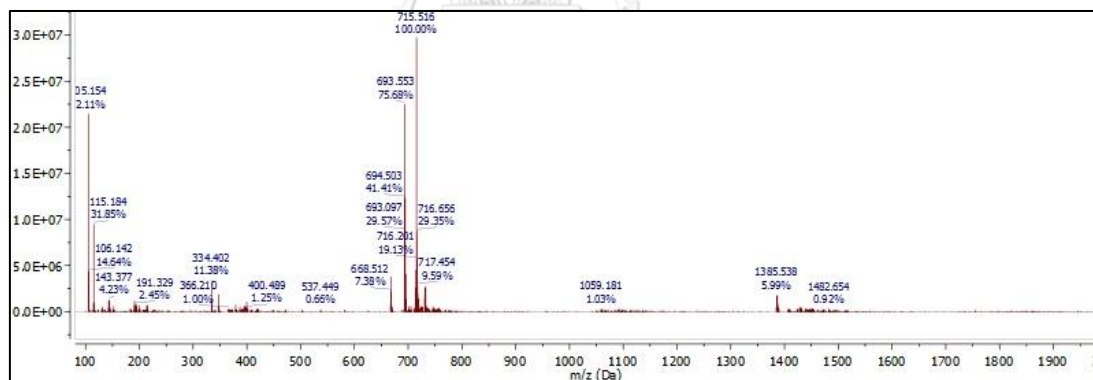


Figure A13. ESI mass spectrum of compound **4c**

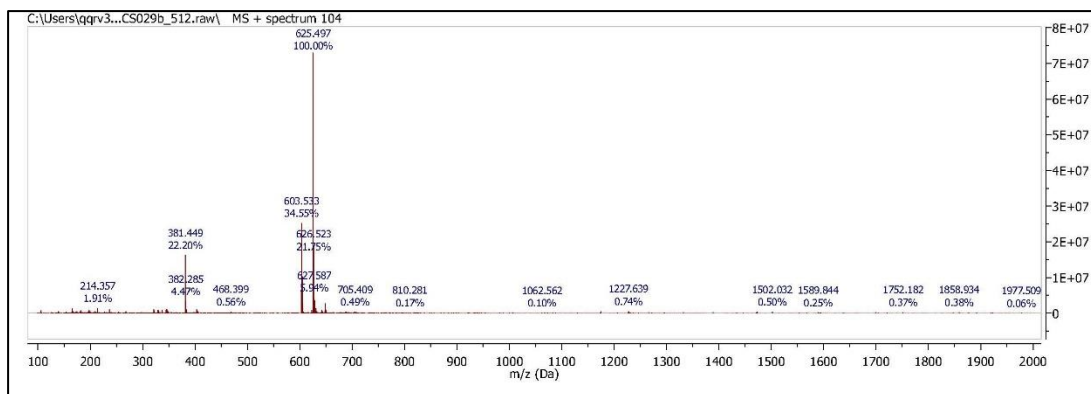


Figure A14. ESI mass spectrum of compound 5.

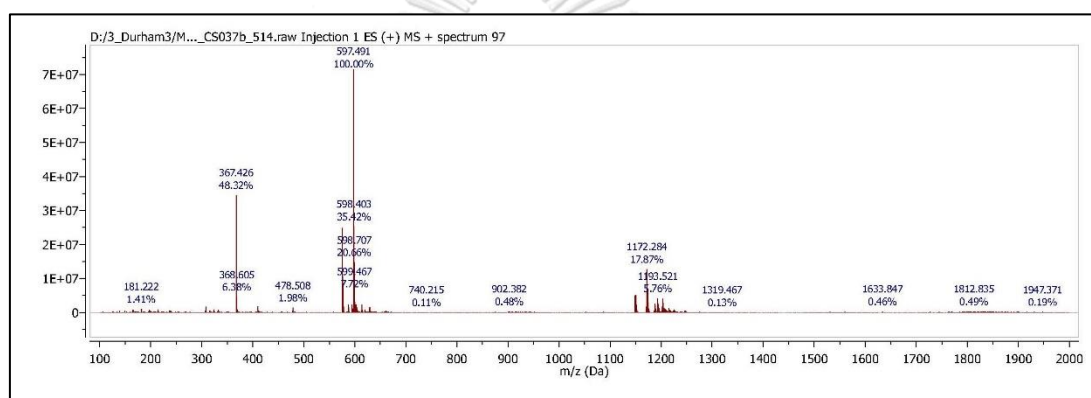


Figure A15. ESI mass spectrum of compound 6a.

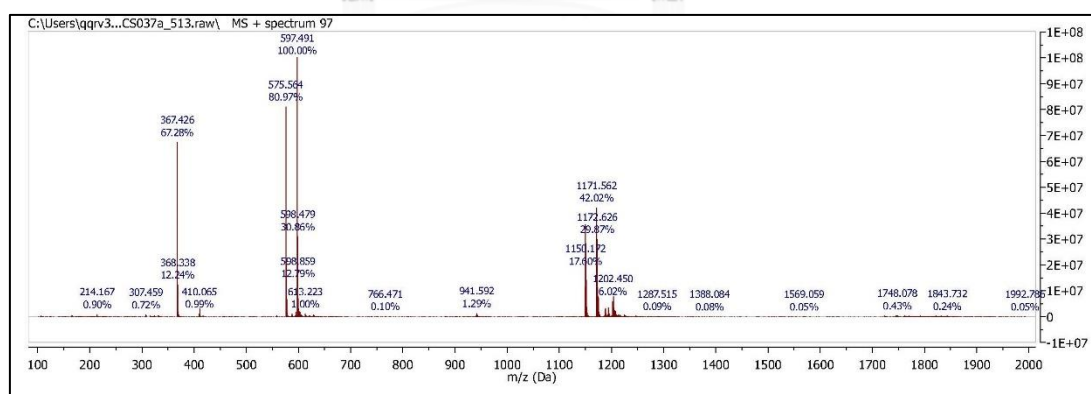


Figure A16. ESI mass spectrum of compound 6b.

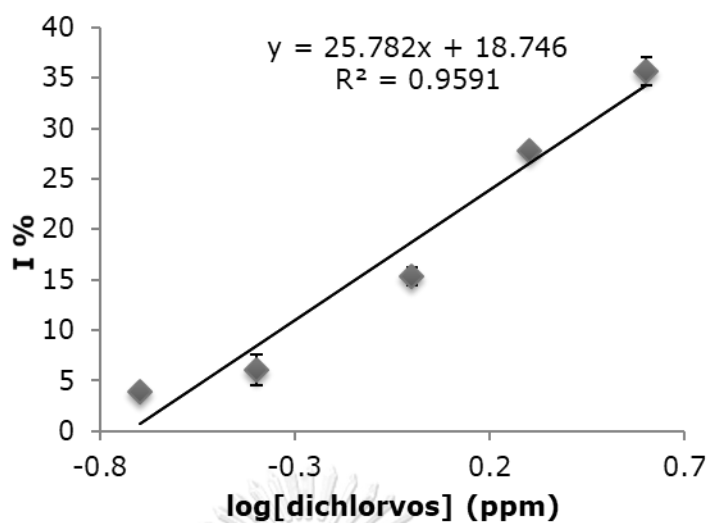


Figure A17. Linear range of dichlorvos detections in *tap water* by using **GQDs/Enz** platform with spiked dichlorvos in log concentration of 0.2 ppm to 4 ppm.

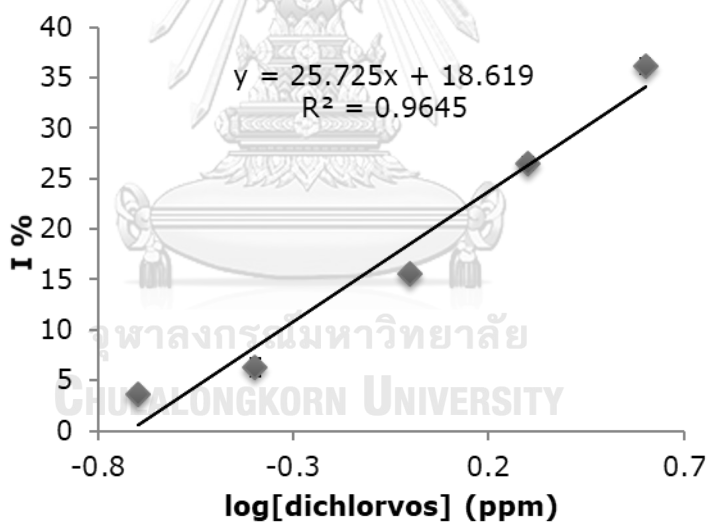


Figure A18. Linear range of dichlorvos detections in *field water 1* by using **GQDs/Enz** platform with spiked dichlorvos in log concentration of 0.2 ppm to 4 ppm.

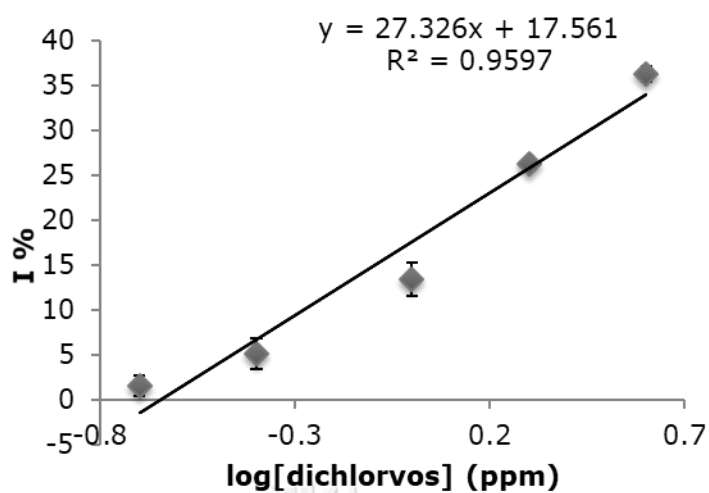


Figure A19. Linear range of dichlorvos detections in *field water 2* by using **GQDs/Enz** platform with spiked dichlorvos in log concentration of 0.2 ppm to 4 ppm.

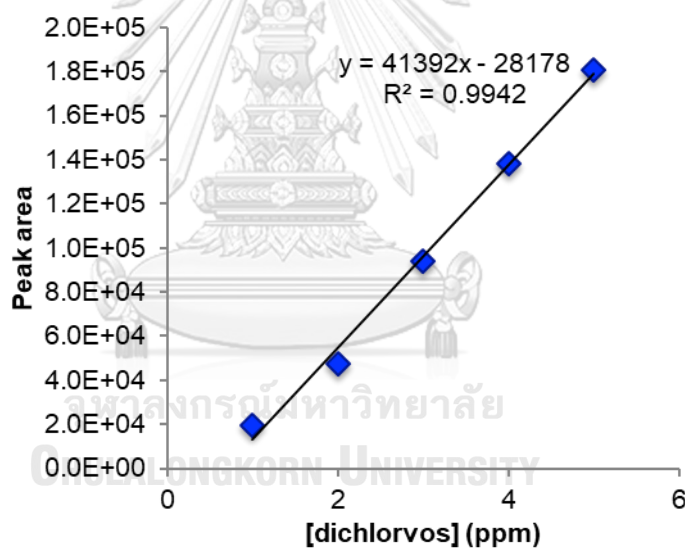


Figure A20. Linear range of dichlorvos detections in *Milli-Q water* by using LC/MS method with spiked dichlorvos in concentration of 1 ppm to 5 ppm.

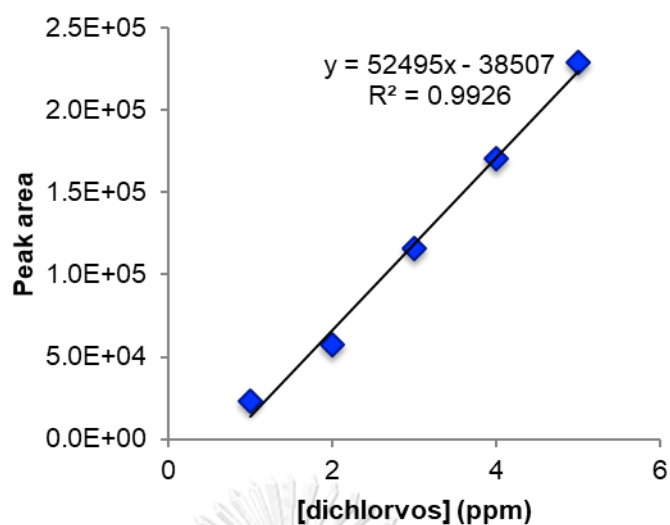


Figure A21. Linear range of dichlorvos detections in *tap water* by using LC/MS method with spiked dichlorvos in concentration of 1 ppm to 5 ppm.

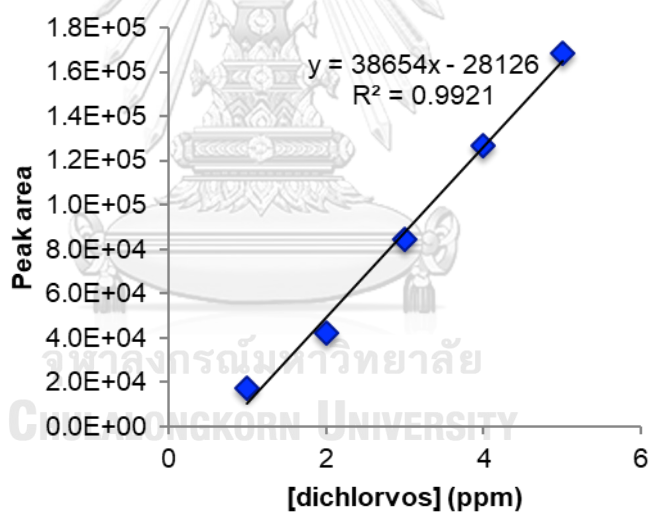


Figure A22. Linear range of dichlorvos detections in *field water 1* by using LC/MS method with spiked dichlorvos in concentration of 1 ppm to 5 ppm.

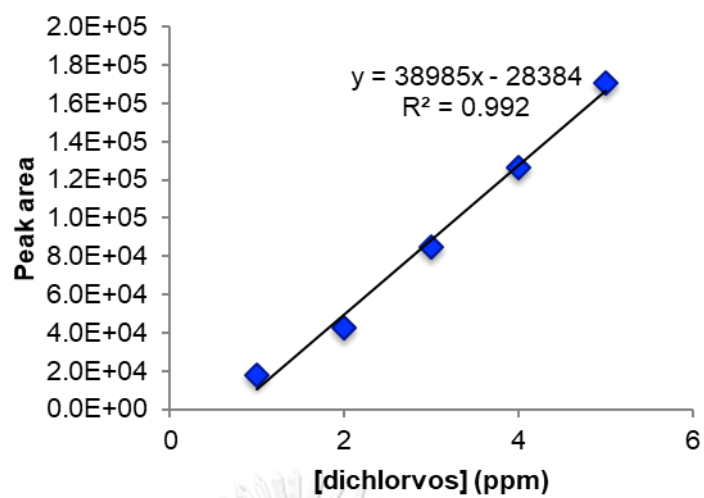
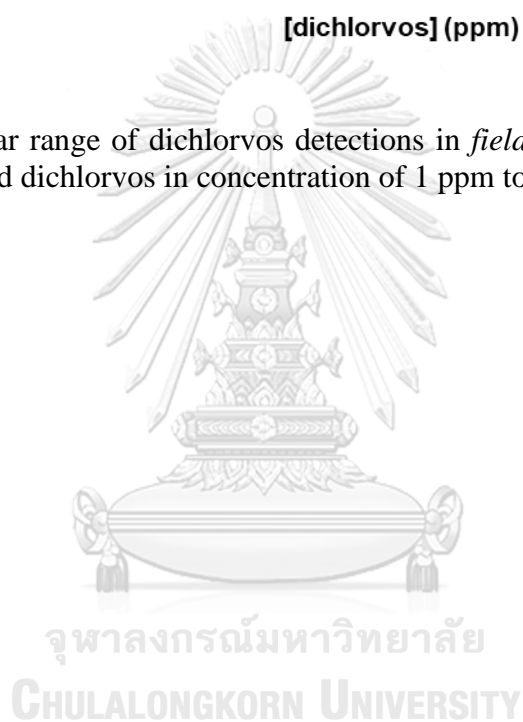


Figure A23. Linear range of dichlorvos detections in *field water 2* by using LC/MS method with spiked dichlorvos in concentration of 1 ppm to 5 ppm.



VITA

NAME Miss Chonticha Sahub

DATE OF BIRTH 31 July 1987

PLACE OF BIRTH Roi Et

INSTITUTIONS ATTENDED A high school diploma from Kaennakhon Wittayalai School (Mathematics and Science Programme), Khon Kaen in 2005, under the scholarship from the Development and Promotion of Science and Technology Talent Project (DPST) since 2003 until present. Bachelor's degree of Science in Chemistry with a first class honor from Khon Kaen University, Khon Kaen, Thailand in 2009. Master's Degree (Chemistry), Chulalongkorn University, Bangkok, Thailand since 2010 to 2013. Doctor of Philosophy degree (Chemistry) and a member of supramolecular research unit at Chulalongkorn University, Bangkok, Thailand since 2013 to 2018.

HOME ADDRESS 204, Moo.1, Photong Sub-District, Phontong District, Roi Et, 45110.

PUBLICATION Sahub, C.; Tumcharern, G.; Tuntulani, T.; Ekgasit, S.; Palaga, T.; Tomapatanaget, B., Study of Novel Self-Assembled Coordination Nanoparticles from Surfactants and Gadolinium ion to Stabilize Curcumin in Buffered Solution. *KKU Research Journal*, 2013; 18(5).

Sahub, C.; Tumcharern, G.; Chirawatkul, P.; Ruangpornvisuti, V.; Ekgasit, S.; Wanichweacharungruang, S.; Tuntulani, T.; Palaga, T.; Tomapatanaget, B., Self-assembly of Gd³⁺/SDS/HEPES complex and curcumin entrapment for enhanced stability, fluorescence image in cellular system. *Colloids Surf B Biointerfaces*, 2017, 156, 254-261.

Jeong, Y.; Tonga, G. Y.; Duncan, B.; Yan, B.; Das, R.; Sahub, C.; Rotello, V. M., Solubilization of Hydrophobic Catalysts Using Nanoparticle Hosts. *Small*, 2018, 14 (7).

Sahub, C.; Tuntulani, T.; Nhujak, T.; Tomapatanaget, B., Effective biosensor based on graphene quantum dots via enzymatic reaction for directly photoluminescence detection of organophosphate pesticide. *Sensors and Actuators B: Chemical*, 2018, 258, 88-97.

Sahub, C.; Andrews, J. L.; Smith J. P.; Asyikin M. A. M.; Tomapatnaget, B., Steed J. W., A hybrid graphene quantum dots/enzyme hydrogel for highly efficient photoluminescence sensing of organophosphate pesticides. *Impressed*, 2018.

AWARD RECEIVED

ACS Sensors Prize in the 5th International Conference on Molecular Sensors and Molecular Logic Gates (MSML 2016), University of Bath, Bath, UK.

Outstanding Awards in Biological Science in the 8th Conference on Synchrotron Light Research Institute (SLRI 2018), 2 June, 2018, Centara Grand at Central Plaza Ladprao, Bangkok, Thailand.



จุฬาลงกรณ์มหาวิทยาลัย
CHULALONGKORN UNIVERSITY